SYNTHESES AND CHARACTERIZATION OF BENZOTRIAZOLE, THIENOPYRROLEDIONE AND BENZODITHIOPHENE CONTAINING CONJUGATED RANDOM TERPOLYMERS FOR ORGANIC SOLAR CELLS

A THESIS SUBMITTED TO
THE GRADUATE SCHOOL OF NATURAL AND APPLIED SCIENCES
OF
MIDDLE EAST TECHNICAL UNIVERSITY

BY

KARDELEN GÖKSU

IN PARTIAL FULFILLMENT OF THE REQUIREMENTS
FOR
THE DEGREE OF MASTER OF SCIENCE
IN
CHEMISTRY

JUNE 2019

Approval of the thesis:

SYNTHESES AND CHARACTERIZATION OF BENZOTRIAZOLE, THIENOPYRROLEDIONE AND BENZODITHIOPHENE CONTAINING CONJUGATED RANDOM TERPOLYMERS FOR ORGANIC SOLAR CELLS

submitted by **KARDELEN GÖKSU** in partial fulfillment of the requirements for the degree of **Master of Science in Chemistry Department, Middle East Technical University** by,

Prof. Dr. Halil Kalıpçılar
Dean, Graduate School of **Natural and Applied Sciences** _____

Prof. Dr. Cihangir Tanyeli
Head of Department, **Chemistry** _____

Prof. Dr. Ali Çırpan
Supervisor, **Chemistry, METU** _____

Examining Committee Members:

Prof. Dr. Levent Toppare
Chemistry, METU _____

Prof. Dr. Ali Çırpan
Chemistry, METU _____

Prof. Dr. Yasemin Arslan Udum
Technical Sciences Vocational School, Gazi University _____

Assoc. Prof. Dr. İrem Erel Göktepe
Chemistry, METU _____

Assoc. Prof. Dr. Görkem Günbaş
Chemistry, METU _____

Date: 18.06.2019

I hereby declare that all information in this document has been obtained and presented in accordance with academic rules and ethical conduct. I also declare that, as required by these rules and conduct, I have fully cited and referenced all material and results that are not original to this work.

Name, Surname: Kardelen Göksu

Signature:

ABSTRACT

SYNTHESES AND CHARACTERIZATION OF BENZOTRIAZOLE, THIENOPYRROLEDIONE AND BENZODITHIOPHENE CONTAINING CONJUGATED RANDOM TERPOLYMERS FOR ORGANIC SOLAR CELLS

Göksu, Kardelen
Master of Science, Chemistry
Supervisor: Prof. Dr. Ali Çırpan

June 2019, 85 pages

Two random terpolymers, PBTS and PBTSe were designed and synthesized successfully as the donor units for polymer organic solar cell. Desired terpolymers contain alkoxy-benzodithiophene as an electron rich unit and N-octylthieno[3,4,c]pyrrole-4,6-dione (TPD) as the electron deficient group. Furthermore, thiophene and selenophene π bridges were introduced to benzotriazole unit as the acceptor moieties into copolymer backbone. The properties of synthesized terpolymers solar cell device were investigated by optical, electrochemical, spectroelectrochemical, kinetic studies. One of the terpolymer, PBTS showed an optical band gap of 1.84 eV with highest occupied molecular orbital (HOMO) energy level of -5.29 eV, open circuit voltage of 0.64 V, short circuit current density of 10.57 mA/cm^2 and fill factor of 63.5%. The power conversion efficiency of bulk heterojunction solar cell device based on PBTS: $PC_{71}BM$ blend film was recorded as 4.30% by introducing 1% 1, 8 diiodooctane (DIO) as the solution process additive. The second terpolymer, PBTSe exhibited lower optical band gap of 1.78 eV with a HOMO energy level of -5.27 eV, open circuit voltage of 0.69 V, short circuit current density of 11.88 mA/cm^2 and fill factor of 62.7%. The power conversion efficiency of bulk heterojunction solar cell device based on PBTS: $PC_{71}BM$ blend film was

recorded as 5.15% by introducing 3% diphenyl ether (DPE) as the solution process additive.

Keywords: Benzotriazole, Thienopyrroledione, Benzodithiophene, Organic Solar Cell, Random Conjugated Polymer

ÖZ

ORGANİK GÜNEŞ HÜCRELERİNDE KULLANILACAK BENZOTRİAZOL, TİYENOPİROLEDİYON VE BENZODİTİYOFEN İÇEREN RASTGELE TERPOLİMERLERİN SENTEZ VE ÖZELLİKLERİİ

Göksu, Kardelen
Yüksek Lisans, Kimya
Tez Danışmanı: Prof. Dr. Ali Çırpan

Haziran 2019, 85 sayfa

Rastgele terpolimerler, PBTS ve PBTSe, foto aktif katmanda kullanılmak üzere organik güneş pili için bir donör ünitesi olarak başarılı bir şekilde tasarlanmış ve sentezi tamamlanmıştır. Elde edilen terpolimerler, elektron bakımından zengin bir birim olarak alkoksi-benzoditiyofen ve elektron eksikliği olan bir grup olarak N-oktiltiyeno [3,4,*c*] pirol-4,6-dion (TPD) içermektedir. Ayrıca, benzotriazol ünitesine kopolimer omurgasına electron alıcı birim olarak tiyofen ve selenofen köprüler sokuldu. Üretilen güneş pili cihazının özellikleri optik, elektrokimyasal, spektroelektrokimyasal, kinetik çalışmalar ile incelenmiştir. Terpolimerden biri olan PBTS, − 5.29 eV'luk en yüksek işgal edilmiş moleküler orbital (HOMO) enerji seviyesine sahip olan 1.84 eV'lik bir optik bant boşluğu, 0.64 V'luk açık devre voltajı, 10.57 mA/cm^2'lik kısa devre akım yoğunluğu ve yüzde 63.5'lik dolum faktörü gösterdi. PBTS: PC71BM yoğun heteroeklem güneş hücre cihazının güç dönüşüm verimliliği, bir çözelti işlem katkısı olarak %1 1,8 diiodooktan (DIO) eklenerek % 4,30 olarak kaydedilmiştir. İkinci terpolimer olan PBTSe, HOMO enerji seviyesi − 5.27 eV, 0.67 V açık devre voltajı, 11.77 mA/cm^2 kısa devre akım yoğunluğu ve % 52.1 dolum faktörü ile 1.78 eV düşük optik bant aralığı sergilemiştir. PBTS: PC71BM harman filmi bazında yoğun heteroeklem güneş hücre cihazının güç dönüşüm

verimliliği, bir çözelti işlem katkısı olarak % 3 difenil eter (DPE) eklenerek % 5.15 olarak kaydedilmiştir.

Anahtar Kelimeler: Benzotriazol, Tiyenopiroldiyon, Benzoditiyofen, Organik Güneş Gözesi, Rastgele Konjüge Polimer

To my family

ACKNOWLEDGEMENTS

I would like to express my special thanks of gratitude to Prof. Dr. Ali Çırpan who gave me the opportunity to do my master which also helped me in doing a lot of research with endless laboratory facilities and I came to know about so many new things.

I am really thankful to him. I own my other special thank Prof. Dr. Levent Toppare for his guidance and valuable questions in our meetings, which help me to think in deeply about my studies and broaden my horizon.

I would like to thank Prof. Dr. Yasemin Arslan Udum and Dr. Şerife Özdemir Hacıoğlu for electrochemical characterization studies.

I would like thank Dr. Gönül Hızalan for studies in photovoltaic applications and she showed me how to process my polymers in device applications.

I would like to thank Assoc. Prof. Dr. Görkem Günbaş for his contributions in organic chemistry field .

I am very grateful to Şevki Can Cevher for his guidance, support and patience during my master adventure.

I would like to express my deeply gratitude to Selin Sağesen for her friendship, motivation, and support during my thesis.

I would like to offer my special thanks to Soner Öztürk who always stands by me whenever I needed and the words are not enough how much I deeply love him. He always supports me and tries to make me remember how much I am strong when I am not believe in myself.

I would like to thank Duygu Güven. She is always with me like my sister anytime when I need her support and valuble thoughts.

I would like to thank all Cırpan’s Research group members for their help and support during my experiments.

I would like to thank NanoMagnetic Instruments for AFM images especially Dr. Selda Keskin Oral and all researchers of NanoMagnetic Intrument AFM laboratory.

I would like to thank METU Central Laboratory for TEM images.

I want to thank Toppare and Günbaş Research group members for their contributions.

The last but not the least, I owe a lot to my precious parents Nevin, Naci and Halim for their endless love, guidance and encouragement my whole life.

TABLE OF CONTENTS

LIST OF TABLES

TABLES

LIST OF FIGURES

FIGURES

LIST OF ABBREVIATIONS

ABBREVIATIONS

CP	Conjugated polymer
BHJ	Bulk Heterojunction
OSC	Organic Solar Cell
EC	Electrochromic
PCE	Power conversion efficiency
HOMO	Highest Occupied Molecular Orbital
LUMO	Lowest Unoccupied Molecular Orbital
CB	Conduction Band
VB	Valence Band
CV	Cyclic Voltammetry
ITO	Indium tin oxide
PSS	Polystyrene Sulfonate
PEDOT	Polyethylene Dioxythiophene
PCBM	[6,6]-Phenyl C_{71}butyric acid Methyl ester
$TBAPF_6$	Tetrabutylammonium hexafluorophosphate
ACN	Acetonitrile
η	Power conversion efficiency
J_{sc}	Short circuit current density
V_{oc}	Open circuit voltage

FF	Fill factor
P_{max}	Maximum power
P_{in}	Power of the incident light
AM 1.5 G	Air mass 1.5 Global
Eg^{op}	Optical band gap
Eg^{el}	Electronic band gap
TA	Thermal Analysis
TGA	Thermal Gravimetric Analysis
DSC	Differential Scanning Calorimetry
UV	Ultraviolet
Vis	Visible
TPD	Thienopyrroledione
BDT	Benzodithiophene
BTz	Benzotriazole
EQE	External Quantum Efficiency

LIST OF SCHEMES

SCHEMES

CHAPTER 1

INTRODUCTION

1.1. Conjugated Polymers (CPs)

One of the most remarkable subject of recent years is conjugated polymers (CPs). Conjugated polymer is a macromolecule which represents a structural system containing alternating double and single bonds that possess semi-conducting ability. The first conjugated polymer polypyrrole (PPy) was investigated in 1960s. In 1977, MacDiarmid and his co-workers[1] doped polyacetylene (PA) with iodine and electrical conductivity of PA was successfully achieved. This study was a breakthrough point for the researchers and contribute to the acceleration of studies on new conjugated polymers[1]. There are many examples of synthesized conjugated polymers as shown in *Figure 1.1*. Discovery of conducting polymers and ability of doping generated a new era of molecules with better mechanical properties and optical, electrical and electronic features[2]. CPs do not conduct electricity in their neutral states. This is overcome after by doping process where the charges can easily flow on the polymer chains and electrical conductivity is enhanced. By doing so, electric current is produced[3].

Conjugated polymers are cheap and easy to manufacture, and have a growing interest in many applications. Organic solar cells, organic light emitting diodes, electrochromic devices and supercapacitors are just a few of the most remarkable areas of these polymers. The overlapping of pz-orbitals forms the highest occupied molecular orbital (HOMO) filled by the π-electrons in the conjugated polymer and the lowest unoccupied molecular orbital (LUMO).

Several optical and electronic properties can be tuned through the π-system while chemical bonding by δ-bonds in the molecular structure is maintained.

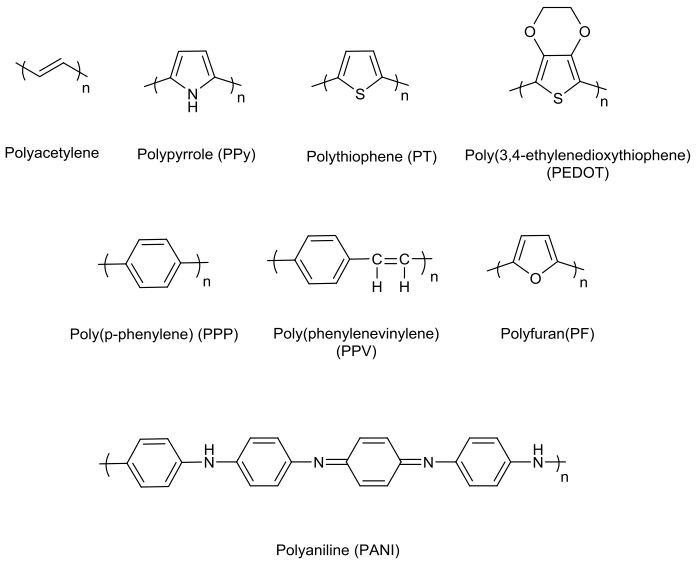

Figure 1.1. Illustrations of Conjugated Polymers (CPs)

The valence band consists of π-orbitals bordered by the HOMO and the conduction band is constituted with π*-orbitals bordered by the LUMO. The difference between HOMO and LUMO energy levels gives band gap of polymer[4–7].

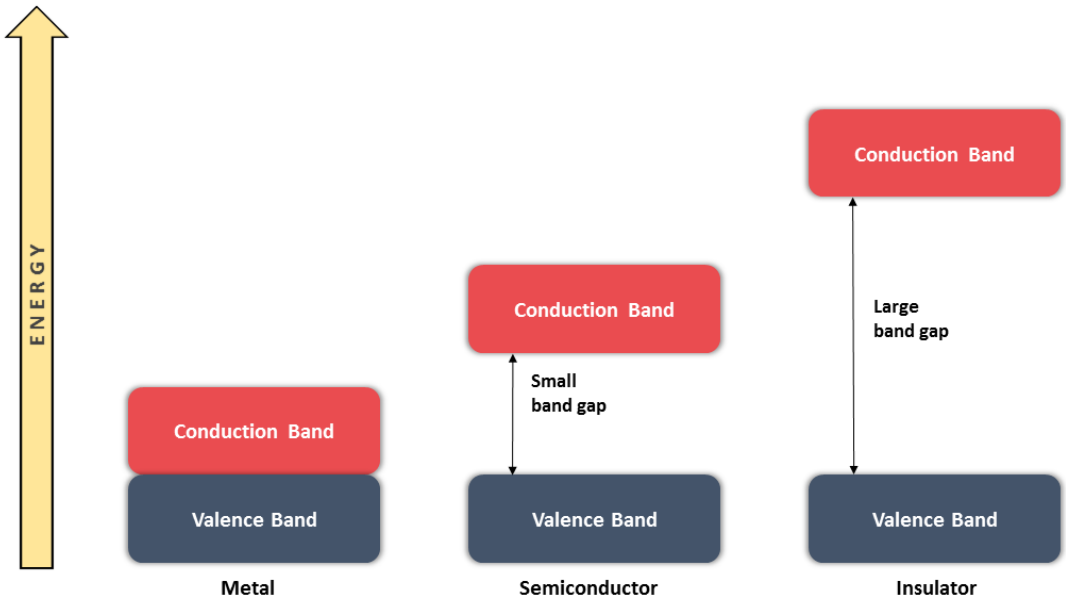

Figure 1.2. Band Gaps of Metal, Semiconductor, Insulator

1.1.1. Doping Process

As previously mentioned, CPs are not conductive in their neutral state due to lack of free charges where electrons can easily flow in order to conduct electricity. The process is called as "doping" in which partial oxidation or reduction of the conjugated polymer occur via charge transfer reaction, and leads to formation of free charges. The polymer is p-dopable when the electrons are removed from polymer chains. On the other part, when electrons are introduced to chains of polymers resulting in anions (negatively charged) and it is defined as n-doping[3]. The conjugated polymer with extended π-orbital causes one dimensional electronic structure with polarons, bipolarons, solitons (non-linear excitations)[8]. The formation of positive and negative charges on the polymer backbone chains are illustrated in below:

Chemically doped Polyacetylene:

$(CH)_n + nyX \longrightarrow [(CH)^{+y} X_y^-]_n$ p-type X=Br_2, I_2 (oxidaiton with halogens)

$(CH)_n + nyM \longrightarrow [(CH)^{+y} M_y^-]_n$ n- type M=Na, Li (reduction with alkali metals)

Electrochemically doped Polythiophene:

$(T)_n + nyX^- \longrightarrow [T_y^+X_y^-]_n + nye^-$ p-type X = ClO_4^-

$(T)_n + nyM^- \longrightarrow [T_y^+X_y^-]_n$ n-type M = Li^+

While free radical are forming, there arise some structural defects on the polymer backbone during the polymerization reaction of polyacetylene[3]. The formation of this structure is named as soliton[3,9] and during oxidation and reduction of polymer, negatively (due to reduction) and positively (due to oxidation) charged solitons are formed illustrated in *Figure 1.3*.

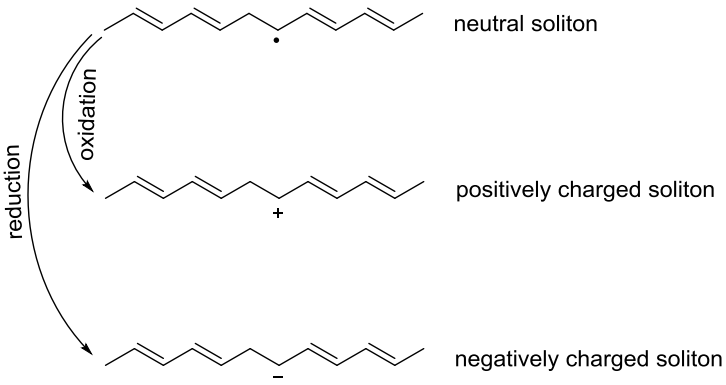

Figure 1.3. Trans-polyacetylene soliton formation

1.2. Electrochromism

Electrochromism (EC) is a phenomenon where a reversible visible color change occurs in the material under applied potential, and many organic and inorganic materials show optical changes in the electromagnetic spectrum[10]. Electrochromical materials exhibit color change between bleached or transparent state and several colored states[11]. The first examples of these materials were suggested by Deb and co-workers[12] studying on amorphous and crystalline metal oxides. Electrochromic materials are divided in three categories: transition metal oxides, inorganic materials and organic materials or organic polymers[13]. Especially, semiconductor tungsten oxide (WO_3) was very promising as a high band-gap material[14]. Prussian blue, oxides of Co and Ni (anodically colored) and V, Nb, Mo oxides (cathodically colored) are the examples of populously studied electrochromic inorganic materials. The third class of EC compounds is conjugated polymers, which have rapid response time, high optical contrast, multicolor electrochromic properties and being processability. Among the conjugated polymers, polythiophene, polypyrrole and polyaniline are extensively used EC materials[11]. In 2000, John R. Reynolds et al.[15] reported a study including many organic polymer structures and showed their neutral and doped state color changes under applied external potential. In *Figure 1.4*, three examples of polymers are shown.

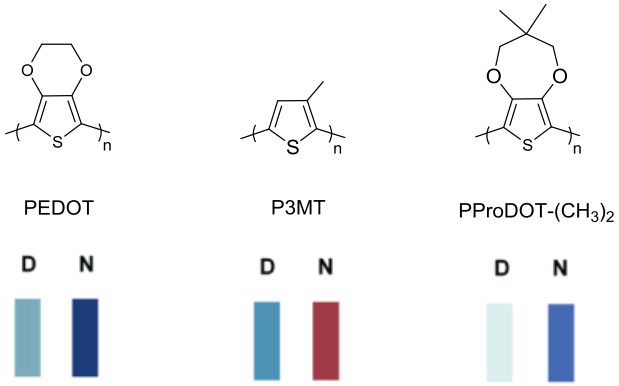

Figure 1.4. Examples of Semiconductor Electrochromic Polymers in Literature[15]

Several parameters are studied for the characterization and identification of electrochromic materials and these parameters affects the properties of electrochromic devices:

The first one is ***optical contrast*** that is percent transmittance change (ΔT %) at altered wavelengths and it gives an idea of the amount of incident light at a specific wavelength where it is absorbed or reflected.

The second is ***switching speed*** which is also called as switching time. It is the time between transitions of two states of materials under external potential and coloring/bleaching or vice versa of EC materials is observed during this period which indicates oxidation and reduction processes are occurring.

The third factor is ***stability*** which is related to active matrix decomposition. When there is an irreversible oxidation or redox reaction at very high potentials, they cause deterioration of active matrices. During oxidation and reduction reactions of materials, electrons are gained or lost and this causes the formation of side products that affects the switching stability.

The last parameter is ***optical memory*** also called as open-circuit memory. It is important that the EC material can be maintained at its absorption state after electric field is ceased. To illustrate, there is no requirement to apply current for days in solid state ECDs while solution ones are changed very rapidly.

1.3. Motivation

In today's world, there exists an enormous amount of energy consumption and this consumption is increasing day by day reaching terawatt magnitude as the human population increase[16–20]. The requirement of supplies are commonly fulfilled from energy sources like oil, natural gas, coal and other fuels[21–23]. The primary concern of using non-renewable energy sources is the emission of greenhouse gases while burning of fuel sources [24]. The shortening of the life of fossil fuels has led researchers to the shift to look for alternative energy sources and to intensify their research toward the greener sources like solar energy which has limitless energy capacity, cleanness and renewability[16]. Most commonly, conjugated polymer structures possess good specific capacitance and this makes them very popular for next-generation energy storage devices[25].

1.4. Organic Solar Cell

Organic photovoltaics (OPVs) are devices which use organic materials such as polymers and small molecules in order to convert sunlight energy into the electricity [26]. Organic materials have the potential to foster a lasting technology that is economically feasible for power generation based on eco-friendly materials with unrestricted accessibility. Organic semiconductors can be an alternative to inorganic semiconductors as these are cost effective and have extremely high optical absorption coefficients which extend the possibility for the construction of ultrathin solar cells. Additionally, organic solar cells have shown the possibilities for flexible devices using high throughput, low temperature approaches that employ well established roll-to-roll process[27,28]. There are very promising low cost manufacturing process in order to construct solar cells: perovskite solar cells (PSCs)[29], dye-sensitized solar cells (DSSCs) [30], organic small molecules or organic polymer solar cells[6,31–33]. Among all of types, bulk heterojunction solar cells (BHJSCs) take great attention due to their low cost, ease of processability and lightness[34,35].

1.4.1. Bulk Heterojunction Solar Cell

The utilization of organic compounds such as polymers and small molecules in the optoelectronic device applications are very popular since light weight, easy reproducibility and low cost fabrication are main advantages of organic solar cells compared to inorganic analogues. In 1993, Sariciftci et al.[36] made first polymer based bulk heterojunction solar cell by using poly[2-methoxy-5-(2-ethylhexyloxy)-1,4-phenylenevinylene] (MEH-PPV) as donor part and buckminsterfullerene (C_{60}) as acceptor part interfacing with each other and power conversion efficiency of device was recorded as 0.04%. This study was a milestone of BHJSCs based on polymers and pioneered to new areas of studies[36].

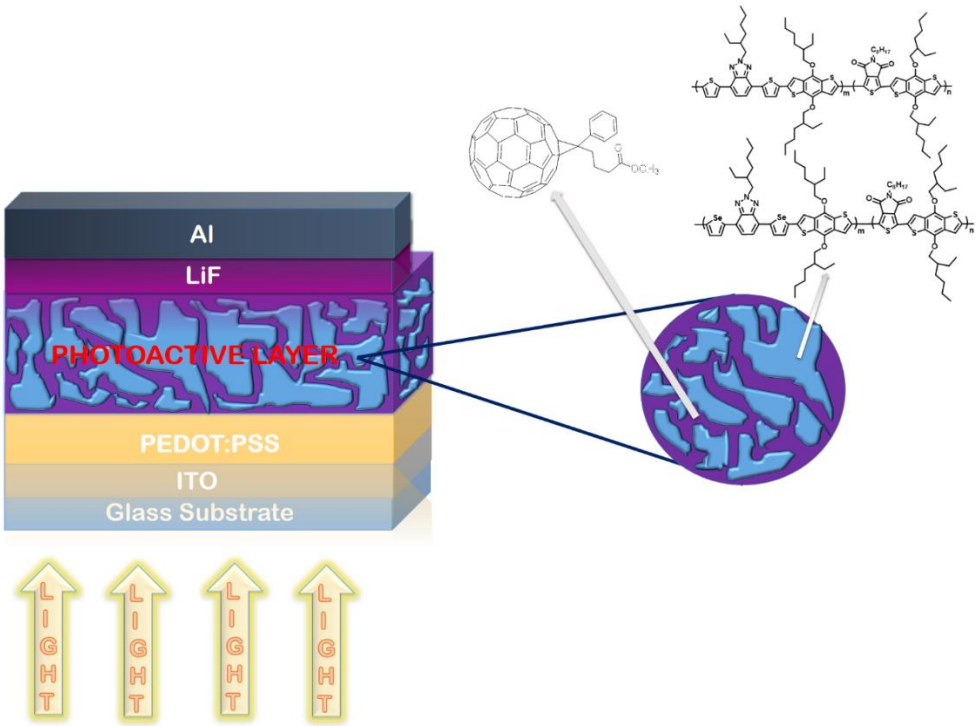

Figure 1.5. Device Construction of a BHJ OSC

A BHJ OSC basically comprises of a multilayer structure in which layers are deposited by individual construction techniques (see *Figure 1.5.*). The photoactive layer involves two constituents: conjugated polymers are used as the donor materials while fullerene derivatives are utilized as the acceptor materials. Between anode and low

work function (WF) cathode, the photoactive layer is placed and interfacial layers which are electron transport layer and hole transport layer are introduced between layers in order to improve performance of BHJ OSCs devices[37]. There are four fundamental steps of working principle of an BHJ OSCs namely (1) absorption of photon and formation of exciton, (2) diffusion of exciton toward donor-acceptor interface, (3) transportation of charges and (4) collection of charges[37–39]. In general, donor material (conjugated polymer) absorbs light and an electron is excited from HOMO energy level of donor polymer to LUMO energy level. As a result of this, exciton, a pair of positive (hole) and negative (electron) charges bonded via electrostatic Coulomb force, is obtained. In order to create exciton, HOMO of the donor and LUMO of the acceptor should be in a range of 0.1 V-1.4 eV. The energy difference is larger for organic semiconductors because enhanced Coulomb interaction between hole and electron is obtained by localized wave functions of hole and electron and low dielectric constants (ε~3–4). The electron-hole pair diffuses toward the donor-acceptor interface and they are divided into separable charges derived by potential energy difference[40]. Then, charge carriers are collected on the bicontinuous interpenetrating pathway through corresponding electrodes without trapping of charges and recombination processes. The working principle steps are mentioned in details below.

1.4.2. Operation Principle of BHJ OSCs

1.4.2.1. Light Absorption and Exciton Generation

First essential rule for high efficiency device is achieved with maximum absorption of incident sunlight by photoactive layer. In general, donor part of the active layer absorbs light. Having high absorption coefficient ($10^7 m^{-1}$) of conjugated polymers lead to absorption of light at their maxima in the absorption spectrum with about 100 nm thickness of photoactive layer [41]. The thickness has a limitation up to 100 nm because only 60% absorption can be achieved by the polymer containing active layer that results in low charge carrier mobilities[41]. Low photocurrent generation is

obtained as a result of low absorption property of conjugated polymers. By lowering the band gap of donor polymers, better light absorption is obtained and hence, higher amounts of photons are harvested resulting in higher device performance. To illustrate, band gap less than 2 eV is evaluated as low band gap material thanks to better overlap with solar spectrum leading to improvement of device efficiency[42,43]. When the sunlight reaches to active layer, excitation of photon from HOMO to LUMO energy level is occurred and exciton (hole-electron pair) is formed. The excitons diffuse toward interface of polymer donor and acceptor interface (see *Figure 1.6*)[40].

1.4.2.2. Diffusion of Exciton and Charge Dissociation

Hole and electron in an exciton are bonded with Coulomb interactions and dissociation is only occurred when attractions between two charges are broken. This process is performed by LUMO energy difference of donor and acceptor material and should be above their binding energy in order to dissociation of free electron and hole[44–46]. Exciton diffusion length is a term defining the distance where time required for travelling before it dissociates. Since most of the conjugated polymers have excitons with shorter lifetime, the distance has a boundary of a few nanometers (less than 20 nm) for proper generation of charge in diffusion length border[47,48]. Better charge migration is resulted from efficient exciton dissociation which requires electric field difference leading to dissociation of charges into free electron and hole. Moreover, when holes go through the material with lower HOMO, free electrons are drifted to material with higher LUMO[42,49].

1.4.2.3. Transportation of Free Charge Carriers

Transportation of free charges through the anode and cathode electrodes is depicted in *Figure 1.6*. The term of hopping process defines the transportation of charge carriers in organic materials from one localized state to other state[50,51]. Fermi level difference of two electrodes leads to migration of free charges in an internal electric field with driving force toward corresponding electrodes in organic semiconductors[52]. The open-circuit voltage (V_{OC}) of the solar cell is affected by low

work function cathode and high work function anode[47]. Further, carrier diffusion and electric field drive the migration of free charge carriers[47].

1.4.2.4. Charge Carriers Collection at Electrodes

Extracted free charges travel through respective electrodes [38]. Since the potential barriers of electrodes and photoactive materials should be optimized, the work function of cathode and anode must be matched with LUMO and HOMO of the materials, respectively [47]. When perfect match is obtained, it is called as Ohmic contact [41].

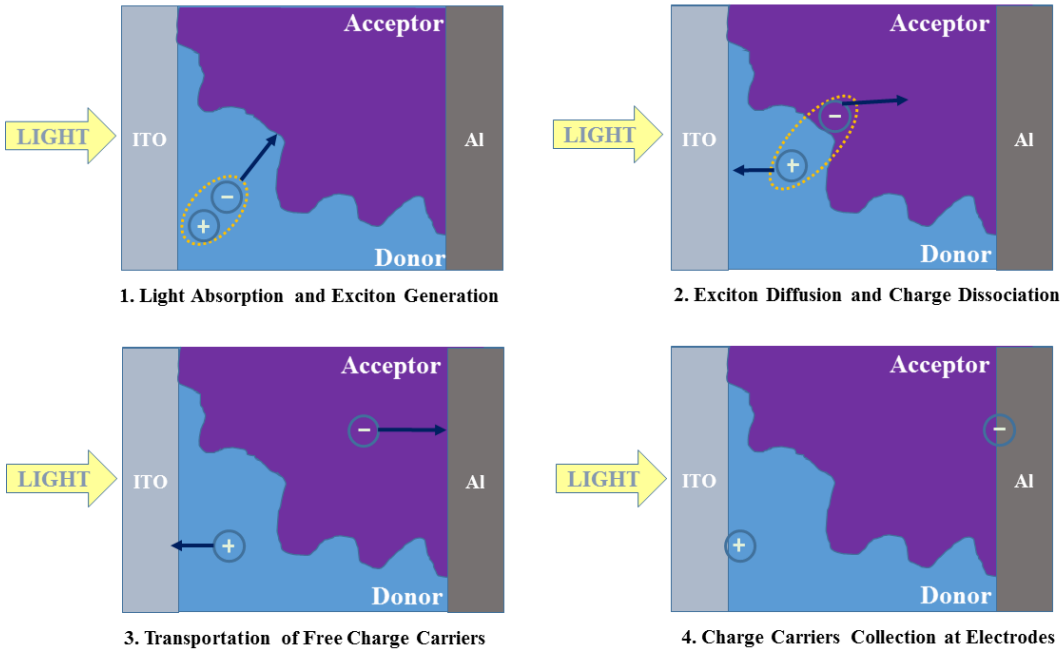

Figure 1.6. Operation of An Organic Solar Cell

1.4.3. Parameters Affecting Device Performance

The solar cell photovoltaic performance is clarified by current density (*J*) where obtained current is divided by the lightened area of cell with respect to external voltage (V). Conventional BHJ OSCs' performances known as power conversion efficiency (PCE) strongly depend on three main parameters which are short-circuit current density (J_{sc}), open-circuit voltage (V_{oc}) and fill factor (FF). The current passing

through the circuit with no external potential is defined as short-circuit current density (J_{sc}). The open-circuit voltage is the voltage with its maxima when no current is passing through in the circuit. The other term is fill factor which gives information about how quality the solar cell is. Finally, device performance is expressed by the term of power conversion efficiency (PCE, η) which is the ratio of product of three parameters and input power (P_{in}) shown in equation (1):

$$\eta = \frac{Pout}{Pin} = \frac{FF\ x\ Voc\ x\ Jsc}{Pin} \qquad \text{(Eq. 1)}$$

The measurements are performed under AM (Air Mass) 1.5 Global conditions. The Air Mass is the distance of travelled light through the atmosphere and it is normalized to the shortest distance. During travel of light, some of the solar power is lost because of absorption by air and dust. The power and incident light spectrum affect solar cell efficiency and a standard spectrum was utilized for accurate calculations at atmosphere and at surface of Earth. AM 1.5G with zenith angle (vertical angle) of 48.2° is the standard spectrum from Earth surface where G indicates global direct and diffuse radiation[53].

1.4.3.1. Short-Circuit Current Density (J_{sc})

The J_{sc} is a term which gives the number of generated and collected charges at corresponding electrodes at zero potential. In other words, it is the maximum current density when applied potential value is zero (V_{oc}=0) in the circuit[47]. The short-circuit current density is approved by external quantum efficiency. EQE is formulated by the ratio incoming photon number to generated charge carriers' number. Therefore, EQE and J_{sc} are related to their parameters. The EQE is expressed by the product of absorption efficiency (η_{abs}), diffusion efficiency (η_{diff}), dissociation efficiency (η_{diss}), transfer efficiency (η_{tr}) and charge collection efficiency (η_{cc})[54].

1.4.3.2. Open circuit voltage (V_{oc})

The open circuit voltage is defined as extracted maximum voltage from a solar cell when there is no available current. A high V_{OC} value is attained by adjusting HOMO energy level of donor which has a direct relationship with HOMO level of donor and LUMO energy level of acceptor moiety i.e. $PC_{71}BM$[55,56]. Earlier studies implies that V_{oc} is obtained from work function differences of two electrodes and is explained by metal-insulator-metal (MIM) model[6,57].

1.4.3.3. Fill Factor (FF)

Another parameter affecting the power conversion efficiency of device is fill factor. It has a relationship between migration of charge carriers and recombination. When the charges are recombined, then low FF value is obtained. Moreover, shape of *J-V* curve is also important and FF determines character of OSC. FF is expressed by ratio of power at its maxima from the solar cell to the product of open-circuit voltage (V_{oc}) and short-circuit current density (J_{sc})[58]. An ideal FF value is 100% when the rectangle is formed in a *J-V* curve (see *Figure 1.6.*). The perfect rectangle shows that ideal solar cell with ease of the photo-carriers generation[59].

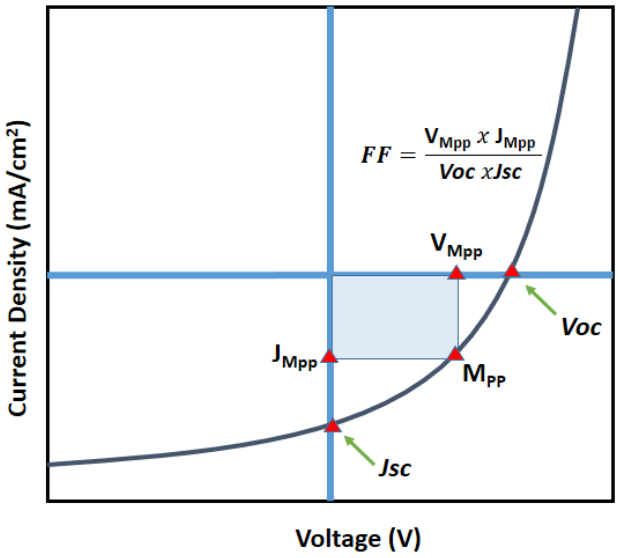

Figure 1.7. J-V curve of Organic Solar Cell Device

1.5. Moieties in Conjugated Random Terpolymers

1.5.1. Thieno[3,4-c]pyrrole-4, 6-dione (TPD)

The thieno[3,4-c]pyrrole-4,6-dione (TPD) moiety (see Figure 6) is commonly used group in the copolymers. In 1996, Tour and Zhang used TPD moiety in donor-acceptor (D-A) type copolymer synthesis for the first time[60]. It has a symmetrical coplanar structure and planarity that enable good electron delocalization. Imide nature provides a strong electron-withdrawing ability and this results in low band gap polymers stabilized by LUMO energy level with strong intramolecular and intermolecular interactions[61]. Soluble derivatives can be achieved by the addition of different alkyl groups to the nitrogen position of imide bond. Furthermore, high crystalline polymers are obtained by introducing TPD unit into polymer backbone chain[62,63].

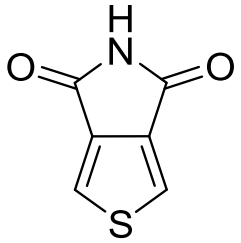

Figure 1.8. Structure of Thienopyrroledione Moiety

1.5.2. Benzotriazole (BTz)

Benzotriazole (BTz) is a heterocyclic nitrogen containing benzazole that have electron deficient nature due to imine bonds (–C=N–). Firstly, Tanimato and Yamamoto[64] synthesized BTz unit. The fused benzene ring leads to get larger conjugation in order to obtain π-π stacking. In addition to this, three nitrogen atoms provide to make hydrogen and coordination bonds. BTz has also functionalizable sides and solubility, one of the most important parameter for processability, can be improved from these sides by introducing different alkyl chains from nitrogen atoms. In addition to improvement of solubility, after addition of alkyl chains, obtained close packing structure increases hole mobility.

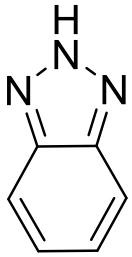

Figure 1.9. Structure of Benzotriazole Moiety

1.5.3. Benzo[1, 2-*b*:4, 5-*b*']dithiophene (BDT)

In the beginning of 1980s, electrical conductivity of benzo[1,2-b:4,5-b']dithiophene (BDT) had been known and synthesized in many molecule designs of molecules[65]. In 2008, Hou and Yang [66] et al. used BDT moiety in the conjugated polymers and it is very promising block to tune optical and electronic properties and intermolecular charge transfer (ICT) from donor to acceptor could be achieved for the high efficient photovoltaic devices[67].

Benzodithiophene (BDT) shows great electron donor properties due to its electron rich π-conjugation system and benzene with coherent thiophene ring increases the planarity[68]. Moreover, high open circuit voltage is achieved by BDT containing polymers having low lying HOMO energy levels. By introducing alkoxy groups to BDT, solubility is increased and the resulting polymers become solution processable for active layer of organic photovoltaic (OPV) devices[69,70]. Besides the solubility, copolymers, containing 4,8- alkoxy–substituted BDT, shows highly crystalline structure and relatively low band gap[71,72].

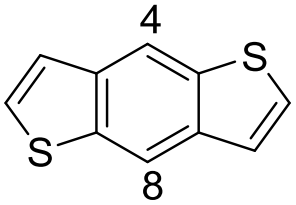

Figure 1.10. Structure of Benzodithiophene Moiety

1.5.4. Group 16 Heterocycles as Π-Bridges: Thiophene and Selenophene

One of the essential parts of the periodic table is group 16 consists of oxygen, sulfur, selenium, tellurium, polonium, and ununhexium in order from top to bottom. This group of elements is called chalcogens containing the first four elements of group 16: oxygen, sulfur, selenium and tellurium and five-membered heterocycles can be obtained from all of these four elements.

Incorporation of heterocycles into conjugated polymers can tune new properties for optoelectronic applications.

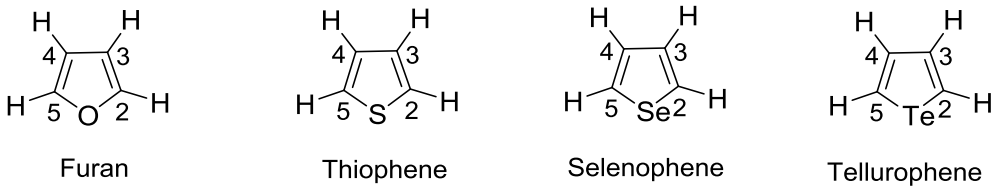

Figure 1.11. Heterocycle Structure of Group 16 members

In 2012, Kim and co-workers have designed polymer structures by altering π-spacer with thiophene and selenophene. According to modification, lower LUMO energy level is expected to obtain thanks to less ionization potential (IP) and close electronegativity of selenium and sulfur atom without any effect on HOMO energy level[73]. Besides a widen absorption band, improved mobility is a result of intermolecular Se···Se interaction for better photo-currents [74]. By using selenophene unit, 1.70 eV lower band gap was obtained than thiophene analogue without a change in HOMO energy level. Enhanced Jsc value of 11.7 mA/cm2 was recorded with almost same HOMO level with high value of Voc and PCE % was reported as 4.12% for PCDSeBT[75].

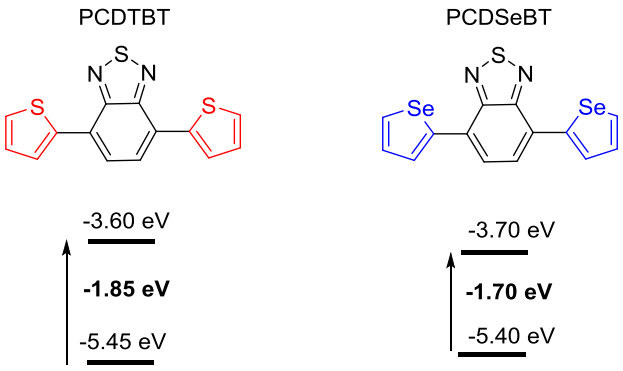

Figure 1.12. Energy-level diagrams of PCDTBT and PCDSeBT

1.6. Literature Review

Donor-acceptor type polymers are one of the most commonly used molecule design for photovoltaic applications. One electron-rich unit and one electron-poor unit are combined covalently by the repetition of these units form conjugated polymer chains. The molecular design construction is necessary to achieve tuned proper optical band gap for maximizing the caption of the solar spectrum[76]. Currently, thiophene[77] with electron-deficient groups and benzodithiophene[78] as the electron donor subunits take great attention[79]. Keller and coauthors[80] have investigated PBT8PT copolymer (see *Figure 1.12*) properties for photovoltaics in 2016. The reported PV efficiency was 6.78% using BDT and TPD moieties in the D-A type conjugated polymer[80].

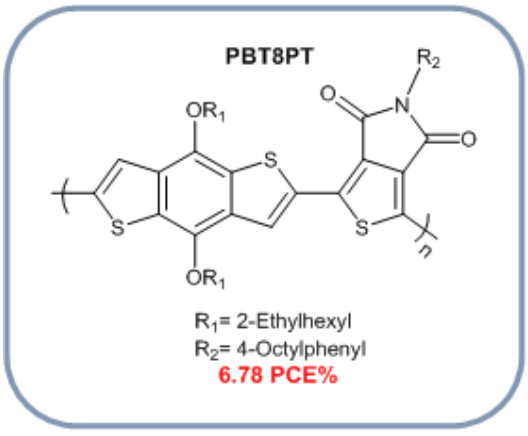

Figure 1.13. Structure of PBT8PT

Furthermore, Zhang et al. designed copolymers called as PBDTBTz (see *Figure 1.14*) containing BDT and BTz via Stille coupling reaction exhibiting 1.4 PCE% with a *J*sc value of 4.8 mA/cm^2, V_{oc} of 0.61 V, and FF of 47%. Moreover, less steric hindrance and lower band gaps were achieved by introducing thiophene to BTz subunit in PBDTDTBTz copolymer (see *Figure 1.14*). They used blended PBDTDTBTz and $PC_{71}BM$ as the active layer showed a device performance of 1.7% with a J_{sc} value of 4.5 mA/cm^2, V_{oc} of 0.61 V, and FF of 62%[81].

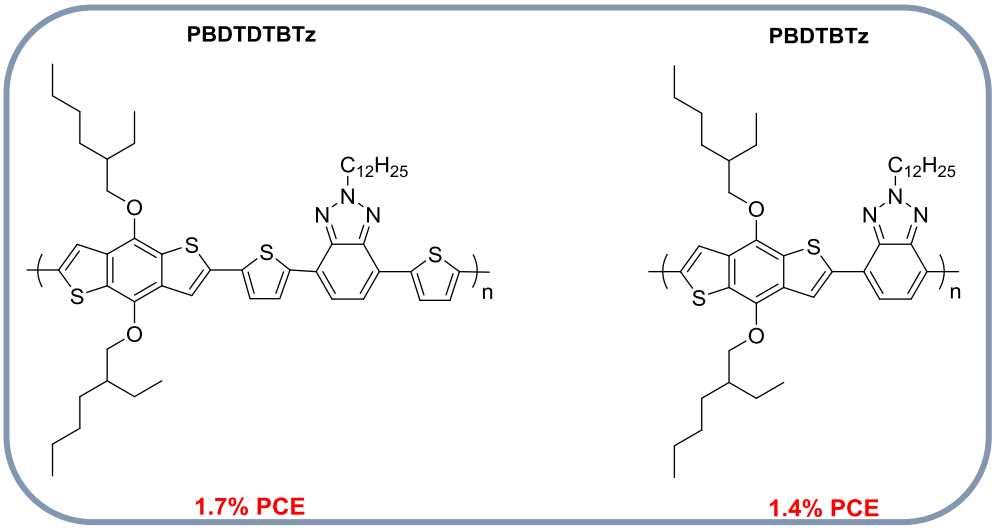

Figure 1.14. Structure of PBDTDTBTz and PBDTBTz

One of the widespread structural design of conjugated polymer is introducing a third component into the carbon backbone chain of the D-A copolymer. Terpolymers contain three different building block that means different properties can be tuned by combining them. By doing so, three units in the terpolymer cause synergetic effects such as improved molecular energy levels, broad light absorption by the appearance of a new π–π* or interchain charge transfer (ICT) peak, solubility, miscibility with fullerene leading to better domain morphology and charge carrier mobility. Lately, terpolymers based solar cell efficiencies have been reported exceeding 9% PCE[82–85]. There are several donor and acceptor segments suitable for the design of copolymers. Among them, benzodithiophene (BDT) shows excellent electron donor properties due to its electron-rich π-conjugation system and benzene with coherent

thiophene ring increases the planarity. There are several donor and acceptor segments suitable for the design of copolymers. Among them, benzodithiophene (BDT) shows excellent electron donor properties due to its electron-rich π-conjugation system and benzene with coherent thiophene ring increases the planarity. Cabanetos and coauthors have designed copolymer based on alkoxy substituted BDT and alkylated-TPD (PBDTTPD) (see *Figure 1.15*) treated with solvent processing additive 5% (v/v) 1-chloronaphthalene having V_{oc} value of 0.93 V, *J*sc value of 12.5 mA/cm^2 and FF of 65% with a PCE of 7.3%[86].

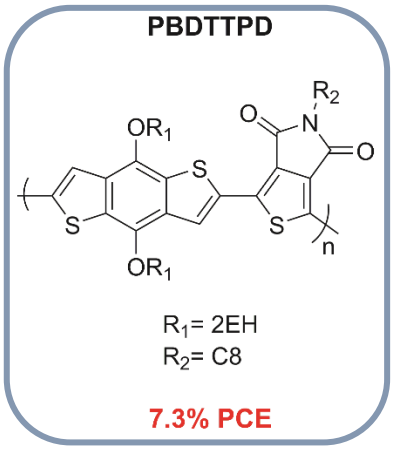

Figure 1.15. Structure of PBDTTPD

Azeri et al. reported a terpolymer based on benzotriazole (BTz), thienopyrrolodione (TPD) and benzodithiophene (BDT) and the efficiency was found to be 2.55% with V_{oc} of 0.84 V, J_{sc} of 4.75 mA/cm^2 and 64% FF (shown in *Figure 1.16*)[31].

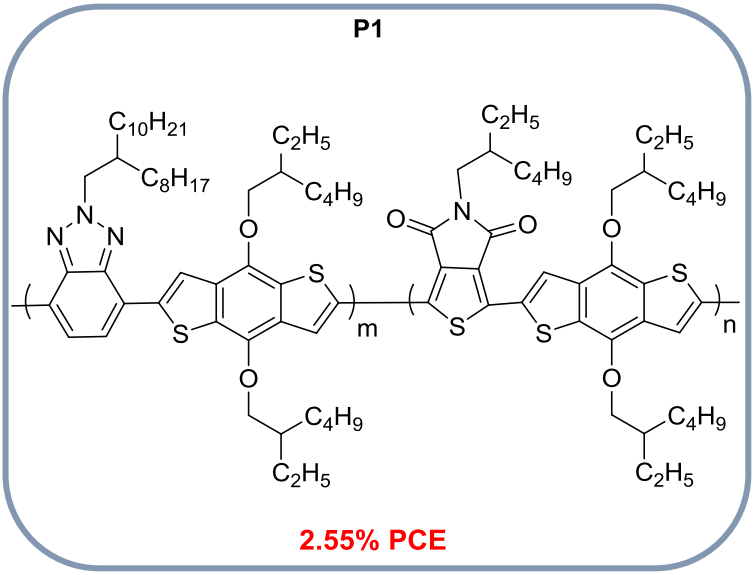

Figure 1.16. Structure of P1

In Kotowski's work, BTz, BDT, and benzothiadiazole moieties have been chosen in order to obtain random donor terpolymers with $PC_{71}BM$ as the acceptor. The treatment of solvent processing additive increases *J*sc value from 4.95 to 10.30 mA/cm^2 since better morphology was obtained with slightly changing Voc and FF values indicating 5.01% PCE raising from 2.63% efficiency.

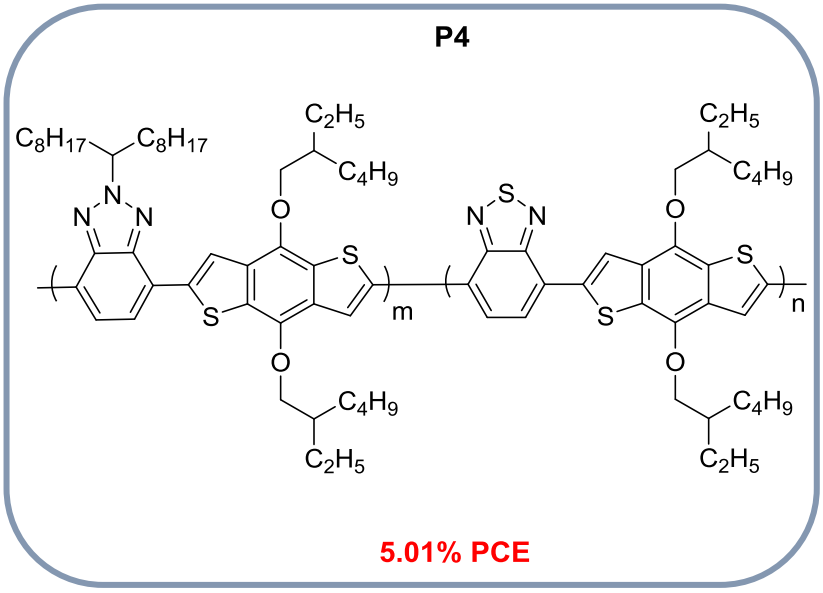

Figure 1.17. Structure of P4

1.7. Aim of Thesis

In the literature, 1D-2A or 2D-1A designs for random terpolymers show better light-harvesting ability. The addition of the third component into the backbone of the polymer chains enable to improve molecular energy levels, have broader photon absorption arising from new π–π* or interchain charge transfer (ICT) peak. Random terpolymerization is a method to facilitate from the properties of three subunits and lower the band gap of desired copolymers, which is essential to exhibit better PV efficiencies. Several donor and acceptor segments are available for the design of copolymers in the literature. Thienopyrrolodione (TPD) is a widely used unit as the acceptor thanks to its electron deficient diimide groups and TPD stabilizes LUMO energy level of the polymer. Besides TPD, BTz is another electron acceptor group having electron deficient imine bonds leading to optimizing photovoltaic performances. As an electron donor segment, benzodithiophene (BDT) was selected since it has an electron-rich π-conjugation system and a more planar structure. Additionally, BDT based polymers have low lying LUMO energy level with high open circuit voltage. In the light of literature reviews, two random terpolymers were designed including BDT, TPD, and BTz. After the synthesis of copolymers, various characterizations were made, and their suitability for solar cells was investigated. The structures of polymers were illustrated in *Figures 1.18* and *1.19.*

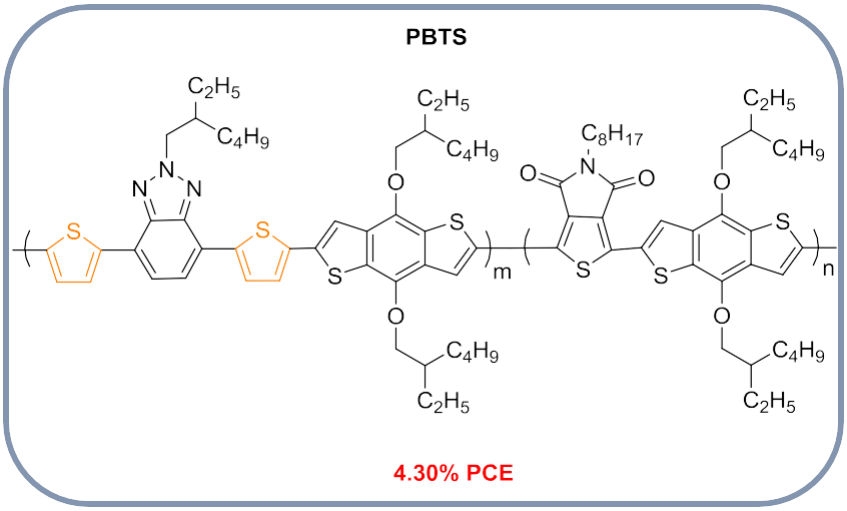

Figure 1.18. Structure of PBTS

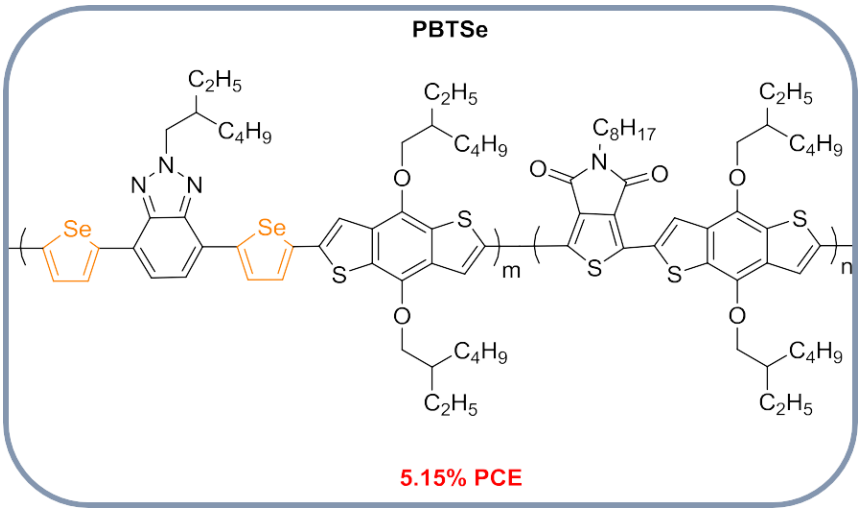

Figure 1.19. Structure of PBTSe

CHAPTER 2

EXPERIMENTAL

2.1. Materials, Measurements and Characterizations

Chemical reagents were commercially available and were used as received. Tetrahydrofuran (THF) was freshly distilled from benzophenone ketyl and sodium metal under inert atmosphere. Other solvents were of analytical grade and used without further purification. For the characterization of synthesized compounds, NMR spectra were taken on Bruker Spectrospin Avance DPX-400 Spectrometer, and chemical shifts were determined relative to internal standard, tetramethylsilane (TMS), for ^{1}H and ^{13}C nuclei in organic deuterochloroform solvent. Gel permeation chromatography (GPC) was performed using Shimadzu RID-20 with chloroform as the eluent and polystyrene as the universal standard to investigate average molecular weights of synthesized polymers. For detection of thermal behaviors of PBTS and PBTSe, thermal gravimetry analysis and differential scanning calorimetry were studied with Perkin Elmer Pyris 1 TGA and Perkin Elmer Diamond DSC, respectively. UV–Vis absorption spectroscopy was performed using a JASCO V-770 spectrophotometer for both solution in chloroform and thin film of PBTS and PBTSe. Emission spectra were obtained on a Perkin Elmer LS 55 Fluorescence spectrometer. Cyclic voltammetry was performed on electrochemical work station with a three-electrode system in a solution of 0.1M $TBAPF_6$ acetonitrile solution at a scan rate of 100 mV/s.

2.2. Synthesis

(1), **(2)** and **(3)** were synthesized according to previously reported procedure[87].

2.2.1. Synthesis of 4,7-Dibromobenzo[c][1,2,5]thiadiazole (1)

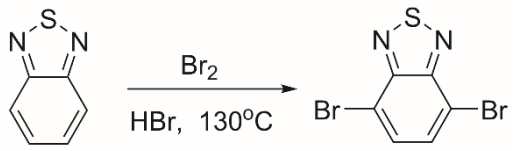

Figure 2.1. Synthesis of 4,7-Dibromobenzo[c][1,2,5]thiadiazole.

A solution of 2,1,3-benzothiadiazole (10.00 g, 73.4 mmol) and 100 mL hydrobromic acid (HBr) (48%) was added in a 500 mL two necked round bottom reaction flask and reflux the reaction for 1 and half hour at 110 ˚C. Then, bromine (11 mL, 216.53 mmol) in 40 mL HBr (48%) was added into the reaction flask dropwise with pressure equalizing dropping funnel. After complete addition of bromine in HBr, reaction was stirred at 130 ˚C overnight. Then, reaction was poured into freshly prepared saturated sodium sulfite ($NaHSO_3$) solution and continued to add sodium bisulfite till orange color compound getting pale yellow color. Before washing with cold diethyl ether, the filtered compound was washed with water several times to obtaine pale yellow stable solid (20.85 g, yield 95%).

2.2.2. Synthesis of 3,6-Dibromobenzene-1,2-diamine (2)

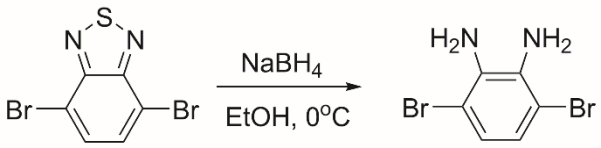

Figure 2.2. Synthesis of 3,6-Dibromobenzene-1,2-diamine.

4,7-Dibromobenzo[c][1,2,5]thiadiazole (10.0 g, 34.0 mmol) was weighed into a round bottom flask and then dissolved in 400 mL ethanol (EtOH). Reaction flask was placed in an ice bath and temperature was controlled while slow addition of sodium borohydride $NaBH_4$ (38.6 g, 1020mmol). Then, the reaction was stirred overnight at ambient temperature. Ethanol was evaporated and obtained solid was extracted with diethyl ether and water. Before removing organic solvent, drying agent,$MgSO_4$, was

used to get rid of remaining water. The obtained product has a pale yellow color. (8.5 g, yield 94%).

2.2.3. Synthesis of 4,7-dibromo-2H-benzo[d][1,2,3]triazole (3)

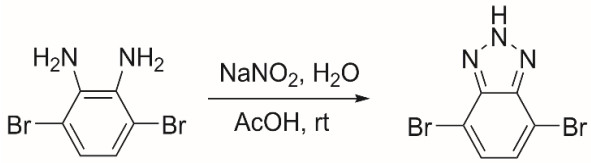

Figure 2.3. Synthesis of 4,7-Dibromo-2H-benzo[d][1,2,3]triazole.

To a solution of 3,6-Dibromobenzene-1,2-diamine (5.00 g, 18.80 mmol) in 65 mL acetic acid (AcOH), a prepared solution of $NaNO_2$ (1.43 g, 20.72 mmol) in 36 mL H_2O was added very slowly. Then, the mixture was stirred for half an hour at room temperature. The precipitate was collected by filtration and washed with distilled water several times till odor of acetic acid was gone. Finally, 4,7-dibromo-2H-benzo[d][1,2,3]triazole was obtained as orange-pale brown powder. (3.25 g, yield 65%)

2.2.4. Tributyl (thiophen-2-yl)stannane (4)

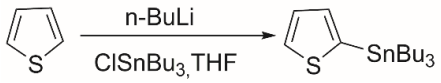

Figure 2.4. Synthesis of Tributyl(thiophen-2-yl)stannane.

Thiophene (2.00 g, 23.77 mmol) was dissolved in 30 mL of freshly distilled THF (dry) under argon atmosphere. The reaction was stirred for a while and flask was placed in a cryostat at -78˚C. n-BuLi (9.00 mL, 22.5 mmol, 2.5 M in hexane) was added drop wise over 6 h, and subsequently, the reaction was stirred for 1 h. Further, tributyltin chloride (8.51 g, 26.15 mmol, 97%) was added slowly over 4 h, and the mixture was stirred for an additional hour. Finally, it was removed from cryostat and stirred overnight at room temperature. THF was evaporated under reduced pressure. About 5 mL distilled water were added to flask and extraction was performed with dichloromethane and brine. The organic residue was dried over $MgSO_4$, and the

solvent was evaporated by rotary evaporator. The viscous pale yellow oil was obtained (8.5 g, yield 96%); ^{1}H NMR (400 MHz, $CDCl_3$), δ (ppm): 7.57 (d, J = 4.7 Hz, 1H), 7.19 (dd, J = 4.6, 3.2 Hz, 1H), 7.12 (d, J = 3.2 Hz, 1H), 1.50 (t, 6H), 1.26 (dd, J = 14.7, 7.4 Hz, 6H), 1.06 – 1.01 (m, 6H), 0.81 (t, J = 7.3 Hz, 9H); ^{13}C NMR (101 MHz, $CDCl_3$), δ(ppm) 136.19, 135.18, 130.58, 127.83, 28.97, 27.27, 13.67, 10.82.

2.2.5. Tributyl(selenophen-2-yl)stannane (5)

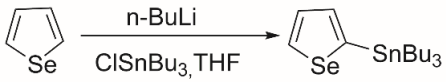

Figure 2.5. Synthesis of Tributyl(selenophen-2-yl)stannane.

Selenophene (2.56 g, 19.54 mmol) was dissolved in 35 mL of freshly distilled THF under an inert atmosphere. The reaction was stirred for a while and flask was placed in a cryostat at -78˚C. n-BuLi (7.42 mL, 18.56 mmol, 2.5 M in hexane) was added drop wise over 6 h and stirred for an additional hour. Tributyltin chloride (7.00 g, 21.49 mmol, 97%) was added slowly over 4 h and stirred further 1 h. The reaction was stirred overnight at room temperature. THF was removed under reduced pressure, and 10 mL distilled water were added to flask and extraction was performed with dichloromethane, sodium bicarbonate ($NaHCO_3$) and brine. The organic residue was dried over $MgSO_4$, and the solvent was evaporated by rotary evaporator. The viscous pale yellow oil was obtained (7.7 g, yield 94%); ^{1}H NMR (400 MHz, $CDCl_3$), δ (ppm): 8.54 (d, J = 4.9 Hz, 1H), 7.76 (d, J = 3.3 Hz, 1H), 7.71 (dd, J = 5.1, 3.4 Hz, 1H), 1.85 (dd, J = 15.1, 7.5 Hz, 6H), 1.65 – 1.58 (m, J = 14.7, 7.3 Hz, 6H), 1.42-1.33 (m, 6H), 1.17 (t, J = 9.4, 5.2 Hz, 9H); ^{13}C NMR (101 MHz, $CDCl_3$), δ(ppm) 143.35, 138.03, 135.45, 130.64, 29.25, 27.54, 13.89, 11.33.

2.2.6. 3-(Bromomethyl)heptane (6)

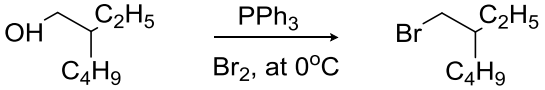

Figure 2.6. Synthesis of 3-(Bromomethyl)heptane.

To a solution of 2-ethylhexan-1-ol (10.00 g, 76.79 mmol) in methylene chloride (DCM) (120 mL), triphenylphosphine (PPh_3) (20.48 g, 78.10 mmol) was added, and the temperature was set to 0 °C in an ice bath. Bromine (11.36 mL, 221.47 mmol) in about 5 mL methylene chloride was added drop wise with pressure equalizing dropping funnel to the reaction mixture at 0 °C and the reaction was stirred overnight at room temperature. The reaction was poured into freshly prepared saturated sodium bisulfite ($NaHSO_3$) solution in water. Extraction was performed with DCM and distilled water several times. The combined organic phase was dried over $MgSO_4$, and the solvent was evaporated under reduced pressure. The obtained product was purified by column chromatography on silica gel using hexane (12.6 g, 85%) to obtain a colorless oil; ^{1}H NMR (400 MHz, $CDCl_3$), δ (ppm): 3.67 – 3.19 (m, 2H), 1.68 – 1.08 (m, 9H), 0.83 (t, J =6.8 Hz, 6H); ^{13}C NMR (101 MHz, $CDCl_3$), δ (ppm): 10.84, 14.02, 22.85, 25.17, 28.83, 31.89, 38.93, 41.04.

2.2.7. 4,7-Dibromo-2-(2- ethylhexyl)-2H-benzo[d][1,2,3]triazole (7)

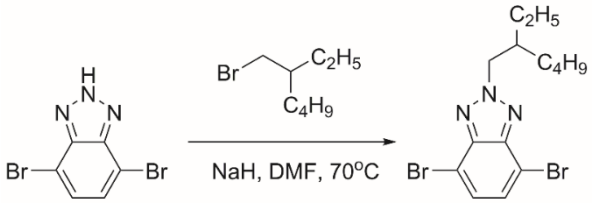

Figure 2.7. Synthesis of 4,7-Dibromo-2-(2- ethylhexyl)-2H-benzo[d][1,2,3]triazole.

Nitrogen purged a two neck round bottom flask was filled with compound **3** (3.00 g, 10.83 mmol) and 20 mL anhydrous dimethylformamide (DMF) at 0 °C. Sodium hydride (NaH) (317 mg, 13.2 mmol, 60% in oil) was added, and the reaction was stirred for 1 h, and then the temperature was raised to 70°C. Now, Compound **6** (2.5 g, 12.97 mmol) was added to the reaction flask and stirred overnight. The crude product was washed four times with chloroform and distilled water. The organic phase was dried with a drying agent ($MgSO_4$). For further purification, column chromatography on silica gel with hexane:ethylacetate (1:1) was performed and desired compound was obtained as a viscous yellow oil (2.0 g, yield 59%); ^{1}H NMR

(400 MHz, $CDCl_3$), δ (ppm): 7.41 (s, 2H), 4.67 (d, J= 7.3 Hz, 2H), 2.29 (m, 1H), 1.41-1.20 (m, 9H), 0.91-0.80 (m, 6H); ^{13}C NMR (101 MHz, $CDCl_3$), δ (ppm): 143.5, 129.18, 109.82, 61.02, 40.23, 30.29, 28.11, 23.74, 22.91, 13.79, 10.33.

2.2.8. 2-(2-Ethylhexyl)-4,7-di(thiophene-2-yl)-2H-benzo[d][1,2,3]triazole (8)

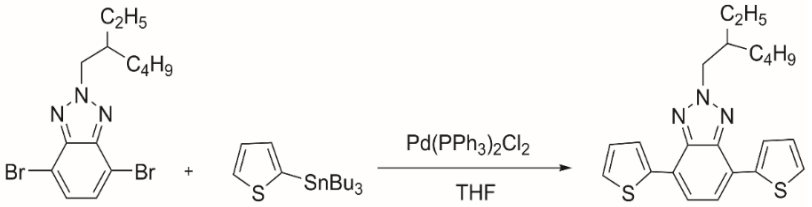

Figure 2.8. Synthesis of 2-(2-ethylhexyl)-4,7-di(thiophen-2-yl)-2H-benzo[d][1,2,3]triazole.

7 (1.11 g, 2.84 mmol) and **4** (3.18 g, 8.52 mmol) were put in a 250 mL two neck round bottom flask under nitrogen atmosphere. Dry THF was added, and bubbling was performed for 45 minutes. Bis(triphenylphosphine)palladium(II) dichloride ($Pd(PPh_3)_2Cl_2$) (99.5 mg, 5 mol%) was added to the reaction media immediately and temperature was raised to 80 °C. The reaction was stirred for 5 h, and an additional 5 mol% catalyst was added to the flask and stirred overnight. The reaction was monitored by thin layer chromatography, and water was added to quench the reaction. Extraction was performed with chloroform and brine. The resulting residue was dried over $MgSO_4$ and chloroform was removed under reduced pressure. Further purification was done with column chromatography (hexane: ethyl acetate) (2:1). The final product was a yellow solid (870 mg, yield 78 %); ^1H NMR (400 MHz, $CDCl_3$) δ (ppm): 8.12 (dd, J = 3.7, 1.0 Hz, 2H), 7.63 (s, 2H), 7.39 (dd, J = 5.1, 1.0 Hz, 2H), 7.20 (dd, J = 5.1, 3.7 Hz, 2H), 4.76 (d, J = 6.7 Hz, 2H), 2.32 – 2.23 (m, 1H), 1.45-1.28 (m, 8H), 1.00 (t, J = 7.4 Hz, 3H), 0.91 (t, J = 7.2 Hz, 3H); ^{13}C NMR (101 MHz, $CDCl_3$) δ (ppm): 142.02, 140.05, 128.09, 126.96, 125.53, 123.58, 122.66, 59.72, 40.46, 30.62, 28.51, 24.02, 22.97, 14.08, 10.59.

2.2.9. 2-(2-Ethylhexyl)-4,7-di(selenophene-2-yl)-2H-benzo[d][1,2,3] triazole (9)

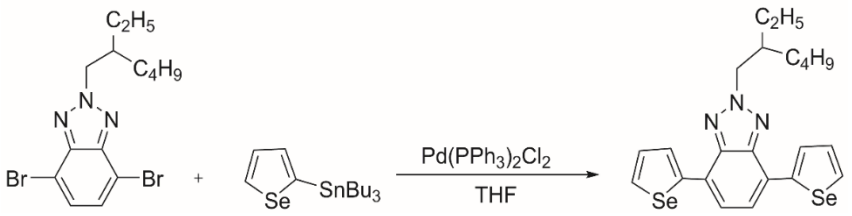

Figure 2.9. Synthesis of 2-(2-ethylhexyl)-4,7-di(selenophen-2-yl)-2H-benzo[d][1,2,3] triazole.

A 100 mL round bottom flask was filled with **7** (700 mg, 1.8 mmol) and **5** (3.02 g, 7.20 mmol) under nitrogen atmosphere in THF. The reaction was stirred for 30 min. $Pd(PPh_3)_2Cl_2$ (63 mg, 5 mol %) was added as a catalyst, and the temperature was raised to 80 °C. The reaction was stirred for 4 h, and an additional 5 mol% catalyst was introduced to the flask and stirred overnight at reflux temperature. The reaction was monitored by thin layer chromatography, and the reaction mixture was poured into water. Extraction was performed with chloroform and brine. The resulting residue was dried over $MgSO_4$, and the solvent was removed under reduced pressure. Further purification was done with column chromatography (hexane: ethyl acetate) (5:1). The final product was a yellow solid (650 mg, yield 74 %); ^{1}H NMR (400 MHz, $CDCl_3$), δ (ppm): 8.20 (dd, J = 3.8, 0.8 Hz, 2H), 8.09 (dd, J = 5.6, 0.8 Hz, 2H), 7.61 (s, 2H), 7.43 (dd, J = 5.6, 3.9 Hz, 2H), 4.76 (d, J = 6.6 Hz, 2H), 2.34 – 2.19 (m, 1H), 1.47 – 1.29 (m, 8H), 1.02 (t, J = 7.4 Hz, 3H), 0.92 (t, J = 7.2 Hz, 3H); ^{13}C NMR (101 MHz, $CDCl_3$) δ 145.19, 141.85, 131.50, 130.46, 128.07, 125.41, 122.84, 59.56, 40.50, 30.68, 28.57, 24.07, 22.97, 14.10, 10.65.

2.2.10. 4,7-Bis (5-bromothiophen-2-yl)- 2- (2-ethylhexyl)- 2H benzo[d] [1,2,3] triazole (10, M1)

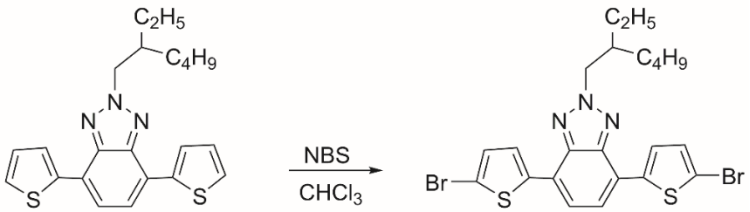

Figure 2.10. Synthesis of 4,7-bis(5-bromothiophen-2-yl)-2-(2-ethylhexyl)-2H-benzo[d][1,2,3]triazole.

8 (500 mg, 1.26 mmol) was dissolved in 50 mL chloroform, and the reaction flask was covered with aluminum foil to protect the reactants from light. *N*- bromosuccinimide (NBS) (562.41 mg, 3.16 mmol) was added in several portions over 6 h, and the reaction was stirred overnight at 30 °C. Extraction was done with chloroform-water for three times, and then he combined organic phase was dried over $MgSO_4$. The crude product was purified by recrystallization from ethanol three times, and obtained crystals were loaded to silica gel column chromatography, using chloroform as the eluent. The desired pure product was collected as a yellow solid (590 mg, yield 84%); ^{1}H NMR (400 MHz, $CDCl_3$) δ (ppm): 7.77 (d, J = 3.9 Hz, 2H), 7.46 (s, 2H), 7.11 (d, J = 3.9 Hz, 2H), 4.72 (d, J = 6.7 Hz, 2H), 2.32 – 2.19 (m, 1H), 1.47 – 1.26 (m, 8H), 0.98 (t, J = 7.4 Hz, 3H), 0.91 (t, J = 7.2 Hz, 3H). ^{13}C NMR (101 MHz, $CDCl_3$) δ 141.61, 141.30, 130.87, 126.90, 122.95, 122.08, 113.18, 59.77, 40.46, 30.59, 28.46, 24.01, 22.98, 14.08, 10.59.

2.2.11. 4,7-Bis(5-bromoselenophen-2-yl)-2-(2-ethylhexyl)-2H-benzo[d][1,2,3] triazole(11, M2)

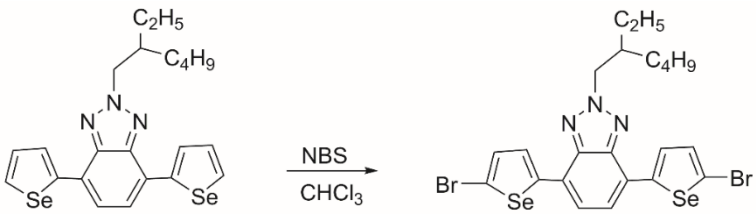

Figure 2.11. Synthesis of 4,7-bis(5-bromoselenophen-2-yl)-2-(2-ethylhexyl)-2H-benzo[d][1,2,3]triazole.

9 (500 mg, 1.02 mmol) was dissolved in 50 mL chloroform, and the reaction flask was protected from light with aluminum foil. *N*- bromosuccinimide (NBS) (454 mg, 2.55 mmol) was added in small portions over 5 h. The reaction was stirred overnight. The crude product was extracted with chloroform-water, and the combined organic phase was dried over $MgSO_4$. The crude product was purified by recrystallization from ethanol two times and then obtained crystals were loaded to silica gel column chromatography, using 10:0.1 petroleum ether, dichloromethane as the eluent couple. The pure product was collected as a yellow solid (550 mg, yield 83%); ^{1}H NMR (400 MHz, CDCl3) δ (ppm): 7.76 (d, J = 4.2 Hz, 2H), 7.49 (s, 2H), 7.32 (d, J = 4.2 Hz, 2H), 4.71 (d, J = 6.5 Hz, 2H), 2.27 – 2.16 (m, J = 10.6, 5.4 Hz, 1H), 1.42 – 1.30 (m, J = 23.2, 13.3, 6.9 Hz, 8H), 1.00 (t, J = 7.4 Hz, 3H), 0.91 (t, J = 7.2 Hz, 3H); ^{13}C NMR (101 MHz, CDCl3) δ 146.46, 141.55, 133.60, 127.10, 124.75, 121.64, 117.73, 77.35, 77.03, 76.71, 59.62, 40.51, 30.68, 28.54, 24.05, 22.98, 14.10, 10.65.

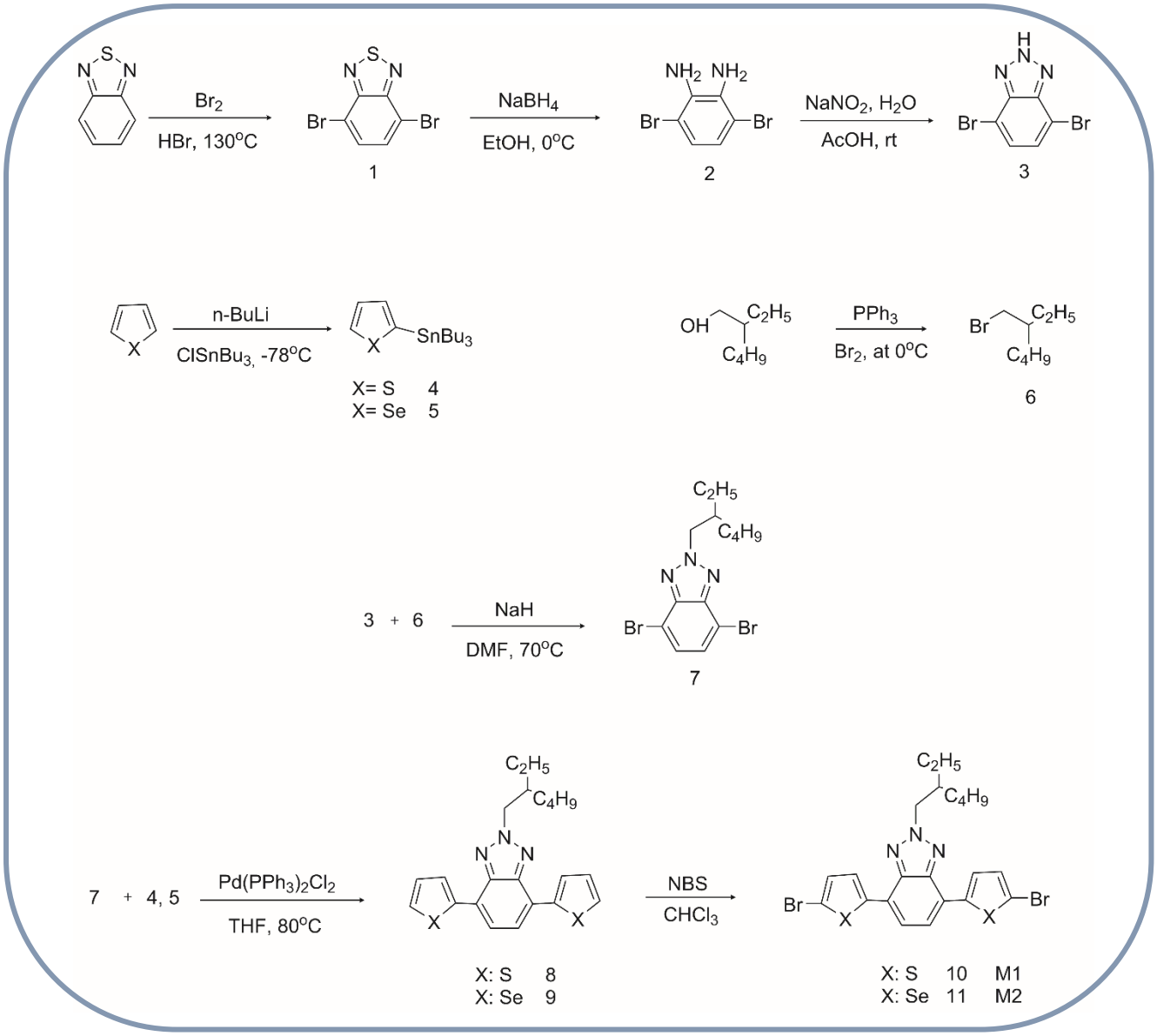

Scheme 2.1. Synthetic routes and chemical structures of the monomers

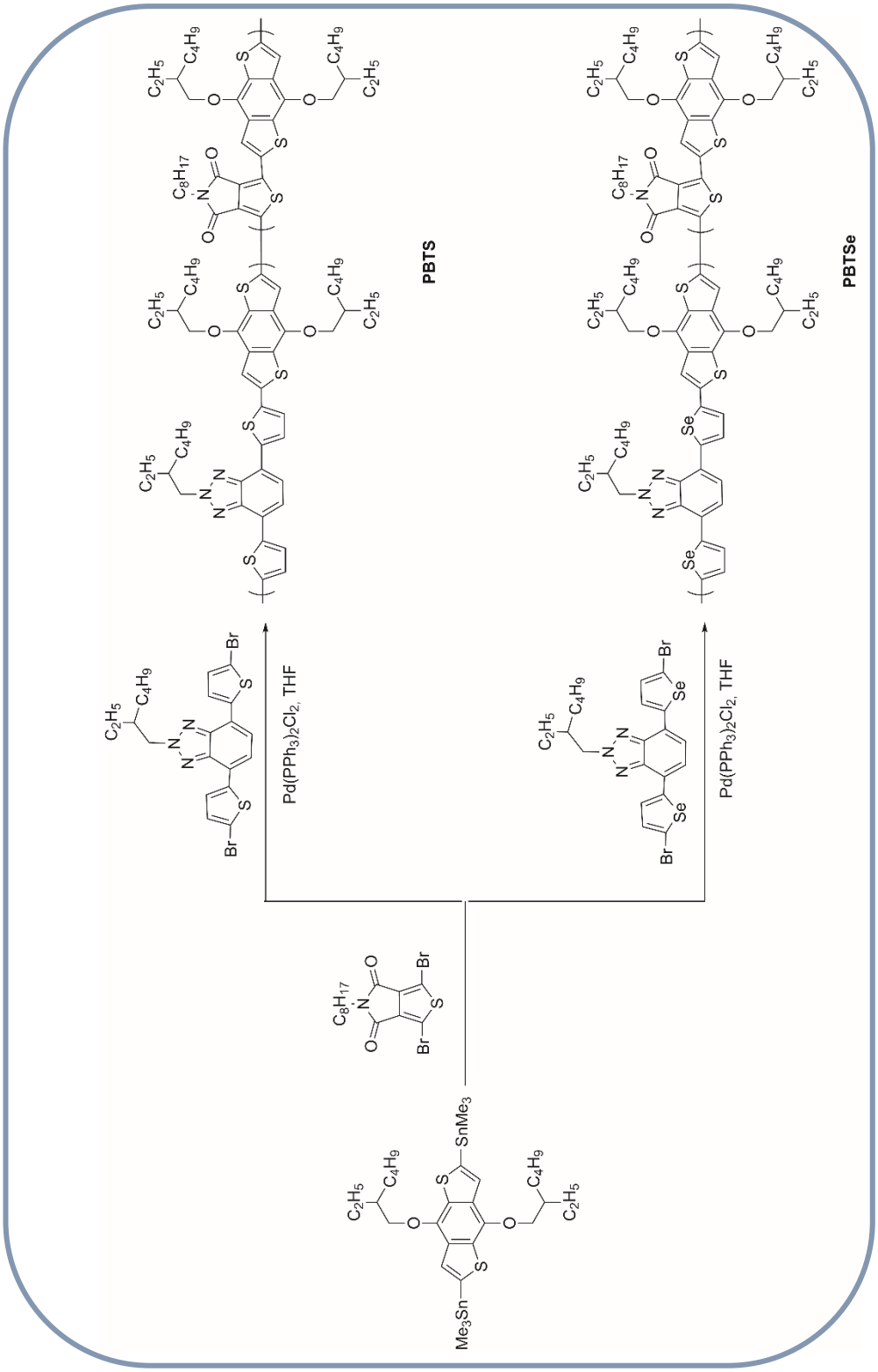

Scheme 2.2. Synthetic routes and chemical structures of the polymers.

2.3. Synthesis of Polymers

2.3.1. Synthesis of PBTS

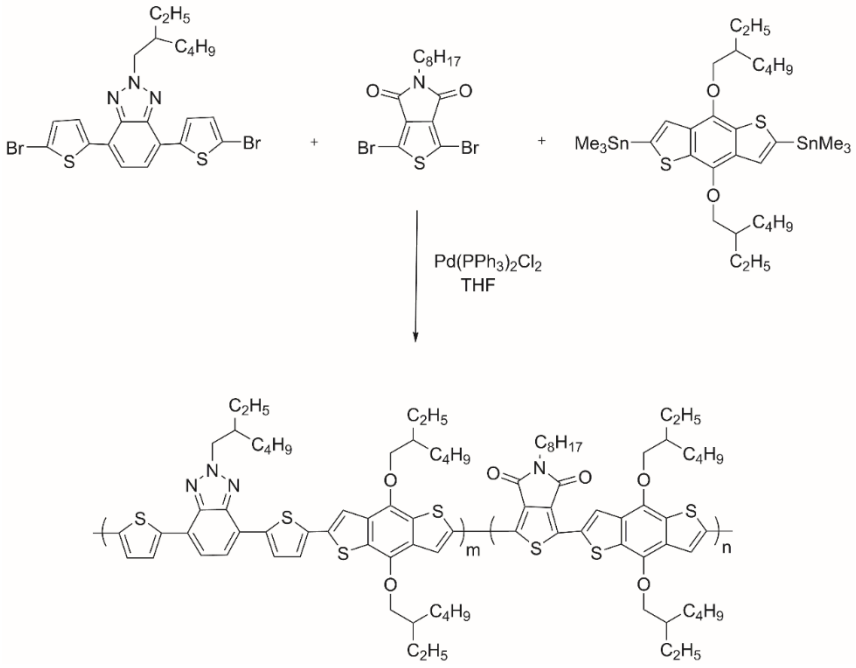

Figure 2.12. Synthetic Pathway for **PBTS**.

A 100 mL of two-necked flask was filled with 4,7-bis(5-bromothiophen-2-yl)-2-(2-ethylhexyl)-2H-benzo[d][1,2,3]triazole (167 mg, 0.29 mmol), 1,3-dibromo-5-octyl-4H-thieno[3,4-c]pyrrole-4,6(5H)-dione (128 mg, 0.29 mmol) and 4,8-bis((2-ethylhexyl)oxy)benzo[1,2-b:4,5-b']dithiophene-2,6 diyl)bis(trimethylstannane) (467 mg, 0.58 mmol) under nitrogen purged atmosphere. Freshly distilled THF was added, and bubbling was performed for 45 minutes. Bis(triphenylphosphine)palladium(II) dichloride ($Pd(PPh_3)_2Cl_2$) (21 mg, 10 mol %) was added to the reaction and temperature raised to 85˚C. The reaction mixture was stirred for 40 hours at the same temperature. Then, bis(triphenylphosphine)palladium(II) dichloride ($Pd(PPh_3)_2Cl_2$) (6.4 mg, 3 mol %) was introduced additionally. The first end capper, 2-bromothiophene, (147 mg, 0.96 mmol) was added. After 4 hours stirring, the second end-capper which is 2-tributylstanylthiophene (676 mg, 1.8 mmol) was added. The reaction mixture was stirred for an additional 6 hours. The solvent was evaporated

under reduced pressure. The residue was dissolved in a minimum amount of $CHCl_3$ and precipitated into cold methanol. Later, Soxhlet was used for polymer purification by using acetone (4 hours) and hexane (12 hours), respectively, to remove dimer, trimer and other oligomers. The polymer was collected with chloroform. Then, the solvent was removed and the remnant was precipitated in cold methanol as dark purple solid beans and filtered to obtain the pure polymer. (410 mg, yield 88%) GPC data were reported as: Number-average molecular weight (M_n) = 24 kDa, Weight-Average molecular weight (M_w) = 36 kDa. Polydispersity index (PDI) = 1.5.

2.3.2. Synthesis of PBTSe

A 100 mL of two-necked flask was filled with 4,7-bis(5-bromoselenophen-2-yl)-2-(2-ethylhexyl)-2H-benzo[d][1,2,3]triazole (150 mg, 0.23 mmol), 1,3-dibromo-5-octyl-4H-thieno[3,4-c]pyrrole-4,6(5H)-dione (98.08 mg, 0.23 mmol) and 4,8-bis((2-ethylhexyl)oxy)benzo[1,2-b:4,5-b']dithiophene-2,6 diyl)bis(trimethylstannane) (358 mg, 0.46 mmol) under nitrogen purged atmosphere and dissolved in dry THF was Bubbling was performed for 45 minutes before adding bis(triphenylphosphine)palladium(II) dichloride ($Pd(PPh_3)_2Cl_2$) (16 mg, 10 mol %). Then, the temperature raised to 85˚C. The reaction mixture was stirred for 40 hours at this temperature. Additional bis(triphenylphosphine) palladium(II) dichloride ($Pd(PPh_3)_2Cl_2$) (5.0 mg, 3 mol %) was introduced to the reaction. The first end capper, 2-bromothiophene (112 mg, 0.69 mmol) was added. After 4 hours stirring, the second end-capper which is 2-tributylstanylthiophene (515 mg, 1.38 mmol) was added. The reaction mixture was stirred for additional 6 hours. The solvent was evaporated under reduced pressure. The residue was dissolved in a minimum amount of $CHCl_3$ and precipitated into cold methanol. Later, Soxhlet thimble was used for polymer purification by using acetone (4 hours) and hexane (12 hours), respectively, to get rid of dimer, trimer and other oligomers. The polymer was collected with chloroform. Then, the solvent was removed and precipitated out in cold methanol as dark purple solids. (350 mg, yield 89 %) GPC data were reported as: Number-average molecular

weight (M_n) = 18 kDa, Weight-Average molecular weight (M_w) = 28 kDa. Polydispersity index (PDI) = 1.55.

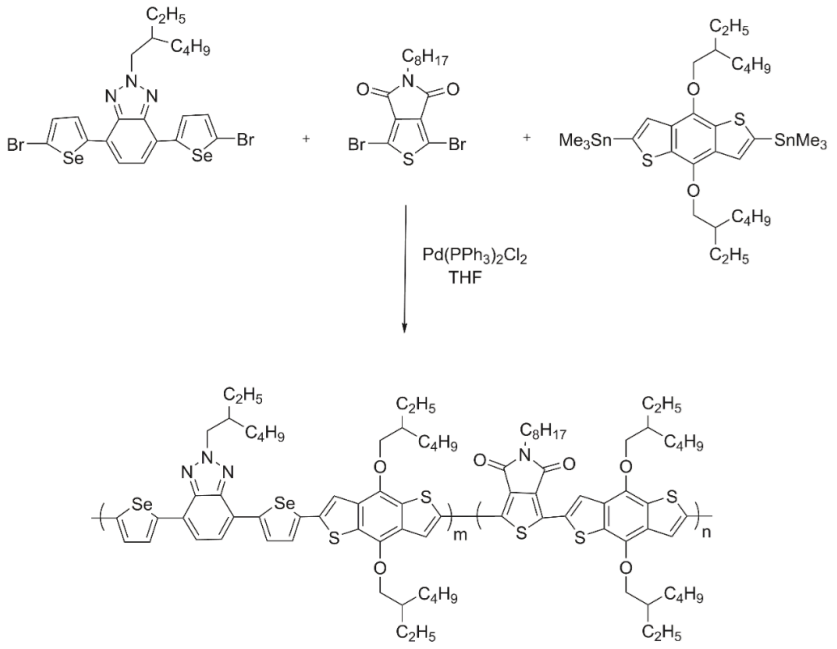

Figure 2.13. Synthetic Pathway for **PBTSe**.

2.4. Characterization of Conducting Polymers

2.4.1. Gel Permeation Chromatography

Gel-permeation chromatography (GPC) is one of the most applied techniques for determination of molecular weight distribution of polymer materials. It is an easy way of obtaining qualitative chromatogram with simple equipment set-up. In this technique, polymers were dissolved in chloroform (2.0 mg/mL), and number-average molecular weights and weight-average molecular weights were obtained from the chromatogram. Heterogeneity index or polydispersity index were calculated from the ratio of weight-average molecular weight to number-average molecular weight.

2.4.2. Thermal Analysis

Thermal analysis (TA) refers to the techniques that find out the properties of materials with a change in temperature [88].

The thermogravimetry analysis (TGA) gives information about weight changes (gain or loss) concerning changes in temperature. Thermal stability of materials is observed, and percent weight loss at decomposition temperature (T_d) was detected for both PBTS and PBTSe terpolymers during the measurements with Perkin Elmer Pyris 1 TGA instrument[89].

Differential Scanning Calorimetry, or DSC, is another technique for thermal analysis. By heating or cooling, heat capacity change is measured with heat flow change. This technique is utilized for the detection of glass transition temperature (T_g) and melting point (T_m) for polymers[89,90].

2.4.3. Electrochemical Studies

Electrochemical studies are used in order to explore the electrochemical behaviors of semiconducting conjugated polymers. A counter electrode (CE), a working electrode (WE) and a reference electrode (RE) are used in the potentiostat. The potential changes are recorded against by the use of working electrode (WE), and the potential difference is investigated between reference and the working electrodes.

Cyclic voltammetry is a commonly used method for many applications. Suitable materials are chosen for the photoactive layer of the device where photoabsorption, exciton generation, migration, and separation occur[91]. Cyclic voltammetry is one of the useful technique for estimating the energy band diagram[92–94]. The required energy for the oxidation process is shown by HOMO and the energy needed for the reduction process is represented by LUMO[94]. Therefore, redox potentials is explored by this technique from oxidation and reduction potentials. Ferrocene is commonly used as the reference in order to get HOMO and LUMO energy levels with the value of -4.75 eV. The given equations (2, 3)[95] are employed for HOMO/LUMO energy level calculations:

$$\boldsymbol{E_{HOMO}(eV) = -(4.75 + E_{oxidation,\,onset})} \qquad \textbf{(Eq.2)}$$

$$\boldsymbol{E_{LUMO}(eV) = -(4.75 + E_{reduction,\,onset})} \qquad \textbf{(Eq.3)}$$

2.4.4. Spectroelectrochemical Studies

Under UV-Visible radiation, the energy is corresponded by the electronic state energy levels in organic molecules. Absorption of energy in the molecule occurs, and this energy is carried by electromagnetic radiation at resonance where an electron can move to higher molecular orbital from lower energy molecular orbital[96]. At this point, UV-Vis spectrophotometer is applied to observe these transitions. Optical band gap identifies the energy of exciton absorption band at the long wavelength side[97] and the onset of longest absorption wavelength (λ_{onset}) is taken for calculation of E_g^{opt}:

$$E_g^{op} = \frac{1241}{\lambda onset} \qquad \textbf{(Eq.4)}$$

2.4.5. Kinetic Studies

It is approved that 95% full contrast is the maxima for the human eye. The switching times are found via Chronoamperometric studies. Further, the kinetic studies is an applied technique in order to determine transmittance change within proper time intervals between two states which are fully oxidized state and neutral states of organic materials at a maximum absorption wavelength of conjugated compounds. The optical contrast is investigated by UV-Vis-NIR spectrophotometer measurements.

2.4.6. Photovoltaic Studies

The construction of a BHJ OSCs is layered as following: ITO/ PEDOT: PSS/ Polymer: $PC_{71}BM$/ LiF/ Al. First, toluene, detergent water, distilled water, acetone, and isopropyl alcohol is generally used in an ultrasonic bath for cleaning of a glass substrate coated with indium-tin oxide (ITO). The oxygen plasma is applied for a further cleaning process. The evaporation of solvents on ITO coated glass is achieved on a hot plate for 15 minutes. Then, poly (ethylenedioxy thiophene): polystyrene sulfonate (PEDOT: PSS from Clevious P VP Al 4083) is spin coated on ITO-glass and let dry on a hot plate for further 15 minutes. Polymer and $PC_{71}BM$ blend ratios are prepared, filtered and spin coated in a glove-box system under an inert atmosphere.

Lithium fluoride and Al are layered by the thermal deposition technique. All device measurements based on current density-voltage (*J*-*V*) are performed under AM 1.5G illumination with Keithley 2400 source meter. Incident-photon-to-current efficiency (IPCE) is used in order to support studies and to control current values matching by a kit of Oriel Quantum Efficiency Measurement.

CHAPTER 3

RESULTS & DISCUSSION

3.1. Electrochemical Studies

Electrochemical characterizations of **PBTS** and **PBTSe** were performed with cyclic voltammetry (CV) techniques to investigate both redox behaviors and HOMO–LUMO energy levels of polymers by using Gamry Instrument Potentiostat/ Galvanostat/ZRA. During measurements, three electrode system was used in 0.1 M tetrabutylammonium hexafluorophosphate ($TBAPF_6$)/ acetonitrile (ACN) electrolyte/solvent couple. For CV characterizations, spray-coated thin films on ITO slides were prepared from the polymer/$CHCl_3$ solutions (5 mg/mL). Cyclic voltammograms (as depicted in *Figure 3.1.*) were recorded in the potential range between -2.0 V and 1.5 V for **PBTS** and between -2.0 V and 1.3 V for **PBTSe** at a scan rate of 100 mV/s. As reported in Table 3.1, **PBTSe** exhibited lower redox potentials at 0.84/1.19 V (p-type doping) and -1.52V /-1.86 V (n-type doping) compared to those of **PBTS** at 0.93 V/1.28V (p-type doping) and -1.77 (n-type doping) which can be attributed to the electron-rich character of selenophene units in the **PBTSe** polymer backbone. Moreover, Se is more polarizable than S. The usage of heavier chalcogens is a way to reduce the oxidation potentials, and as result of this, better electrochemical and optical properties can be tuned[98,99].

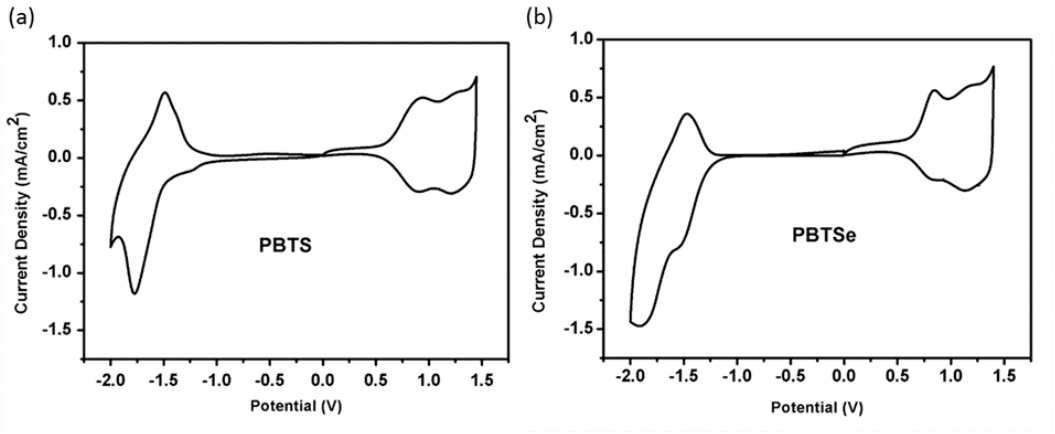

Figure 3.1. Single scan cyclic voltammograms of **PBTS** (a) and **PBTSe** (b) in 0.1 M TBAPF6/ACN electrolyte solution.

In *Figure 3.1.*, both polymers exhibited ambipolar characters; in other words, they have both p and n-type doping behaviors. HOMO and LUMO energy levels of conducting polymers are crucial to test their usability in different applications, especially OPV applications, and can be calculated from CV results. HOMO and LUMO energy levels of **PBTS** and **PBTSe** were calculated from the onset of the oxidation/reduction potentials of the p-doping/n-doping states as -5.29 eV/ 3.30 eV and -5.36 eV/ -3.50 eV, respectively.

Following equations were used for HOMO/LUMO energy level calculations according to reference energy level of ferrocene/ferrocenium redox couple (4.75 eV below the vacuum level).

$$E_{HOMO}(eV) = -(4.75 + E_{oxidation,\,onset}) \qquad \textbf{(Eq.5)}$$

$$E_{LUMO}(eV) = -(4.75 + E_{reduction,\,onset}) \qquad \textbf{(Eq.6)}$$

All the electrochemical results are summarized in Table 3.1. The lower redox potentials of Se comprising **PBTSe** can be attributed to the different electron densities on polymer chains. The stronger electron donating ability of selenophene unit increases the electron density in the polymer backbone and enables doping/dedoping process at lower potentials[100].

Table 3.1. *Summary of electrochemical and spectroelectrochemical properties of **PBTS** and **PBTSe***

	$E_{p\text{-doping}}$ (V)	$E_{n\text{-doping}}$ (V)	HOMO (eV)	LUMO (eV)	E_g^{ec} (eV)	λmax (nm)	E_g^{op} (eV)
PBTS	0.93/1.28	-1.77	-5.29	-3.30	1.99	550/591	1.84
PBTSe	0.84/1.19	-1.52/-1.86	-5.36	-3.50	1.86	580	1.78

3.2. Spectroelectrochemical Studies

The electronic and optical changes were explored via spectroelectrochemical studies, where incrementally increasing potentials were applied during UV-Vis spectra recording, for both **PBTS** and **PBTSe.** For spectroelectrochemical studies, polymers were dissolved in $CHCl_3$ as described before and spray-coated on ITO coated glass electrodes, then dipped into 0.1 M $TBAPF_6$ /ACN solutions in order to investigate their absorption characters between a range 0 V and 1.8 V for both polymers.

Before stepwise oxidation, true neutral state absorptions were achieved via constant potential application to remove the trapped charges. As seen in *Figure 3.2*, neutral state absorption bands were recorded at 550 nm and 580 nm for **PBTS** and **PBTSe**, which corresponded to the π-π* inter-band transitions. During the stepwise potential applications, while the corresponding neutral absorptions were depleted, new absorption bands appeared at around 800 nm and 1600 nm. The formation of the new bands at longer wavelengths proves the formation of polaronic and bipolaronic charge carriers on the polymer backbone.

As mentioned earlier, both polymers were designed and synthesized in order to use them in the active layer of bulk heterojunction OPVs. For that reason, their band gaps are critical to increasing the PCEs. The optical band gaps of both polymers were

calculated from the onset absorption wavelengths of the π-π* transitions as 1.84 eV and 1.78 eV, respectively for PBTS and PBTSe. Similar to the electrochemical results, the stronger electron donating ability of selenophene unit compared to that of thiophene group increases the electron density in the polymer chain which resulted in the red shift in the neutral state absorption and lower band gap for Se comprising **PBTSe** (see Table 3.1.).

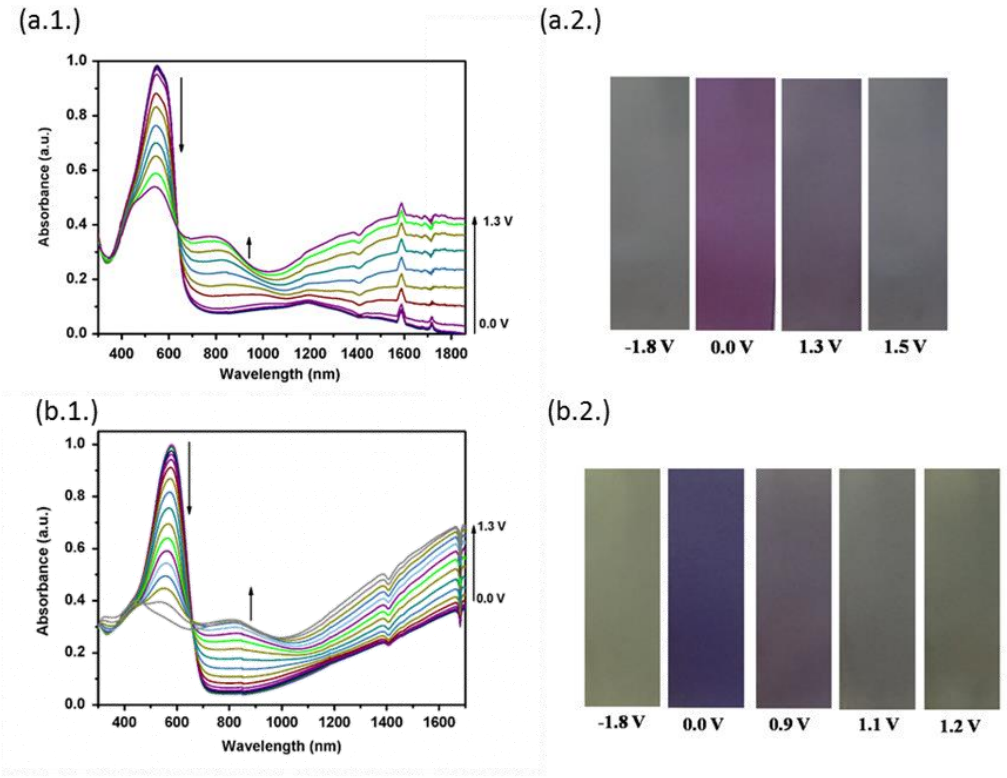

Figure 3.2. Electronic absorption spectra of **PBTS** (a.1.) and **PBTSe** (b.1.) in 0.1 M TBAPF6/ACN electrolyte solution and corresponding colors of **PBTS** (a.2.) and **PBTSe** (b.2.) in the neutral, oxidized and reduced forms.

3.3. Optical and Kinetic Studies

The optical properties of both **PBTS** and **PBTSe** were investigated in a film and as a dilute chloroform solution and the results were depicted in *Figures 3.3.a* and ***3.3.c***. Maximum absorptions in solution and thin film were recorded at 550 nm and 580 nm nm for **PBTS** and 577 nm and 580 nm for **PBTSe**, respectively. **PBTS** exhibited a 10

nm red shift in the thin film, but **PBTSe** showed very similar absorptions in both forms with a 3 nm red shift. The red shifts in the thin films could be dedicated to the more ordered structures of π-conjugated polymers, higher conjugation length and intermolecular polymer chains' interactions[101]. Also, PL emission spectra of **PBTS** and **PBTSe** both in dilute chloroform and film states were shown in *Figures 3.3.b* and *3.3.d*. **PBTS** and **PBTSe** showed large Stoke's shifts of 192 nm and 162 nm, respectively in the film states with electron rich and electron deficient interchain moieties in the copolymers. The interchain exciton transportation is proved by the difference of PL spectra in solution and in the film of **PBTS** and **PBTSe** copolymers. Expectedly, the bathochromic shift is observed for a film with respect to solution by virtue of improved interchain exciton migration in the solid states[102].

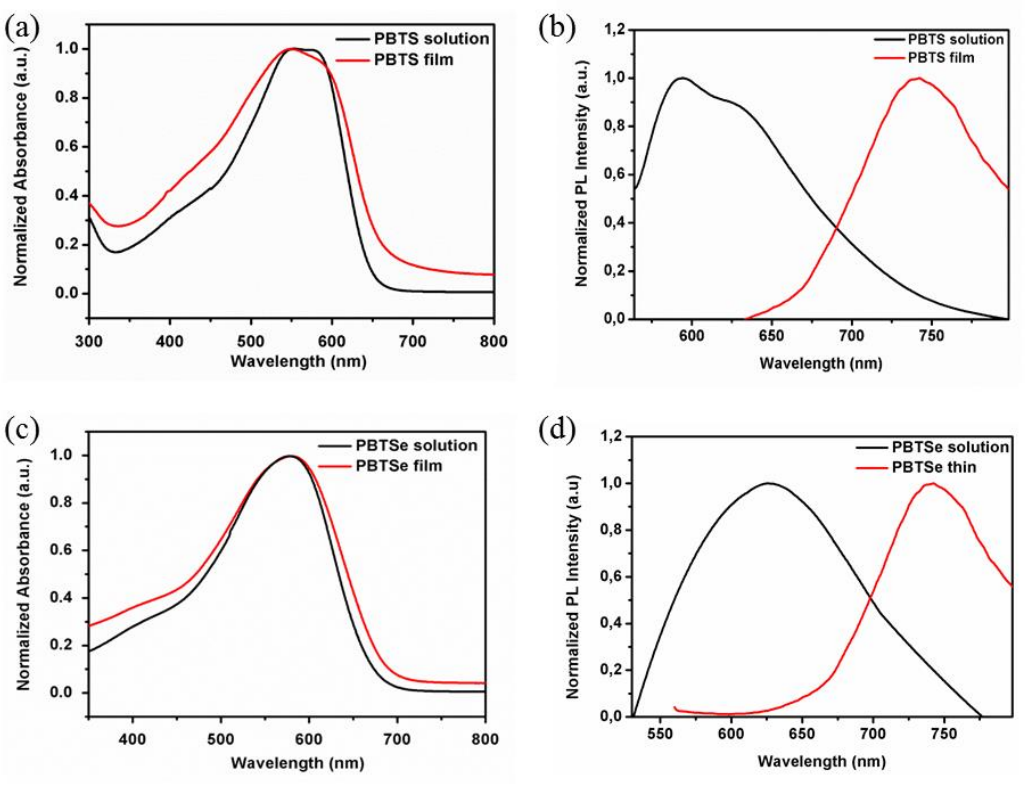

Figure 3.3. Normalized absorption and photoluminescence spectra of polymers in solution (chloroform) and thin film with the polymer structure.

Furthermore, kinetic studies were performed in order to calculate and report the optical contrast and switching time values. The measurements were done at their λ_{max} values from spectroelectrochemical studies between the two extreme states (neutral and fully oxidized states) of the polymers by giving the potential for 5 s. Switching time is the time needed for one full switch between two extreme states, and optical contrast is the transmittance change between those states.

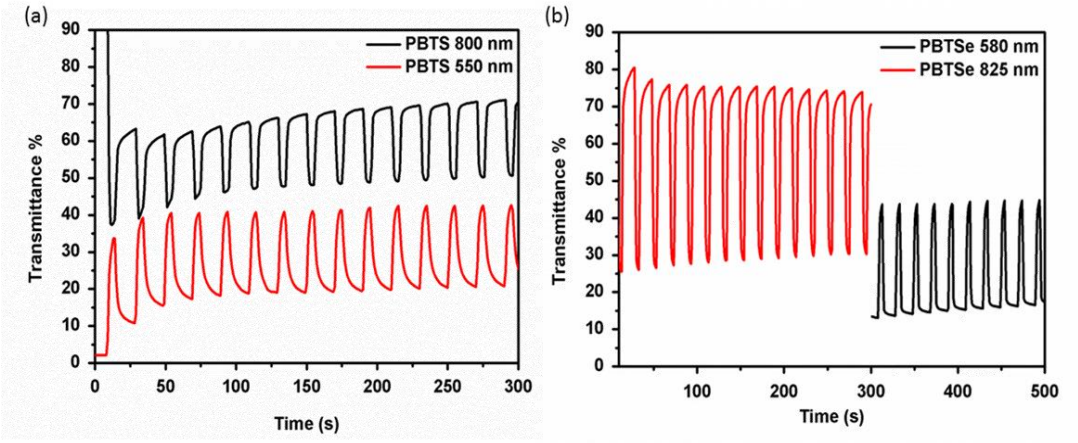

Figure 3.4. Optical transmittance changes of **PBTS** (a) at 550, 800 nm and **PBTSe** (b) at 580, 825 nm in 0.1 M ACN/TBAPF$_6$ solution.

It can be concluded from *Figures 3.4* and Table 3.2; both polymers showed promising optical contrasts and moderate switching times for the corresponding λmax values. The highest optical contrasts recorded for thiophene comprising **PBTS** are 28% at 550 nm, and 23% at 800 nm and those for selenophene based **PBTSe** is 30% at 580 nm, 52% at 825 nm. Corresponding switching times are also illustrated in Table 3.2.

Table 3.2. *Summary of kinetic studies of **PBTS** and **PBTSe***

	Optical contrast (ΔT %)	**Wavelength (nm)**	**Switching times (s)**
PBTS	28	550 nm	3.2
	23	800 nm	4.9
PBTSe	30	580 nm	3.4
	52	825 nm	5.6

3.4. Photovoltaic Studies

The conventional BHJ photovoltaic devices were fabricated with the following structural order; ITO/ PEDOT: PSS/ **PBTS-PBTSe**: PCBM/ LiF/ Al. *Figure 3.5* represents the *J-V* curves for optimization studies of terpolymers under AM 1.5G stimulated solar illumination at 100 mV/cm^2. Optimized open circuit voltage, short circuit current density, fill factor and power conversion efficiency values of PBTS and PBTSe terpolymers are summarized in Table 3.3.

Polymer: $PC_{71}BM$ weight ratios were changed from 1:1 to 1:3 and higher power conversion efficiencies were obtained by replacement of thiophene with selenophene π-spacer in the polymer backbone structure[103,104]. It is an effective strategy for the design of semiconducting polymers where the LUMO energy level can be lower with less affected HOMO due to smaller ionization potential. The results for thiophene and selenophene based BHJ OPVs are depicted in Table 3.1 in various conditions. It can be seen that Se containing polymer **PBTSe** shows higher J_{sc} than S containing **PBTS** analog at 1:1 and 1:2 weight ratios. The higher J_{sc} value in case of PBTSe means a

large number of incoming photons from the solar spectrum can be absorbed in selenophene containing solar cell device[103]. Moreover, the V_{oc} values are directly proportional with the HOMO energy level of donor groups and LUMO energy levels of acceptor groups in the polymer backbone structure. V_{oc} value was 0.66 V for **PBTS** with a 1:2.5 ratio of Polymer: $PC_{71}BM$ and 0.69 V for **PBTSe** with a 1:2 weight ratio of Polymer: $PC_{71}BM$.

Exciton dissociation and charge carriers transport strongly depend on the molecular arrangement of electron donor and electron acceptor groups[41,105]. Adjustment of active morphology can be achieved by using common solvent additives such as 1,8 diiodooctane (DIO), diphenyl ether (DPE) and 1-chloronaphthalene (CN)[26]. In this study, the device performance based on **PBTS** increased from 3.32% to 4.30% at 1:2.5 weight ratio (PBTS: $PC_{71}BM$) by introducing DIO (1%). Another common solvent additive DPE (3%) was added to active layer to obtain better morphology and PCE was increased from 3.19% to 5.15% at 1:2 (PBTSe: $PC_{71}BM$) weight ratio (see Tables 3.3 and 3.4)[26].

Table 3.3. *Photovoltaic Studies Based on* ***PBTS***

	Solvent	V_{oc} **(V)**	J_{sc} **(mA/cm^2)**	**FF (%)**	**PCE (%)**	**Treatment**
PBTS: $PC_{71}BM$						
1:1	*o*-dcb	0.65	6.62	59.7	2.57	-
1:2	*o*-dcb	0.66	8.03	57.9	3.07	-
1:3	*o*-dcb	0.66	7.89	60.6	3.16	-
1:2.5	*o*-dcb	0.66	8.79	57.2	3.32	-
1:2.5	***o*-dcb**	**0.64**	**10.57**	**63.5**	***4.30***	**1% DIO**
1:2.5	*o*-dcb	0.62	11.50	60.1	4.29	3% DPE

Table 3.4. *Photovoltaic Studies Based on* ***PBTSe***

	Solvent	**V_{oc} (V)**	**J_{sc} (mA/cm^2)**	**FF (%)**	**PCE (%)**	**Treatment**
PBTSe: $PC_{71}BM$						
1:1	*o*-dcb	0.67	7.62	57.2	2.92	-
1:2	*o*-dcb	0.69	8.06	57.3	3.19	-
1:3	*o*-dcb	0.69	7.15	58.2	2.87	-
1:2	*o*-dcb	0.66	8.55	52.5	2.96	1% DIO
1:2	***o*-dcb**	**0.69**	**11.88**	**62.7**	***5.15***	**3% DPE**

The device performances using **PBTS** and **PBTSe** were accurate with EQE studies as displayed in *Figures 3.5.b* and *3.5.d*. Broad monochromatic spectrums are presented for both **PBTS** and **PBTSe** containing active layer with and without solvent additives. The spectrum shown in *Figure 3.5.b* gives response from 400 nm to 720 nm with maximum EQE value of almost 70% at 520 nm, while device containing **PBTSe** shows broad spectrum from 400 nm to 720 nm with almost 50% of EQE value at 490 nm[106,107].

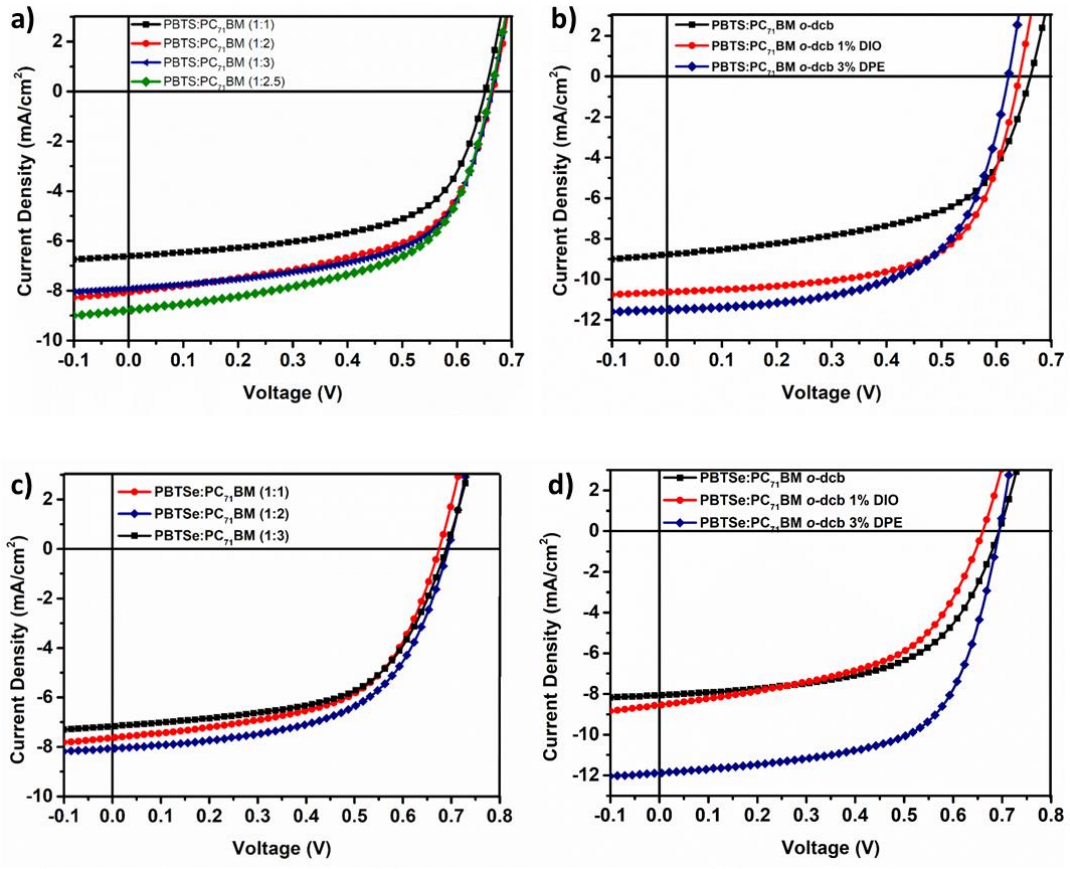

Figure 3.5. J-V characteristic of devices from solar cell simulator of PBTS (a, b) and PBTSe (c, d)

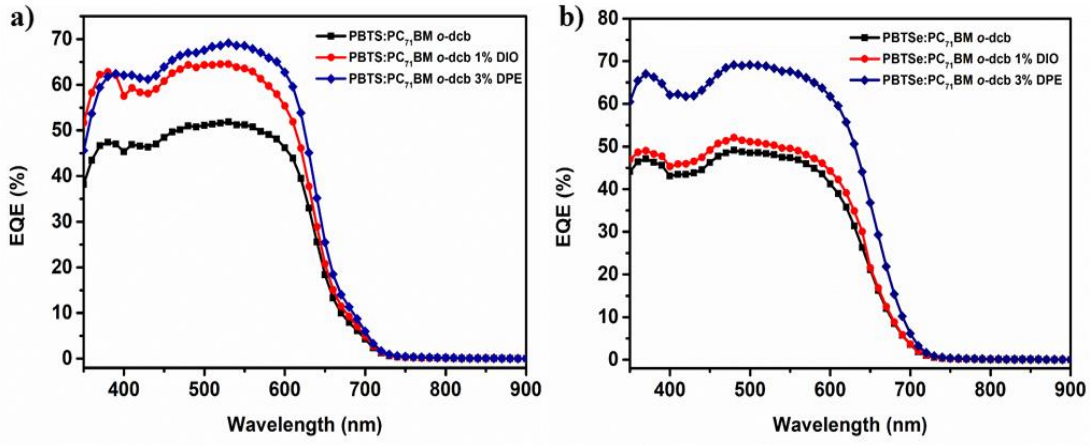

Figure 3.6. EQE curves of PBTS (a) and PBTSe (b)

3.5. Morphology

The bi-continuous charge transport network is required to achieve better performance for devices since domain sizes are essential for excitons (hole-electron pair) to reach the donor-acceptor interface where charge generates[108]. Morphology control is a critical issue for a solar cell with fullerenes because the p-type donor and n-type acceptor materials have close mechanical properties that cause spontaneous phase separation. There are several strategies to obtain uniform nanoscale morphology of the active layer, and one of the simple and effective methods is introducing solvent additive to host solvent. The morphologies of active layers were studied by atomic force microscopy (AFM) and transmission electron microscopy (TEM) (see *Figures 3.7* and *3.8*).

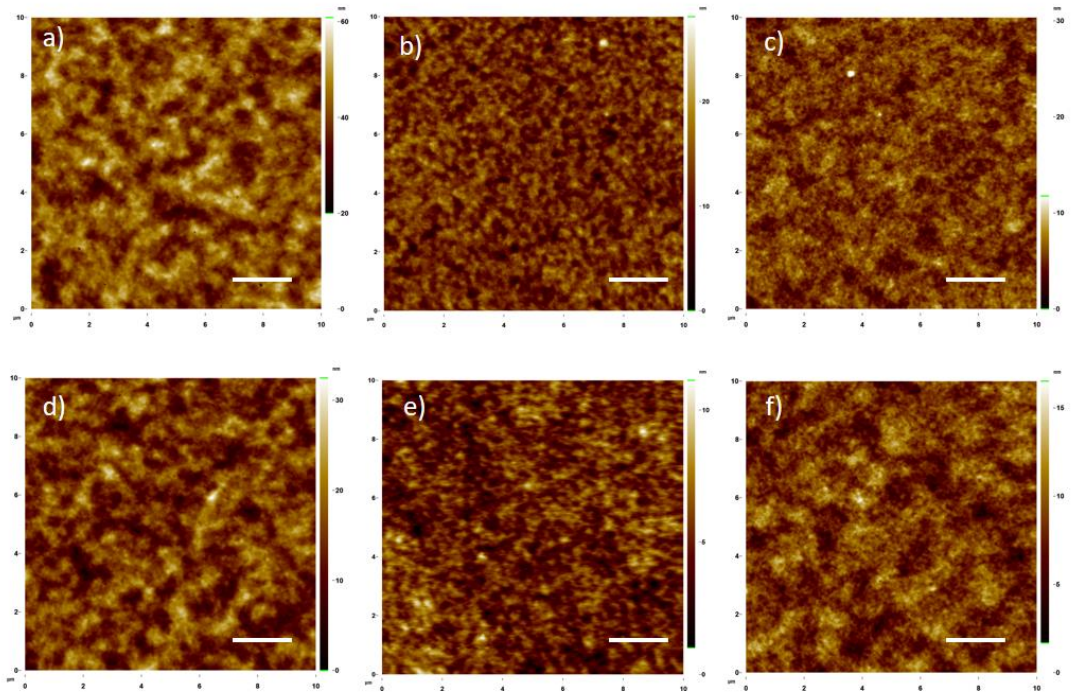

Figure 3.7. AFM images of a) **PBTS**: $PC_{71}BM$ b) **PBTS**: $PC_{71}BM$ with DIO additive c) **PBTS**: $PC_{71}BM$ with DPE additive d) **PBTSe**: $PC_{71}BM$ e) **PBTSe**: $PC_{71}BM$ with DIO additive f) **PBTSe**: $PC_{71}BM$ with DPE additive. Scale bar is 200 nm.

Photoactive layer containing **PBTS**: $PC_{71}BM$ (1:2.5, w/w) was introduced with 1% DIO and uniform surface morphology was obtained as seen in *Figures 3.7b* and *3.7.e*

because DIO can dissolve selectively fullerenes and aggregated $PC_{71}BM$ molecules can intercalate into polymer chain domains[109,110]. Yet, after introducing 3% DPE, PBTSe: $PC_{71}BM$ (1:2, w/w) showed the best performance for the device thanks to better separation of layers. It is known that DPE acts like a theta solvent where polymer chains can behave as ideal and form nano-fibrillar morphology[110]. The homogeneous distribution of **PBTSe** and fullerene can be easily seen from the TEM image shown in *Figure 3.8.f*, after adding DPE. It is seen from AFM and TEM images; pinholes are small enough for exciton dissociation and charge carrier transports.

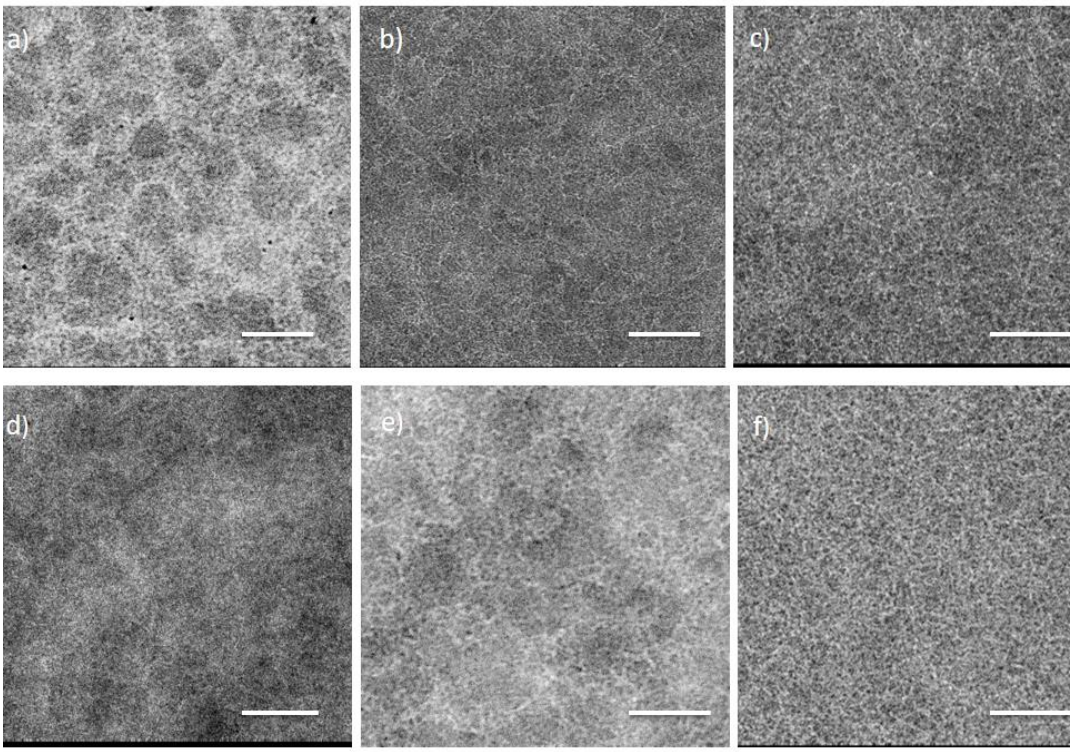

Figure 3.8. TEM micrographs of a) PBTS: $PC_{71}BM$ b) PBTS: $PC_{71}BM$ with DIO additive c) PBTS: $PC_{71}BM$ with DPE additive d) PBTSe: $PC_{71}BM$ e) PBTSe: $PC_{71}BM$ with DIO additive f) PBTSe: $PC_{71}BM$ with DPE additive. Scale bar is 200 nm.

CHAPTER 4

CONCLUSIONS

In the present study, two medium-band gap conjugated terpolymers, **PBTS** and **PBTSe** (containing benzotriazole, benzodithiophene and thienopyrrolodione with altering π-bridges) were synthesized and OSC device fabrications were studied. Synthesized polymers were used as donors and were blended with $PC_{71}BM$. By changing thionephene π bridge by selenophene, performance of devices was improved with increased J_{sc}. Solvent processing additives DIO and DPE with parent *o*-dcb solvent give the best device performances with 1:2.5 and 1:2 weight ratios of **PBTS** and **PBTSe** with $PC_{71}BM$, respectively. Under these observations, introducing π-spacers in π-conjugated polymers, optimizations for polymer: fullerene ratios and using solvent additives can be effective strategies to obtain better performances of organic photovoltaic cells.

REFERENCES

[1] H. Shirakawa, E.J. Louis, A.G. MacDiarmid, C.K. Chiang, A.J. Heeger, Synthesis of electrically conducting organic polymers: halogen derivatives of polyacetylene, (CH) x, J. Chem. Soc. Chem. Commun. (1977) 578. doi:10.1039/c39770000578.

[2] A. Kausar, S.T. Hussain, Effect of multi-walled carbon nanotube reinforcement on the physical properties of poly(thiourea-azo-ether)-based nanocomposites, J. Plast. Film Sheeting. 29 (2013) 365–383. doi:10.1177/8756087913487003.

[3] J.L. Bredas, G.B. Street, Polarons, bipolarons, and solitons in conducting polymers, Acc. Chem. Res. 18 (1985) 309–315. doi:10.1021/ar00118a005.

[4] C. Winder, N.S. Sariciftci, Low bandgap polymers for photon harvesting in bulk heterojunction solar cells, J. Mater. Chem. 14 (2004) 1077. doi:10.1039/b306630d.

[5] A.J. Mozer, N.S. Sariciftci, Conjugated polymer photovoltaic devices and materials, Comptes Rendus Chim. 9 (2006) 568–577. doi:10.1016/j.crci.2005.03.033.

[6] S. Günes, H. Neugebauer, N.S. Sariciftci, Conjugated Polymer-Based Organic Solar Cells, Chem. Rev. 107 (2007) 1324–1338. doi:10.1021/cr050149z.

[7] T. Tadesse, Application of Conjugated Organic Polymers for Photovoltaic's: Review, J. Phys. Chem. Biophys. 08 (2018). doi:10.4172/2161-0398.1000263.

[8] D. Kumar, R.C. Sharma, Advances in conductive polymers, Eur. Polym. J. 34 (1998) 1053–1060. doi:10.1016/S0014-3057(97)00204-8.

[9] J.L. Brédas, J.C. Scott, K. Yakushi, G.B. Street, Polarons and bipolarons in polypyrrole: Evolution of the band structure and optical spectrum upon doing, Phys. Rev. B. 30 (1984) 1023–1025. doi:10.1103/PhysRevB.30.1023.

[10] B. Speiser, Electrochromism. Fundamentals and applications. VonP. M. S. Monk, R. J. Mortimer und D. R. Rosseinsky. VCH Verlagsgesellschaft, Weinheim, 1995. 216 S., geb. 168.00 DM. - ISBN 3-527-29063-X, Angew. Chemie. 108 (1996) 853–854. doi:10.1002/ange.19961080733.

[11] R.J. Mortimer, Electrochromic materials, Chem. Soc. Rev. 26 (1997) 147. doi:10.1039/cs9972600147.

[12] S.K. Deb, A Novel Electrophotographic System, Appl. Opt. 8 (1969) 192. doi:10.1364/AO.8.S1.000192.

[13] M.A. Habib, Electrochromism, in: Electrochem. Transit., Springer US, Boston,

MA, 1992: pp. 51–62. doi:10.1007/978-1-4615-9576-2_4.

[14] C.G. Granqvist, Electrochromic tungsten oxide films: Review of progress 1993-1998, Sol. Energy Mater. Sol. Cells. (2000). doi:10.1016/S0927-0248(99)00088-4.

[15] B.C. Thompson, P. Schottland, K. Zong, J.R. Reynolds, In Situ Colorimetric Analysis of Electrochromic Polymers and Devices, Chem. Mater. 12 (2000) 1563–1571. doi:10.1021/cm000097o.

[16] I. INTERNATIONAL ENERGY AGENCY, World Energy Outlook 2014, OECD, 2014. doi:10.1787/weo-2014-en.

[17] K. Zweibel, The Terawatt Challenge for Thin Film Photovoltaics, in: Thin Film Sol. Cells, John Wiley & Sons, Ltd, Chichester, UK, 2006: pp. 427–462. doi:10.1002/0470091282.ch11.

[18] G. Li, R. Zhu, Y. Yang, Polymer solar cells, Nat. Photonics. 6 (2012) 153–161. doi:10.1038/nphoton.2012.11.

[19] H.A. J., 25th Anniversary Article: Bulk Heterojunction Solar Cells: Understanding the Mechanism of Operation, Adv. Mater. (2013). doi:10.1002/adma.201304373.

[20] C.J. Brabec, M. Heeney, I. McCulloch, J. Nelson, Influence of blend microstructure on bulk heterojunction organic photovoltaic performance, Chem. Soc. Rev. 40 (2011) 1185–1199. doi:10.1039/C0CS00045K.

[21] J. Peng, L. Lu, H. Yang, Review on life cycle assessment of energy payback and greenhouse gas emission of solar photovoltaic systems, Renew. Sustain. Energy Rev. 19 (2013) 255–274. doi:10.1016/j.rser.2012.11.035.

[22] T. Bhattacharya, A.K. Chakraborty, K. Pal, Effects of Ambient Temperature and Wind Speed on Performance of Monocrystalline Solar Photovoltaic Module in Tripura, India, J. Sol. Energy. 2014 (2014) 1–5. doi:10.1155/2014/817078.

[23] V.V. Tyagi, N.A.A. Rahim, N.A. Rahim, J.A.L. Selvaraj, Progress in solar PV technology: Research and achievement, Renew. Sustain. Energy Rev. 20 (2013) 443–461. doi:10.1016/j.rser.2012.09.028.

[24] A. Poullikkas, Implementation of distributed generation technologies in isolated power systems, Renew. Sustain. Energy Rev. (2007). doi:10.1016/j.rser.2006.01.006.

[25] H. Ago, K. Petritsch, M.S.P. Shaffer, A.H. Windle, R.H. Friend, Composites of carbon nanotubes and conjugated polymers for photovoltaic devices, Adv. Mater. (1999). doi:10.1002/(SICI)1521-4095(199910)11:15<1281::AID-ADMA1281>3.0.CO;2-6.

[26] L. Lu, T. Zheng, Q. Wu, A.M. Schneider, D. Zhao, L. Yu, Recent Advances in Bulk Heterojunction Polymer Solar Cells, Chem. Rev. 115 (2015) 12666–12731. doi:10.1021/acs.chemrev.5b00098.

[27] S.E. Shaheen, R. Radspinner, N. Peyghambarian, G.E. Jabbour, Fabrication of bulk heterojunction plastic solar cells by screen printing, Appl. Phys. Lett. 79 (2001) 2996–2998. doi:10.1063/1.1413501.

[28] G. Gustafsson, Y. Cao, G.M. Treacy, F. Klavetter, N. Colaneri, A.J. Heeger, Flexible light-emitting diodes made from soluble conducting polymers, Nature. 357 (1992) 477–479. doi:10.1038/357477a0.

[29] F. Arabpour Roghabadi, V. Ahmadi, K. Oniy Aghmiuni, High coverage solution-processed planar perovskite solar cell grown based on the Stranski–Krastanov mechanism at low temperature and short time, RSC Adv. 6 (2016) 112677–112685. doi:10.1039/C6RA23074A.

[30] E. Ghadiri, N. Taghavinia, S.M. Zakeeruddin, M. Grätzel, J.-E. Moser, Enhanced Electron Collection Efficiency in Dye-Sensitized Solar Cells Based on Nanostructured TiO 2 Hollow Fibers, Nano Lett. 10 (2010) 1632–1638. doi:10.1021/nl904125q.

[31] Ö. Azeri, E. Aktas, C. Istanbulluoglu, S.O. Hacioglu, S.C. Cevher, L. Toppare, A. Cirpan, Efficient benzodithiophene and thienopyrroledione containing random polymers as components for organic solar cells, Polymer (Guildf). 133 (2017) 60–67. doi:10.1016/j.polymer.2017.11.024.

[32] P. Deng, Y. Lei, B. Wu, X. Zheng, Y. Lu, F. Zhu, B.S. Ong, Synthesis, field-effect and photovoltaic properties of random difluorobenzothiadiazole-isoindigo electron donor-acceptor polymers, Dye. Pigment. (2016). doi:10.1016/j.dyepig.2016.07.022.

[33] R. Lampande, G.W. Kim, M.J. Park, B.Y. Kang, J.H. Kwon, Efficient light harvesting in inverted polymer solar cells using polymeric 2D-microstructures, Sol. Energy Mater. Sol. Cells. (2016). doi:10.1016/j.solmat.2016.03.005.

[34] F. Arabpour Roghabadi, N. Ahmadi, V. Ahmadi, A. Di Carlo, K. Oniy Aghmiuni, A. Shokrolahzadeh Tehrani, F.S. Ghoreishi, M. Payandeh, N. Mansour Rezaei Fumani, Bulk heterojunction polymer solar cell and perovskite solar cell: Concepts, materials, current status, and opto-electronic properties, Sol. Energy. 173 (2018) 407–424. doi:10.1016/j.solener.2018.07.058.

[35] S.H. Park, A. Roy, S. Beaupré, S. Cho, N. Coates, J.S. Moon, D. Moses, M. Leclerc, K. Lee, A.J. Heeger, Bulk heterojunction solar cells with internal quantum efficiency approaching 100%, Nat. Photonics. 3 (2009) 297–302. doi:10.1038/nphoton.2009.69.

[36] N.S. Sariciftci, L. Smilowitz, A.J. Heeger, F. Wudl, Semiconducting polymers

(as donors) and buckminsterfullerene (as acceptor): photoinduced electron transfer and heterojunction devices, Synth. Met. 59 (1993) 333–352. doi:10.1016/0379-6779(93)91166-Y.

[37] A. Facchetti, Polymer donor–polymer acceptor (all-polymer) solar cells, Mater. Today. 16 (2013) 123–132. doi:10.1016/j.mattod.2013.04.005.

[38] C. Deibel, V. Dyakonov, C.J. Brabec, Organic bulk-heterojunction solar cells, IEEE J. Sel. Top. Quantum Electron. (2010). doi:10.1109/JSTQE.2010.2048892.

[39] L. Dou, J. You, Z. Hong, Z. Xu, G. Li, R.A. Street, Y. Yang, 25th Anniversary Article: A Decade of Organic/Polymeric Photovoltaic Research, Adv. Mater. 25 (2013) 6642–6671. doi:10.1002/adma.201302563.

[40] A.C. Mayer, S.R. Scully, B.E. Hardin, M.W. Rowell, M.D. McGehee, Polymer-based solar cells, Mater. Today. 10 (2007) 28–33. doi:10.1016/S1369-7021(07)70276-6.

[41] P.W.M. Blom, V.D. Mihailetchi, L.J.A. Koster, D.E. Markov, Device Physics of Polymer:Fullerene Bulk Heterojunction Solar Cells, Adv. Mater. 19 (2007) 1551–1566. doi:10.1002/adma.200601093.

[42] N. Yeh, P. Yeh, Organic solar cells: Their developments and potentials, Renew. Sustain. Energy Rev. 21 (2013) 421–431. doi:10.1016/j.rser.2012.12.046.

[43] C.J. Brabec, C. Winder, N.S. Sariciftci, J.C. Hummelen, A. Dhanabalan, P.A. van Hal, R.A.J. Janssen, A Low-Bandgap Semiconducting Polymer for Photovoltaic Devices and Infrared Emitting Diodes, Adv. Funct. Mater. 12 (2002) 709–712. doi:10.1002/1616-3028(20021016)12:10<709::AID-ADFM709>3.0.CO;2-N.

[44] S. Holliday, Y. Li, C.K. Luscombe, Recent advances in high performance donor-acceptor polymers for organic photovoltaics, Prog. Polym. Sci. 70 (2017) 34–51. doi:10.1016/j.progpolymsci.2017.03.003.

[45] C.M. Proctor, M. Kuik, T.-Q. Nguyen, Charge carrier recombination in organic solar cells, Prog. Polym. Sci. 38 (2013) 1941–1960. doi:10.1016/j.progpolymsci.2013.08.008.

[46] F. Gao, O. Inganäs, Charge generation in polymer–fullerene bulk-heterojunction solar cells, Phys. Chem. Chem. Phys. 16 (2014) 20291–20304. doi:10.1039/C4CP01814A.

[47] D.D.S. Fung, W.C.H. Choy, Introduction to Organic Solar Cells, in: Green Energy Technol., 2013: pp. 1–16. doi:10.1007/978-1-4471-4823-4_1.

[48] M.C. Scharber, N.S. Sariciftci, Efficiency of bulk-heterojunction organic solar cells, Prog. Polym. Sci. (2013). doi:10.1016/j.progpolymsci.2013.05.001.

[49] S. Rafique, S.M. Abdullah, K. Sulaiman, M. Iwamoto, Fundamentals of bulk heterojunction organic solar cells: An overview of stability/degradation issues and strategies for improvement, Renew. Sustain. Energy Rev. 84 (2018) 43–53. doi:10.1016/j.rser.2017.12.008.

[50] S.D. Baranovskii, H. Cordes, F. Hensel, G. Leising, Charge-carrier transport in disordered organic solids, Phys. Rev. B. 62 (2000) 7934–7938. doi:10.1103/PhysRevB.62.7934.

[51] A. Pivrikas, N.S. Sariciftci, G. Juška, R. Österbacka, A review of charge transport and recombination in polymer/fullerene organic solar cells, Prog. Photovoltaics Res. Appl. 15 (2007) 677–696. doi:10.1002/pip.791.

[52] Y. Zhou, M. Eck, M. Krüger, Bulk-heterojunction hybrid solar cells based on colloidal nanocrystals and conjugated polymers, Energy Environ. Sci. 3 (2010) 1851. doi:10.1039/c0ee00143k.

[53] F. Kasten, A.T. Young, Revised optical air mass tables and approximation formula, Appl. Opt. 28 (1989) 4735. doi:10.1364/AO.28.004735.

[54] E. BUNDGAARD, F. KREBS, Low band gap polymers for organic photovoltaics, Sol. Energy Mater. Sol. Cells. 91 (2007) 954–985. doi:10.1016/j.solmat.2007.01.015.

[55] F. Zhang, K.G. Jespersen, C. Björström, M. Svensson, M.R. Andersson, V. Sundström, K. Magnusson, E. Moons, A. Yartsev, O. Inganäs, Influence of Solvent Mixing on the Morphology and Performance of Solar Cells Based on Polyfluorene Copolymer/Fullerene Blends, Adv. Funct. Mater. 16 (2006) 667–674. doi:10.1002/adfm.200500339.

[56] M.-H. Chen, J. Hou, Z. Hong, G. Yang, S. Sista, L.-M. Chen, Y. Yang, Efficient Polymer Solar Cells with Thin Active Layers Based on Alternating Polyfluorene Copolymer/Fullerene Bulk Heterojunctions, Adv. Mater. 21 (2009) 4238–4242. doi:10.1002/adma.200900510.

[57] V.D. Mihailetchi, P.W.M. Blom, J.C. Hummelen, M.T. Rispens, Cathode dependence of the open-circuit voltage of polymer:fullerene bulk heterojunction solar cells, J. Appl. Phys. 94 (2003) 6849–6854. doi:10.1063/1.1620683.

[58] B. Qi, J. Wang, Fill factor in organic solar cells, Phys. Chem. Chem. Phys. (2013). doi:10.1039/c3cp51383a.

[59] V.A. Trukhanov, V. V. Bruevich, D.Y. Paraschuk, Fill factor in organic solar cells can exceed the Shockley-Queisser limit, Sci. Rep. (2015). doi:10.1038/srep11478.

[60] Q.T. Zhang, J.M. Tour, Low Optical Bandgap Polythiophenes by an Alternating Donor/Acceptor Repeat Unit Strategy, J. Am. Chem. Soc. 119

(1997) 5065–5066. doi:10.1021/ja9640399.

[61] S.-M. Bang, J. Park, S. Kang, Y.-S. Lee, B. Lim, H. Heo, J. Lee, Y. Lee, S.-I. Na, Thienopyrroledione and benzodithiophene/thiophene-based random terpolymer for polymer solar cells with improved fill factor, Dye. Pigment. 140 (2017) 229–235. doi:10.1016/j.dyepig.2017.01.049.

[62] P. Berrouard, S. Dufresne, A. Pron, J. Veilleux, M. Leclerc, Low-Cost Synthesis and Physical Characterization of Thieno[3,4- c]pyrrole-4,6-dione-Based Polymers, J. Org. Chem. 77 (2012) 8167–8173. doi:10.1021/jo301512e.

[63] B.A. Alqurashy, A. Iraqi, Y. Zhang, D.G. Lidzey, Preparation and photovoltaic properties of pyrene-thieno[3,4-c]pyrrole-4,6-dione-based donor-acceptor polymers, Eur. Polym. J. 85 (2016) 225–235. doi:10.1016/j.eurpolymj.2016.10.018.

[64] A. Tanimoto, T. Yamamoto, Synthesis of n-Type Poly(benzotriazole)s Having p-Conducting and Polymerizable Carbazole Pendants, Macromolecules. 39 (2006) 3546–3552. doi:10.1021/ma052688b.

[65] H. Yao, L. Ye, H. Zhang, S. Li, S. Zhang, J. Hou, Molecular Design of Benzodithiophene-Based Organic Photovoltaic Materials, Chem. Rev. 116 (2016) 7397–7457. doi:10.1021/acs.chemrev.6b00176.

[66] J. Hou, M.-H. Park, S. Zhang, Y. Yao, L.-M. Chen, J.-H. Li, Y. Yang, Bandgap and Molecular Energy Level Control of Conjugated Polymer Photovoltaic Materials Based on Benzo[1,2- b :4,5- b ′]dithiophene, Macromolecules. 41 (2008) 6012–6018. doi:10.1021/ma800820r.

[67] C. Duan, F. Huang, Y. Cao, Recent development of push–pull conjugated polymers for bulk-heterojunction photovoltaics: rational design and fine tailoring of molecular structures, J. Mater. Chem. 22 (2012) 10416. doi:10.1039/c2jm30470h.

[68] P. Sista, M.C. Biewer, M.C. Stefan, Benzo[1,2-b:4,5-b′]dithiophene Building Block for the Synthesis of Semiconducting Polymers, Macromol. Rapid Commun. 33 (2012) 9–20. doi:10.1002/marc.201100671.

[69] S.C. Price, A.C. Stuart, L. Yang, H. Zhou, W. You, Fluorine Substituted Conjugated Polymer of Medium Band Gap Yields 7% Efficiency in Polymer–Fullerene Solar Cells, J. Am. Chem. Soc. 133 (2011) 8057–8057. doi:10.1021/ja202672c.

[70] S.C. Price, A.C. Stuart, W. You, Low Band Gap Polymers Based on Benzo[1,2-b :4,5- b′]dithiophene: Rational Design of Polymers Leads to High Photovoltaic Performance, Macromolecules. 43 (2010) 4609–4612. doi:10.1021/ma100051v.

[71] L. Huo, J. Hou, Benzo[1,2-b:4,5-b′]dithiophene-based conjugated polymers:

band gap and energy level control and their application in polymer solar cells, Polym. Chem. 2 (2011) 2453. doi:10.1039/c1py00197c.

[72] P. Sista, M.C. Biewer, M.C. Stefan, Benzo[1,2-b:4,5-b′]dithiophene Building Block for the Synthesis of Semiconducting Polymers, Macromol. Rapid Commun. 33 (2012) 9–20. doi:10.1002/marc.201100671.

[73] M. Heeney, W. Zhang, D.J. Crouch, M.L. Chabinyc, S. Gordeyev, R. Hamilton, S.J. Higgins, I. McCulloch, P.J. Skabara, D. Sparrowe, S. Tierney, Regioregular poly(3-hexyl)selenophene: A low band gap organic hole transporting polymer, Chem. Commun. (2007). doi:10.1039/b712398a.

[74] A. Patra, M. Bendikov, Polyselenophenes, J. Mater. Chem. (2010). doi:10.1039/b908983g.

[75] B. Kim, H.R. Yeom, M.H. Yun, J.Y. Kim, C. Yang, A selenophene analogue of PCDTBT: Selective fine-tuning of LUMO to lower of the bandgap for efficient polymer solar cells, Macromolecules. (2012). doi:10.1021/ma302133h.

[76] B.-G. Kim, X. Ma, C. Chen, Y. Ie, E.W. Coir, H. Hashemi, Y. Aso, P.F. Green, J. Kieffer, J. Kim, Energy Level Modulation of HOMO, LUMO, and Band-Gap in Conjugated Polymers for Organic Photovoltaic Applications, Adv. Funct. Mater. 23 (2013) 439–445. doi:10.1002/adfm.201201385.

[77] O.G. Reid, R.D. Pensack, Y. Song, G.D. Scholes, G. Rumbles, Charge Photogeneration in Neat Conjugated Polymers, Chem. Mater. 26 (2014) 561–575. doi:10.1021/cm4027144.

[78] J. Hou, M.-H. Park, S. Zhang, Y. Yao, L.-M. Chen, J.-H. Li, Y. Yang, Bandgap and Molecular Energy Level Control of Conjugated Polymer Photovoltaic Materials Based on Benzo[1,2- b :4,5- b ′]dithiophene, Macromolecules. 41 (2008) 6012–6018. doi:10.1021/ma800820r.

[79] H. Zhou, L. Yang, W. You, Rational Design of High Performance Conjugated Polymers for Organic Solar Cells, Macromolecules. 45 (2012) 607–632. doi:10.1021/ma201648t.

[80] B. Keller, A. McLean, B.G. Kim, K. Chung, J. Kim, T. Goodson, Ultrafast spectroscopic study of donor-acceptor benzodithiophene light harvesting organic conjugated polymers, J. Phys. Chem. C. (2016). doi:10.1021/acs.jpcc.6b01727.

[81] Z. Zhang, B. Peng, B. Liu, C. Pan, Y. Li, Y. He, K. Zhou, Y. Zou, Copolymers from benzodithiophene and benzotriazole: synthesis and photovoltaic applications, Polym. Chem. 1 (2010) 1441. doi:10.1039/c0py00136h.

[82] T.E. Kang, K.-H. Kim, B.J. Kim, Design of terpolymers as electron donors for highly efficient polymer solar cells, J. Mater. Chem. A. 2 (2014) 15252.

doi:10.1039/C4TA02426E.

[83] H.J. Cho, Y.J. Kim, S. Chen, J. Lee, T.J. Shin, C.E. Park, C. Yang, Over 10% efficiency in single-junction polymer solar cells developed from easily accessible random terpolymers, Nano Energy. 39 (2017) 229–237. doi:10.1016/j.nanoen.2017.06.051.

[84] S. Qu, H. Wang, D. Mo, P. Chao, Z. Yang, L. Li, L. Tian, W. Chen, F. He, Fine Tuning of Open-Circuit Voltage by Chlorination in Thieno[3,4- b]thiophene–Benzodithiophene Terpolymers toward Enhanced Solar Energy Conversion, Macromolecules. 50 (2017) 4962–4971. doi:10.1021/acs.macromol.7b00785.

[85] T. Ma, K. Jiang, S. Chen, H. Hu, H. Lin, Z. Li, J. Zhao, Y. Liu, Y.-M. Chang, C.-C. Hsiao, H. Yan, Efficient Low-Bandgap Polymer Solar Cells with High Open-Circuit Voltage and Good Stability, Adv. Energy Mater. 5 (2015) 1501282. doi:10.1002/aenm.201501282.

[86] C. Cabanetos, A. El Labban, J.A. Bartelt, J.D. Douglas, W.R. Mateker, J.M.J. Fréchet, M.D. McGehee, P.M. Beaujuge, Linear Side Chains in Benzo[1,2-b :4,5- b ′]dithiophene–Thieno[3,4- c]pyrrole-4,6-dione Polymers Direct Self-Assembly and Solar Cell Performance, J. Am. Chem. Soc. 135 (2013) 4656–4659. doi:10.1021/ja400365b.

[87] B.A.D. Neto, A.A.M. Lapis, E.N. da Silva Júnior, J. Dupont, 2,1,3-Benzothiadiazole and Derivatives: Synthesis, Properties, Reactions, and Applications in Light Technology of Small Molecules, European J. Org. Chem. 2013 (2013) 228–255. doi:10.1002/ejoc.201201161.

[88] P. Gabbott, ed., Principles and Applications of Thermal Analysis, Blackwell Publishing Ltd, Oxford, UK, 2008. doi:10.1002/9780470697702.

[89] A.S. Mukasyan, DTA/TGA-Based Methods, in: Concise Encycl. Self-Propagating High-Temperature Synth., Elsevier, 2017: pp. 93–95. doi:10.1016/B978-0-12-804173-4.00040-5.

[90] D. a Skoog, F.J. Holler, T. a Nieman, Principles of Instrumental Analysis, Brooks/Cole, 1998. doi:10.1090/S0002-9904-1936-06390-1.

[91] L. Leonat, G. Sbârcea, I.V. Branzoi, Cyclic voltammetry for energy levels estimation of organic materials, UPB Sci. Bull. Ser. B Chem. Mater. Sci. (2013).

[92] M. Al-Ibrahim, H.K. Roth, M. Schrödner, A. Konkin, U. Zhokhavets, G. Gobsch, P. Scharff, S. Sensfuss, The influence of the optoelectronic properties of poly(3-alkylthiophenes) on the device parameters in flexible polymer solar cells, Org. Electron. Physics, Mater. Appl. (2005). doi:10.1016/j.orgel.2005.02.004.

[93] A.P. Kulkarni, C.J. Tonzola, A. Babel, S.A. Jenekhe, Electron transport

materials for organic light-emitting diodes, Chem. Mater. (2004). doi:10.1021/cm049473l.

[94] B.W. D'Andrade, S. Datta, S.R. Forrest, P. Djurovich, E. Polikarpov, M.E. Thompson, Relationship between the ionization and oxidation potentials of molecular organic semiconductors, Org. Electron. Physics, Mater. Appl. (2005). doi:10.1016/j.orgel.2005.01.002.

[95] J.L. Brédas, R. Silbey, D.S. Boudreaux, R.R. Chance, Chain-Length Dependence of Electronic and Electrochemical Properties of Conjugated Systems: Polyacetylene, Polyphenylene, Polythiophene, and Polypyrrole, J. Am. Chem. Soc. (1983). doi:10.1021/ja00360a004.

[96] D.R.T. Zahn, G.N. Gavrila, M. Gorgoi, The transport gap of organic semiconductors studied using the combination of direct and inverse photoemission, Chem. Phys. (2006). doi:10.1016/j.chemphys.2006.02.003.

[97] P.I. Djurovich, E.I. Mayo, S.R. Forrest, M.E. Thompson, Measurement of the lowest unoccupied molecular orbital energies of molecular organic semiconductors, Org. Electron. Physics, Mater. Appl. (2009). doi:10.1016/j.orgel.2008.12.011.

[98] F.A. Devillanova, W.-W. Du Mont, Handbook of Chalcogen Chemistry, Royal Society of Chemistry, Cambridge, 2007. doi:10.1039/9781847557575.

[99] D. Cortizo-Lacalle, P.J. Skabara, T.D. Westgate, CHAPTER 11.2. Chalcogen-Rich Compounds as Electron Donors, in: n.d.: pp. 99–126. doi:10.1039/9781849737463-00099.

[100] J.-M. Jiang, P. Raghunath, H.-K. Lin, Y.-C. Lin, M.C. Lin, K.-H. Wei, Location and Number of Selenium Atoms in Two-Dimensional Conjugated Polymers Affect Their Band-Gap Energies and Photovoltaic Performance, Macromolecules. 47 (2014) 7070–7080. doi:10.1021/ma501720k.

[101] I. Meager, R.S. Ashraf, S. Mollinger, B.C. Schroeder, H. Bronstein, D. Beatrup, M.S. Vezie, T. Kirchartz, A. Salleo, J. Nelson, I. McCulloch, Photocurrent Enhancement from Diketopyrrolopyrrole Polymer Solar Cells through Alkyl-Chain Branching Point Manipulation, J. Am. Chem. Soc. 135 (2013) 11537–11540. doi:10.1021/ja406934j.

[102] G.M. Farinola, A. Cardone, F. Babudri, C. Martinelli, F. Naso, G. Bruno, M. Losurdo, Fluorinated Poly(p-phenylenevinylene)s: Synthesis and Optical Properties of an Intriguing Class of Luminescent Polymers, Materials (Basel). 3 (2010) 3077–3091. doi:10.3390/ma3053077.

[103] H.-Y. Chen, S.-C. Yeh, C.-T. Chen, C.-T. Chen, Comparison of thiophene- and selenophene-bridged donor–acceptor low band-gap copolymers used in bulk-heterojunction organic photovoltaics, J. Mater. Chem. 22 (2012) 21549.

doi:10.1039/c2jm33735e.

[104] L. Gao, Z.-G. Zhang, H. Bin, L. Xue, Y. Yang, C. Wang, F. Liu, T.P. Russell, Y. Li, High-Efficiency Nonfullerene Polymer Solar Cells with Medium Bandgap Polymer Donor and Narrow Bandgap Organic Semiconductor Acceptor, Adv. Mater. 28 (2016) 8288–8295. doi:10.1002/adma.201601595.

[105] X. Zhu, F. Zhang, Q. An, H. Huang, Q. Sun, L. Li, F. Teng, W. Tang, Effect of solvent additive and ethanol treatment on the performance of PIDTDTQx:PC 71 BM polymer solar cells, Sol. Energy Mater. Sol. Cells. 132 (2015) 528–534. doi:10.1016/j.solmat.2014.10.006.

[106] M.K. Pola, K.M. Boopathi, H. Padhy, P. Raghunath, A. Singh, M.-C. Lin, C.-W. Chu, H.-C. Lin, Synthesis of fluorinated benzotriazole (BTZ)- and benzodithiophene (BDT)-based low-bandgap conjugated polymers for solar cell applications, Dye. Pigment. 139 (2017) 349–360. doi:10.1016/j.dyepig.2016.12.007.

[107] E. Kaya, D.H. Apaydın, D.E. Yıldız, L. Toppare, A. Cirpan, Solution processable benzotriazole and fluorene containing copolymers for photovoltaic applications, Sol. Energy Mater. Sol. Cells. 99 (2012) 321–326. doi:10.1016/j.solmat.2011.12.021.

[108] C. V. Hoven, X.-D. Dang, R.C. Coffin, J. Peet, T.-Q. Nguyen, G.C. Bazan, Improved Performance of Polymer Bulk Heterojunction Solar Cells Through the Reduction of Phase Separation via Solvent Additives, Adv. Mater. 22 (2010) E63–E66. doi:10.1002/adma.200903677.

[109] H.N. Tran, D.H. Kim, S. Park, S. Cho, The effect of various solvent additives on the power conversion efficiency of polymer-polymer solar cells, Curr. Appl. Phys. 18 (2018) 534–540. doi:10.1016/j.cap.2018.03.003.

[110] T.H. Lee, S.Y. Park, B. Walker, S.-J. Ko, J. Heo, H.Y. Woo, H. Choi, J.Y. Kim, A universal processing additive for high-performance polymer solar cells, RSC Adv. 7 (2017) 7476–7482. doi:10.1039/C6RA27944A.

APPENDICES

A. NMR DATA

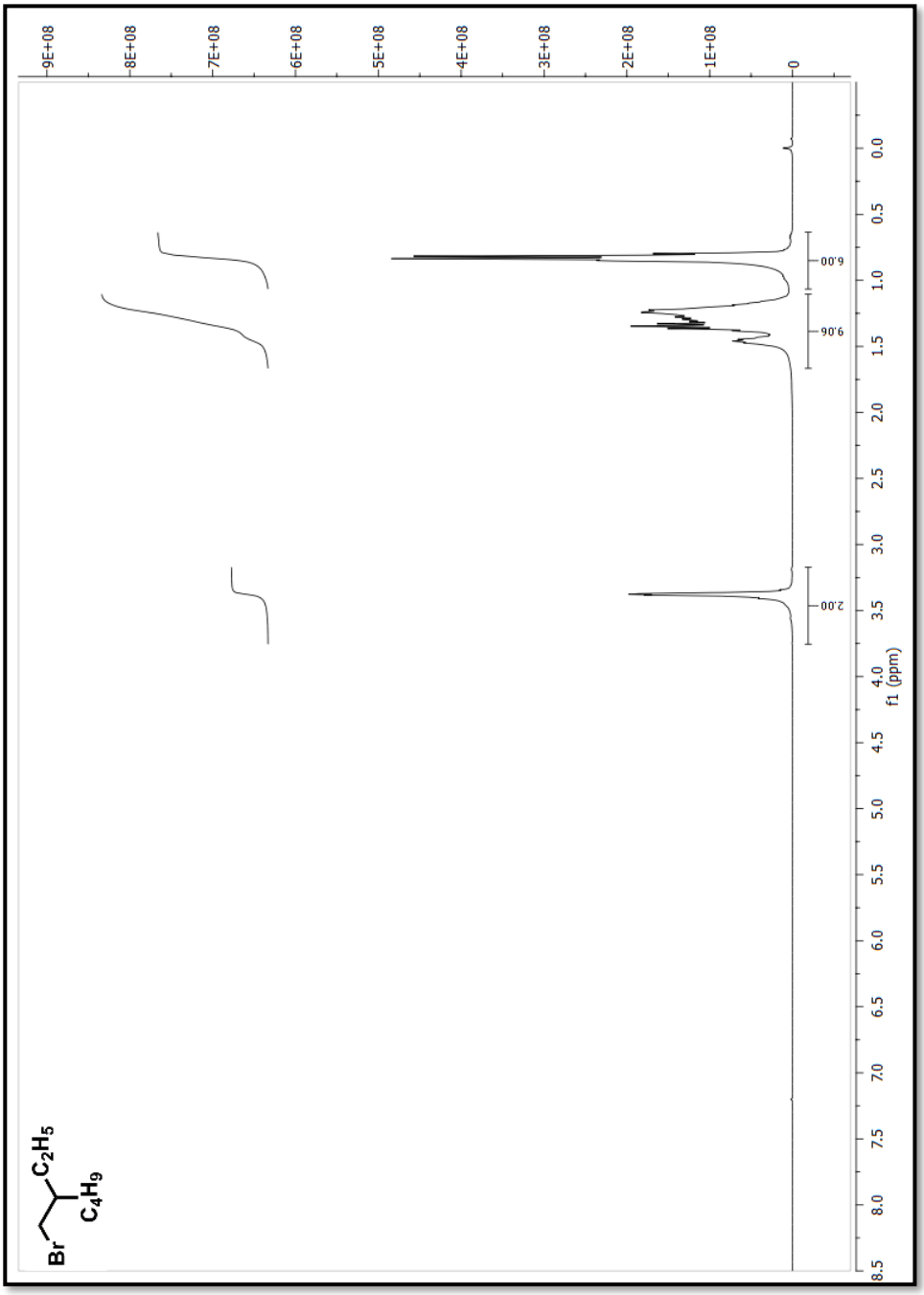

Figure A. 1. ^{1}H NMR of 3-(bromomethyl) heptane

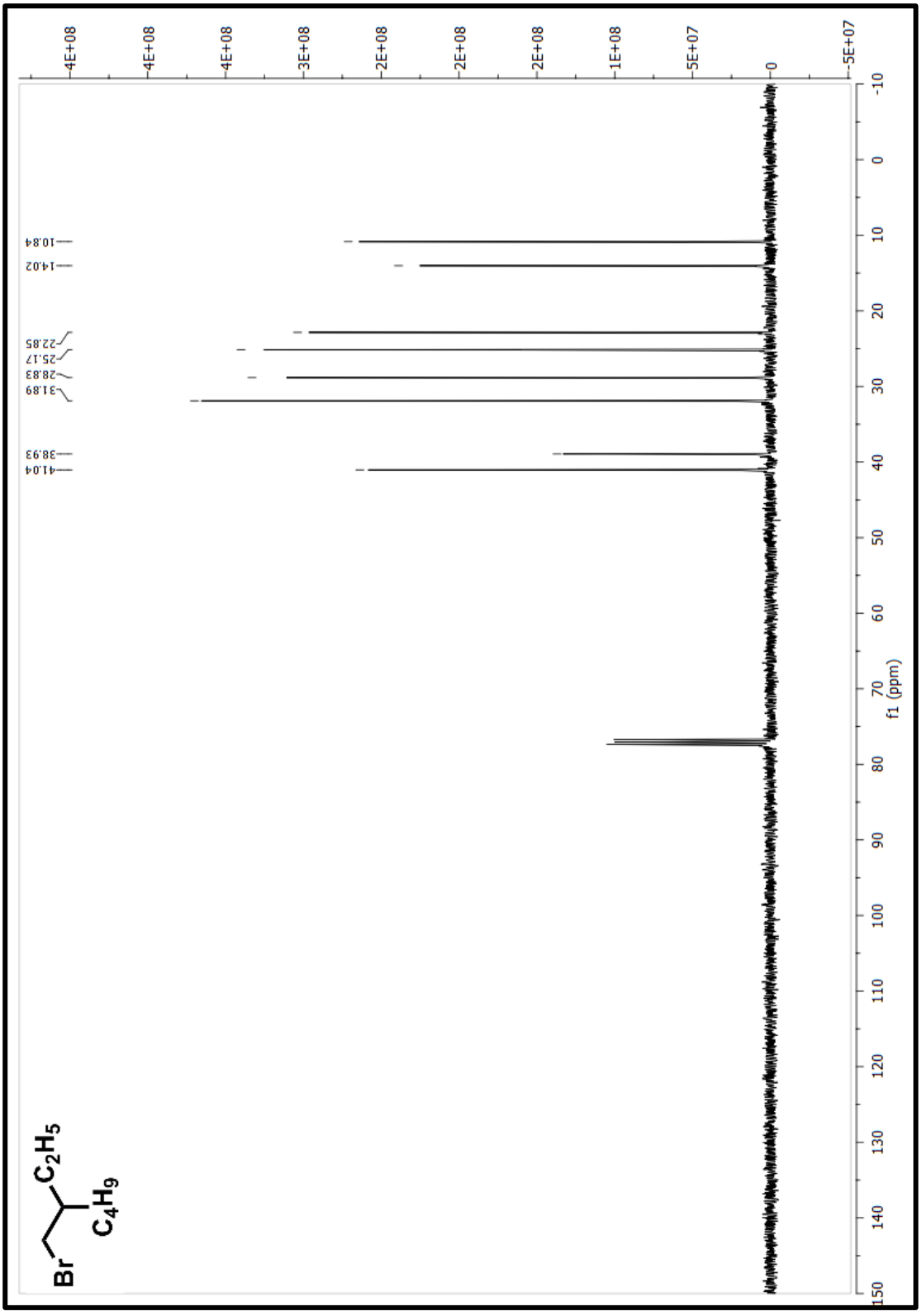

Figure A. 2. ^{13}C NMR of 3-(bromomethyl) heptane

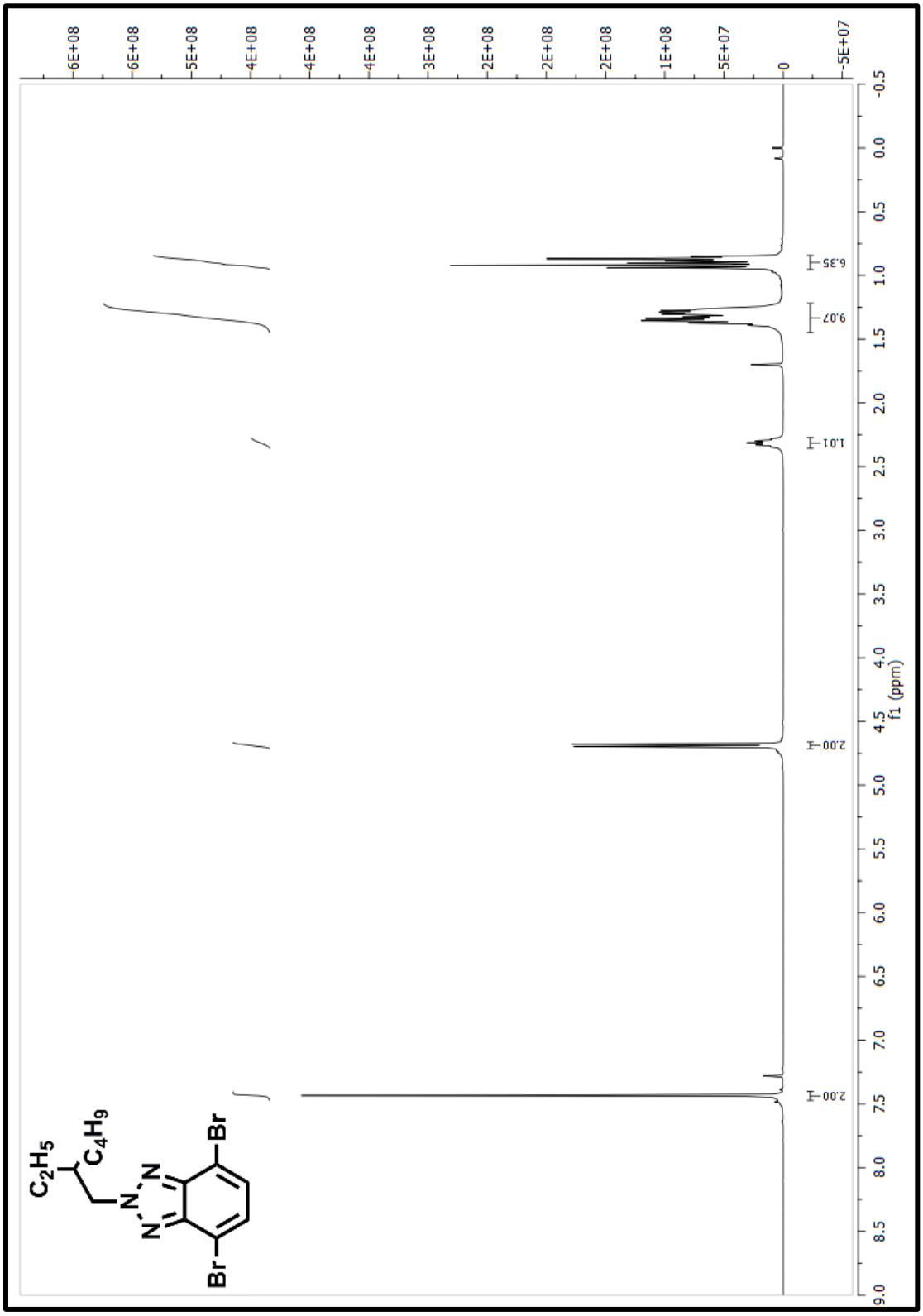

Figure A. 3. ^{1}H NMR of 4,7-Dibromo-2-(2- ethylhexyl)-2H-benzo[d][1,2,3]triazole

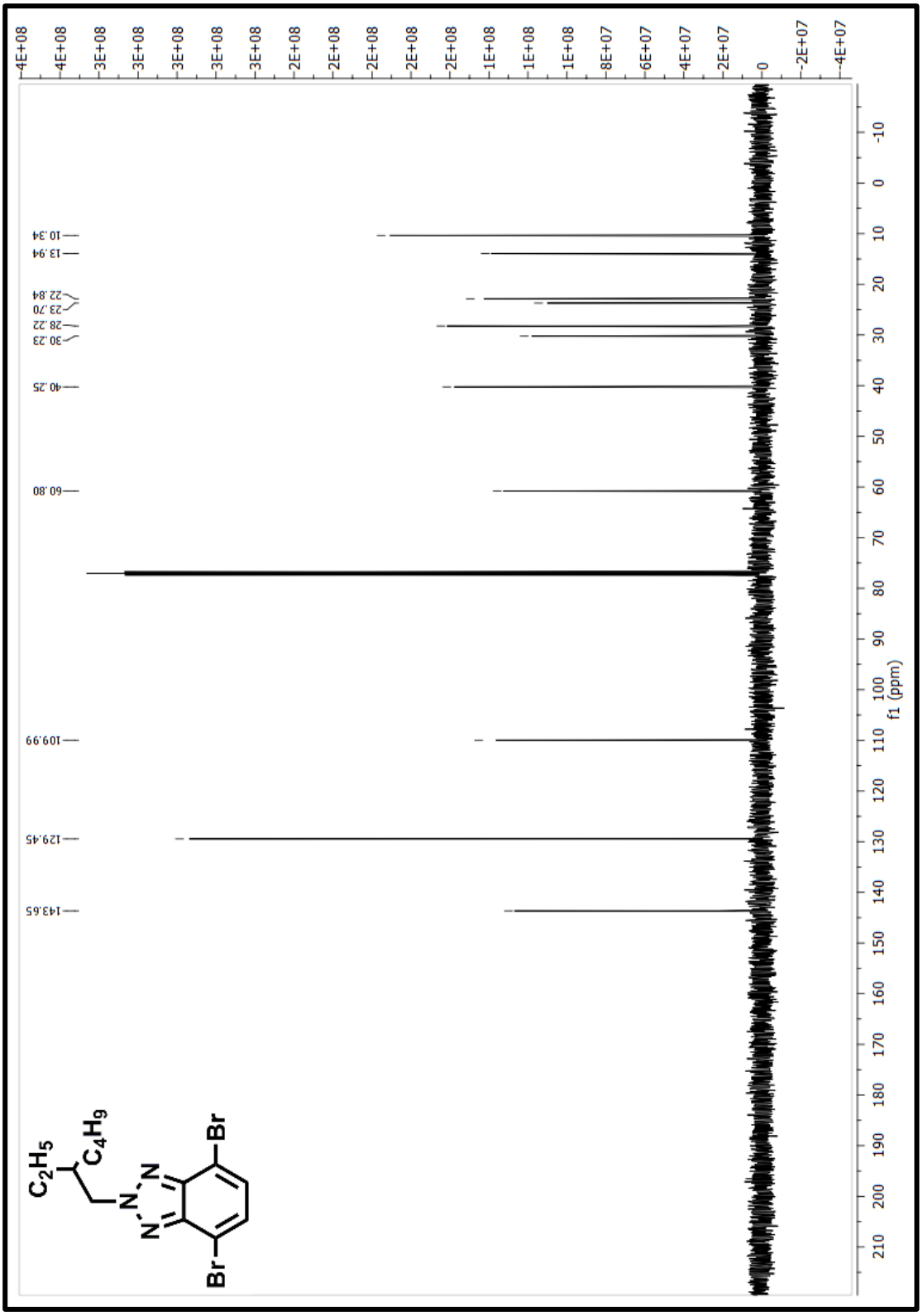

Figure A. 4. ^{13}C NMR of 4,7-Dibromo-2-(2- ethylhexyl)-2H-benzo[d] [1,2,3]triazole

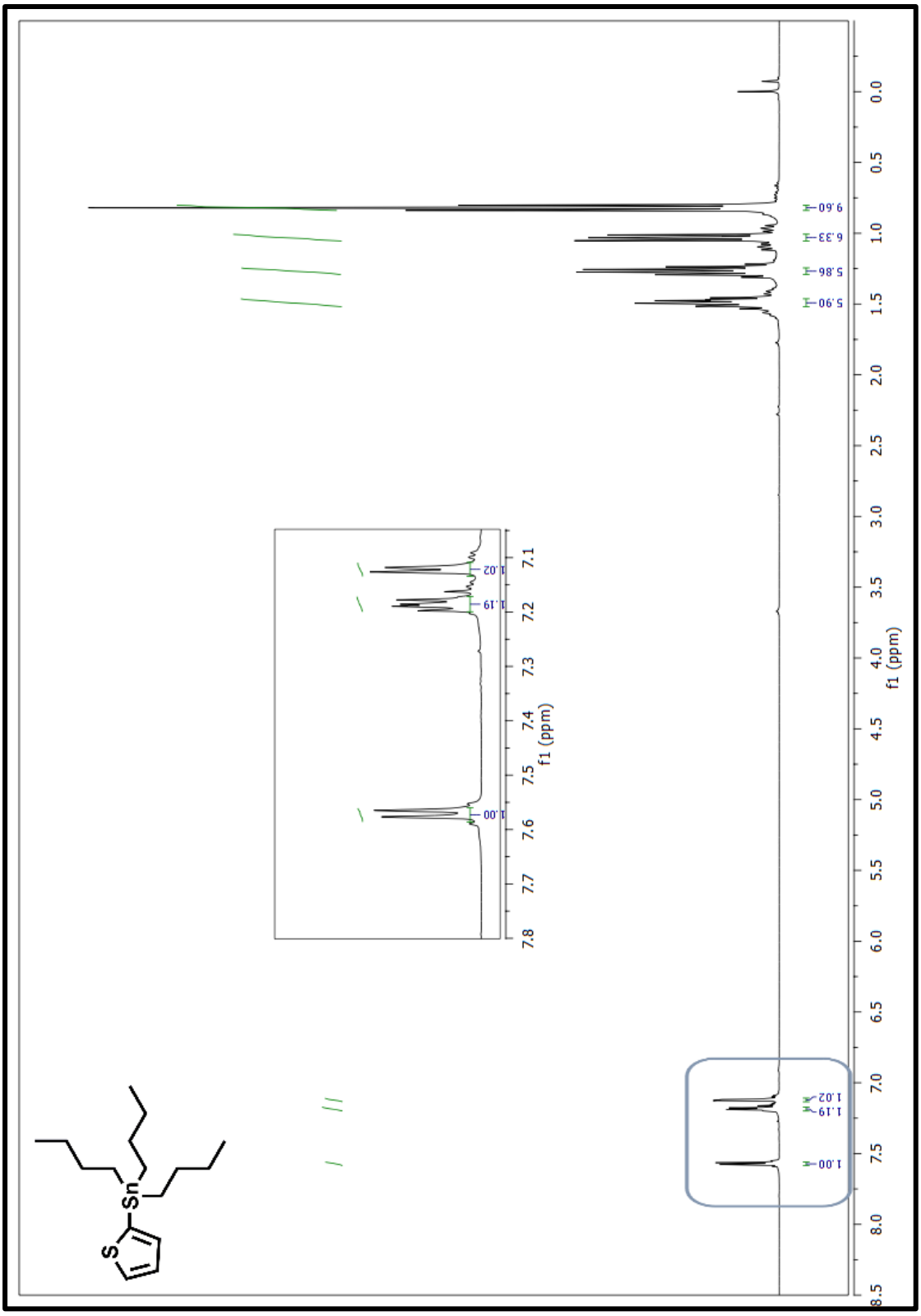

Figure A. 5. ^{1}H NMR of Tributyl(thiophen-2-yl)stannane

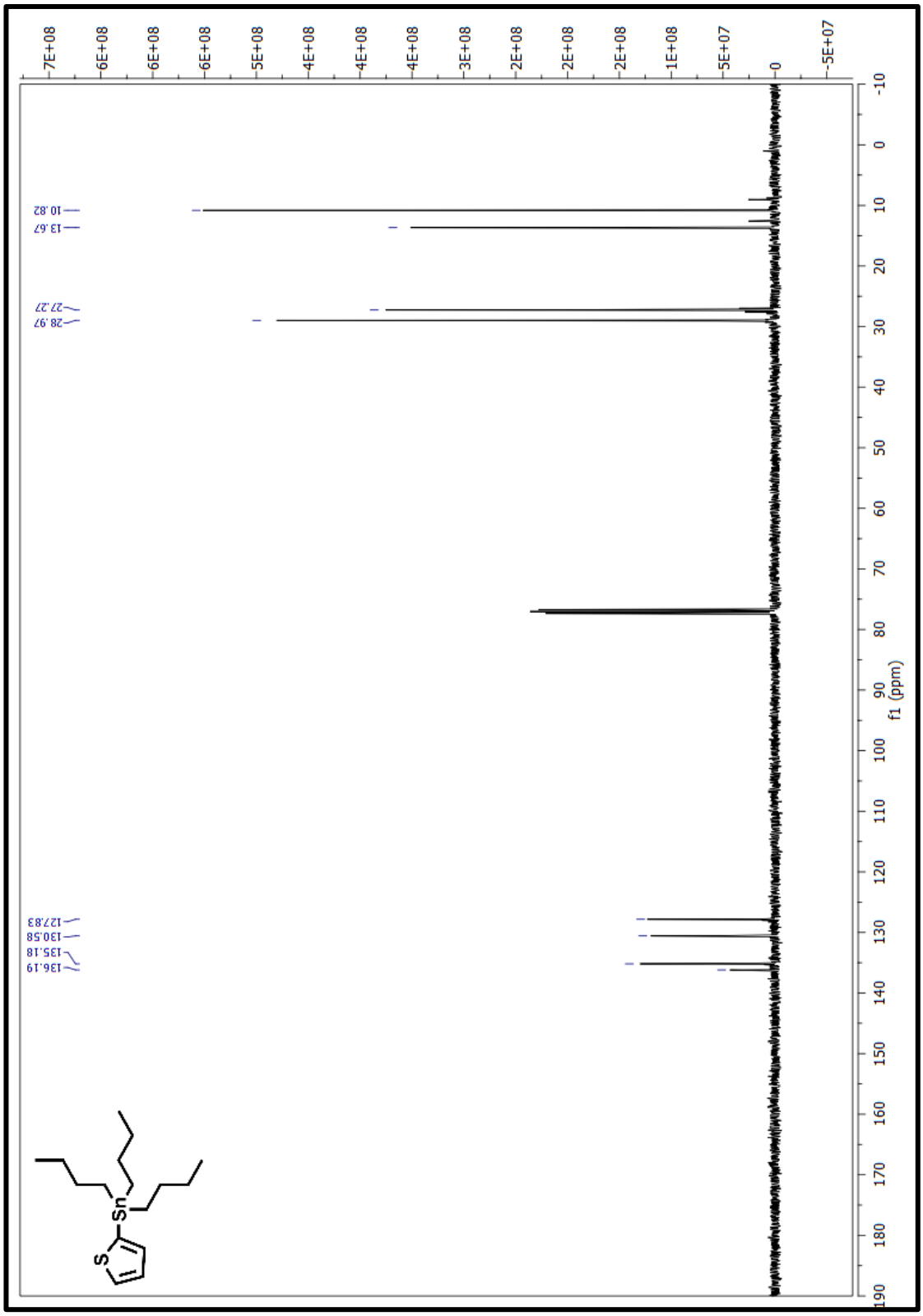

Figure A. 6. ^{13}C NMR of Tributyl(thiophen-2-yl)stannane

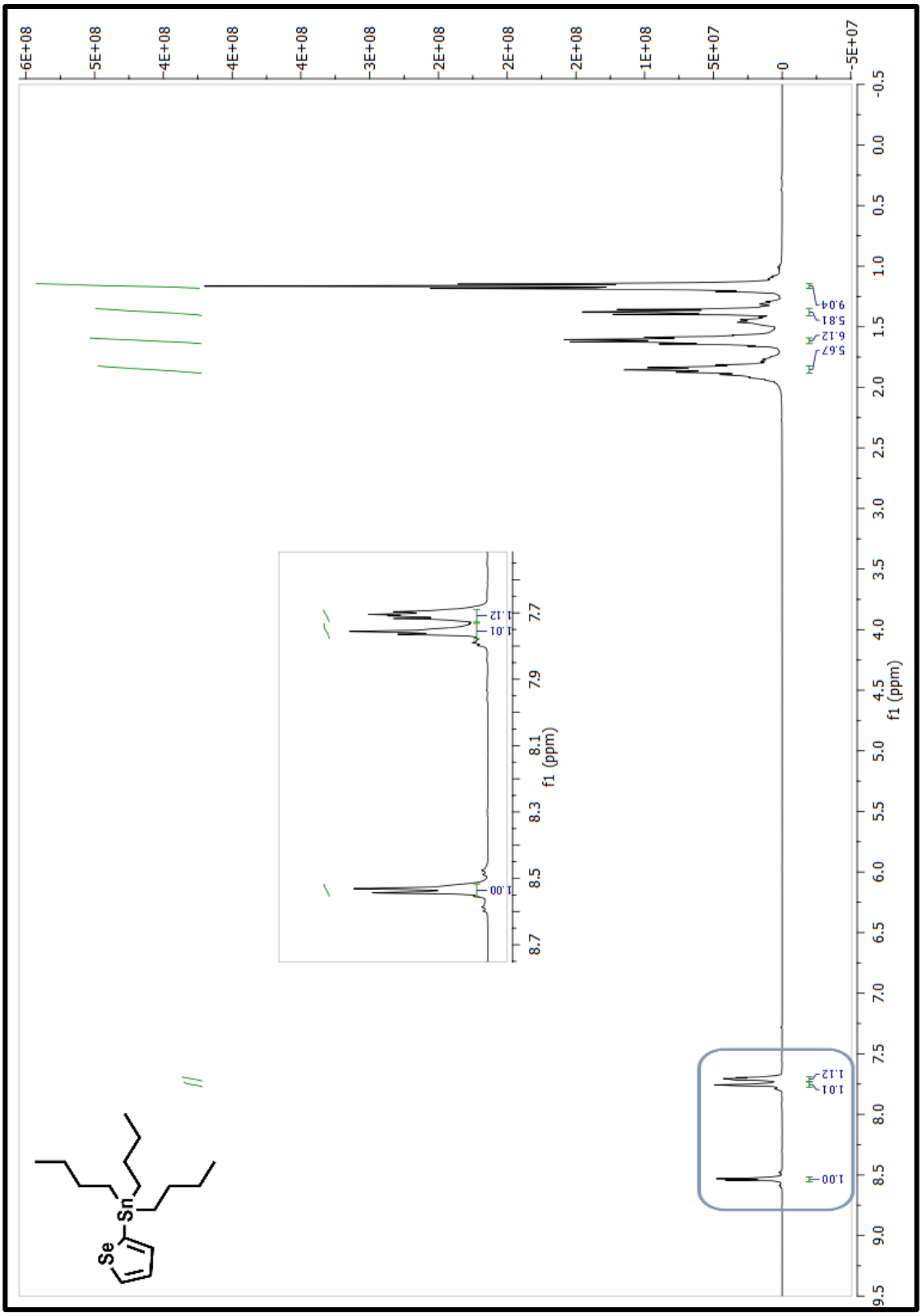

Figure A. 7. [1]H NMR of Tributyl(selenophen-2-yl)stannane

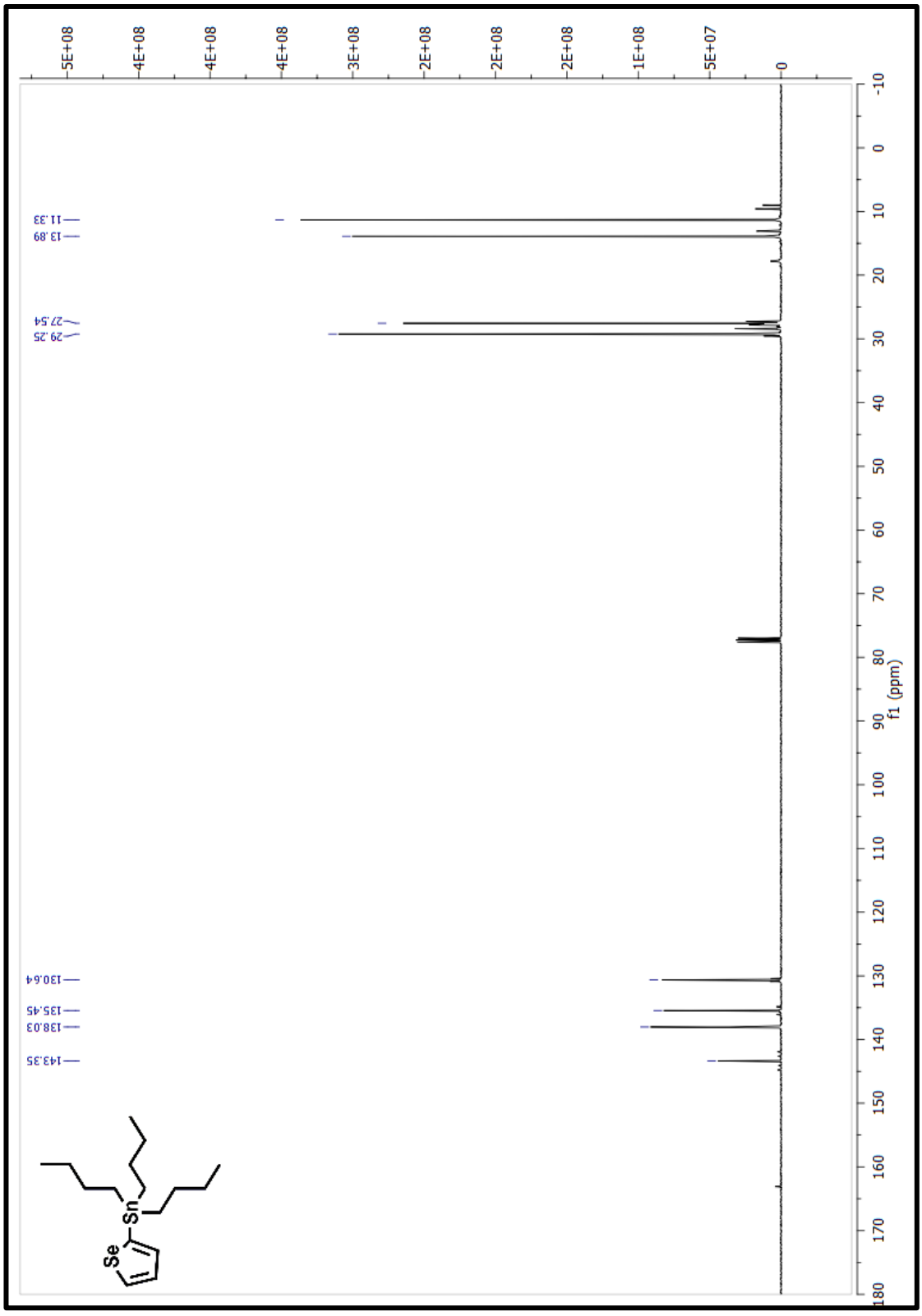

Figure A. 8. ^{13}C NMR of Tributyl(selenophen-2-yl)stannane

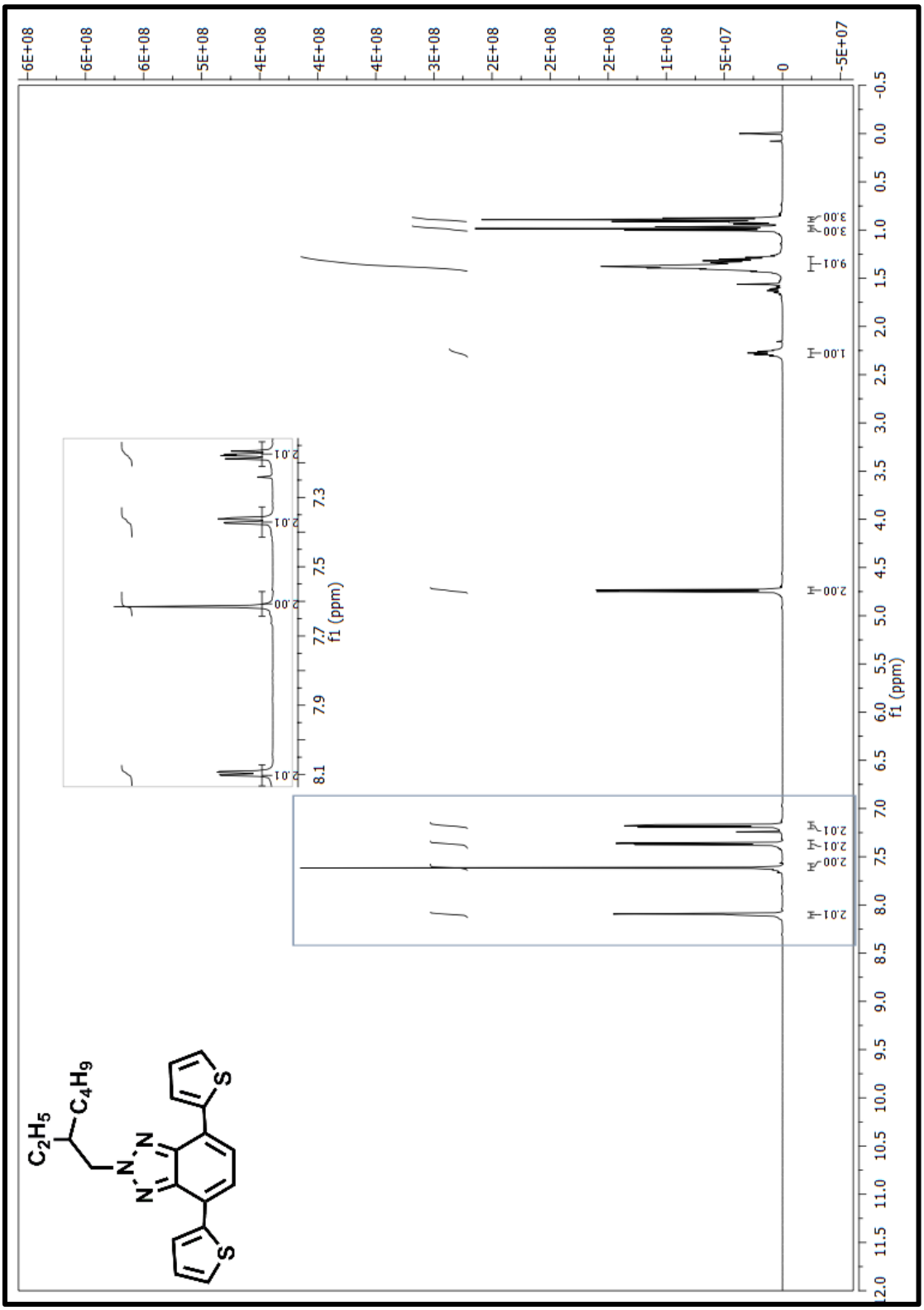

Figure A. 9. [1]H NMR of 2-(2-ethylhexyl)-4,7-di(thiophen-2-yl)-2H-benzo[d][1,2,3]triazole

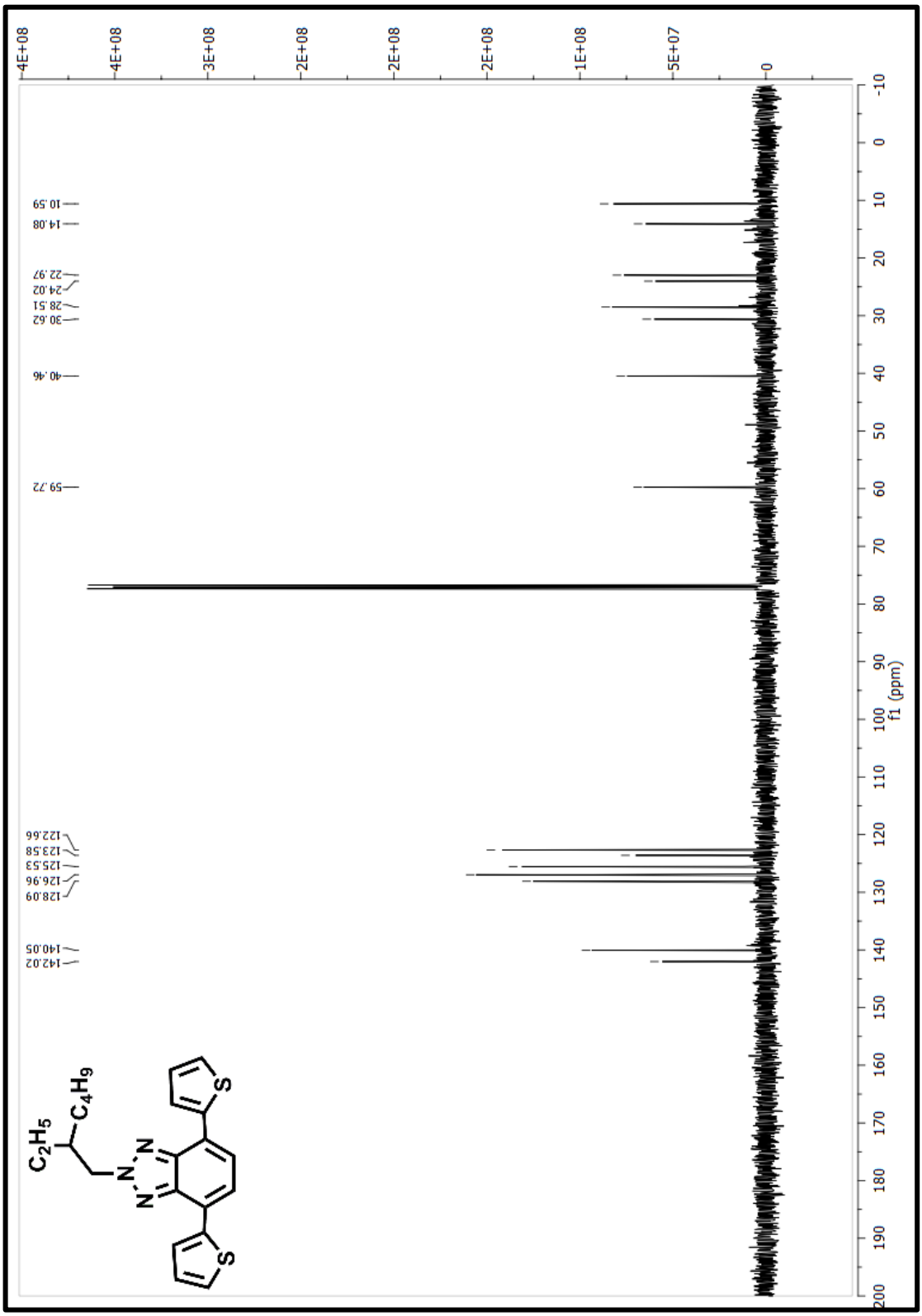

Figure A. 10. ^{13}C NMR of 2-(2-ethylhexyl)-4,7-di(thiophen-2-yl)-2H-benzo[d][1,2,3]triazole

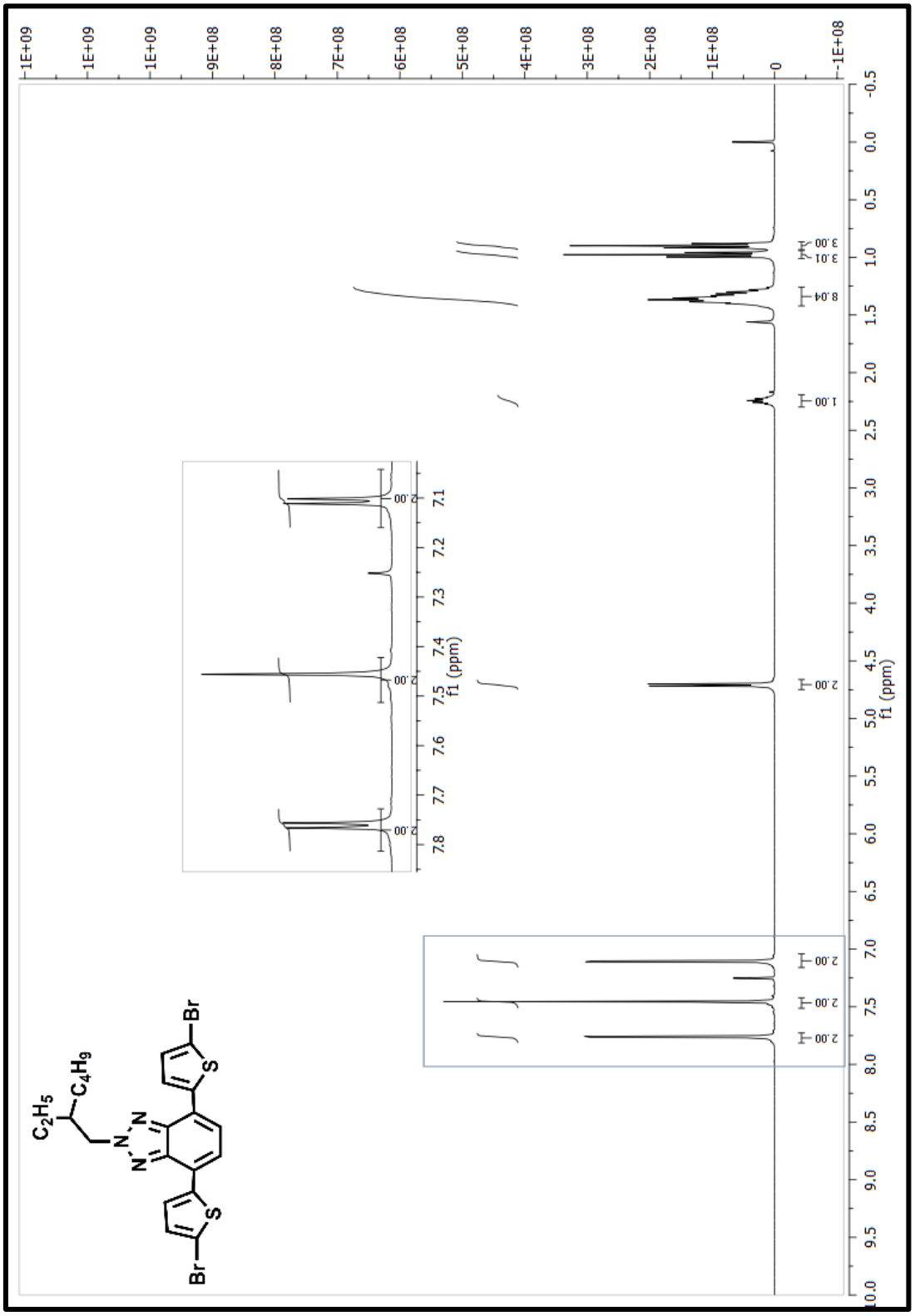

Figure A. 11. ^{1}H NMR of 4,7-bis(5-bromothiophen-2-yl)-2-(2-ethylhexyl)-2H-benzo[d][1,2,3]triazole

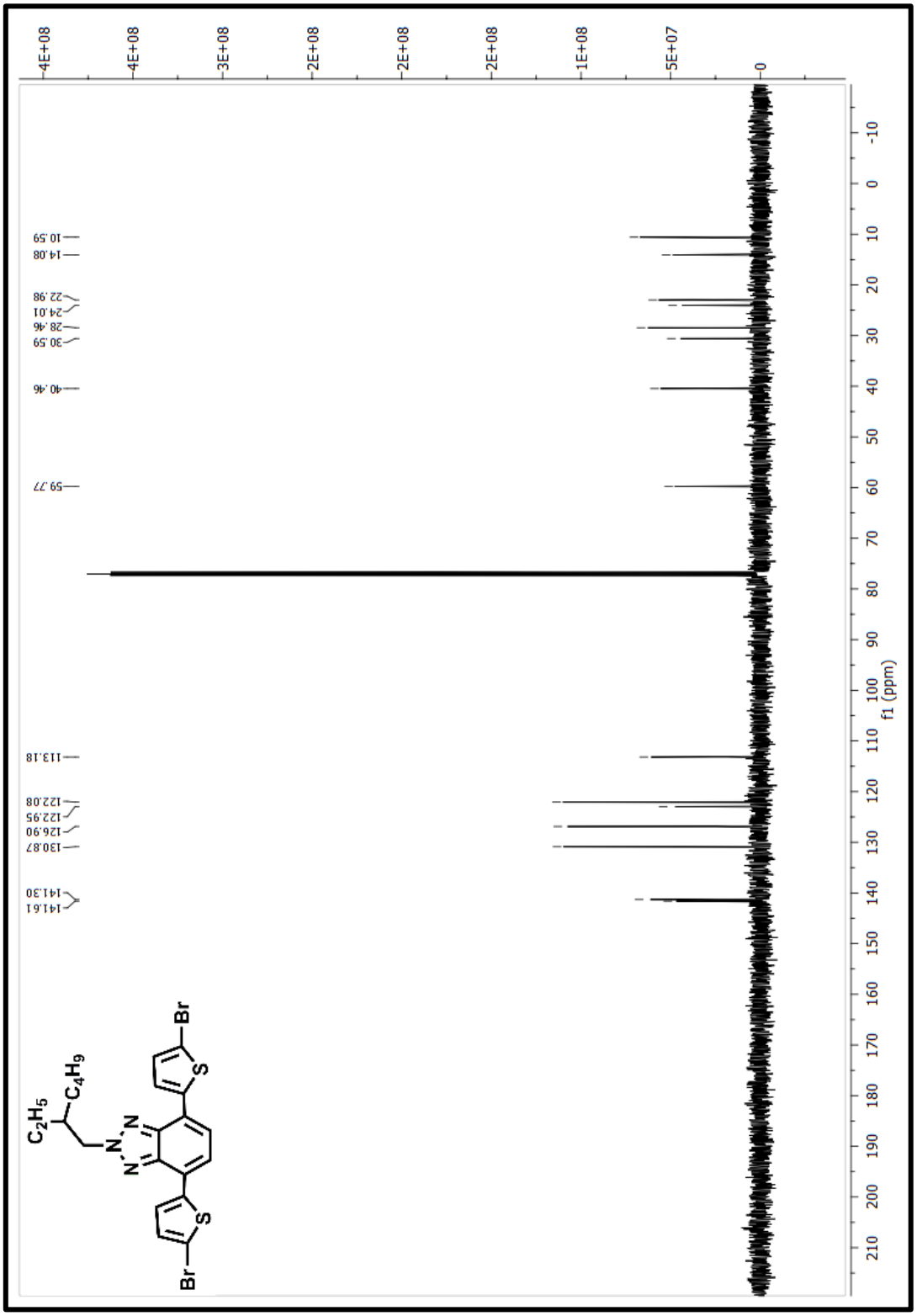

Figure A. 12. ^{13}C NMR of 4,7-bis(5-bromothiophen-2-yl)-2-(2-ethylhexyl)-2H-benzo[d][1,2,3]triazole

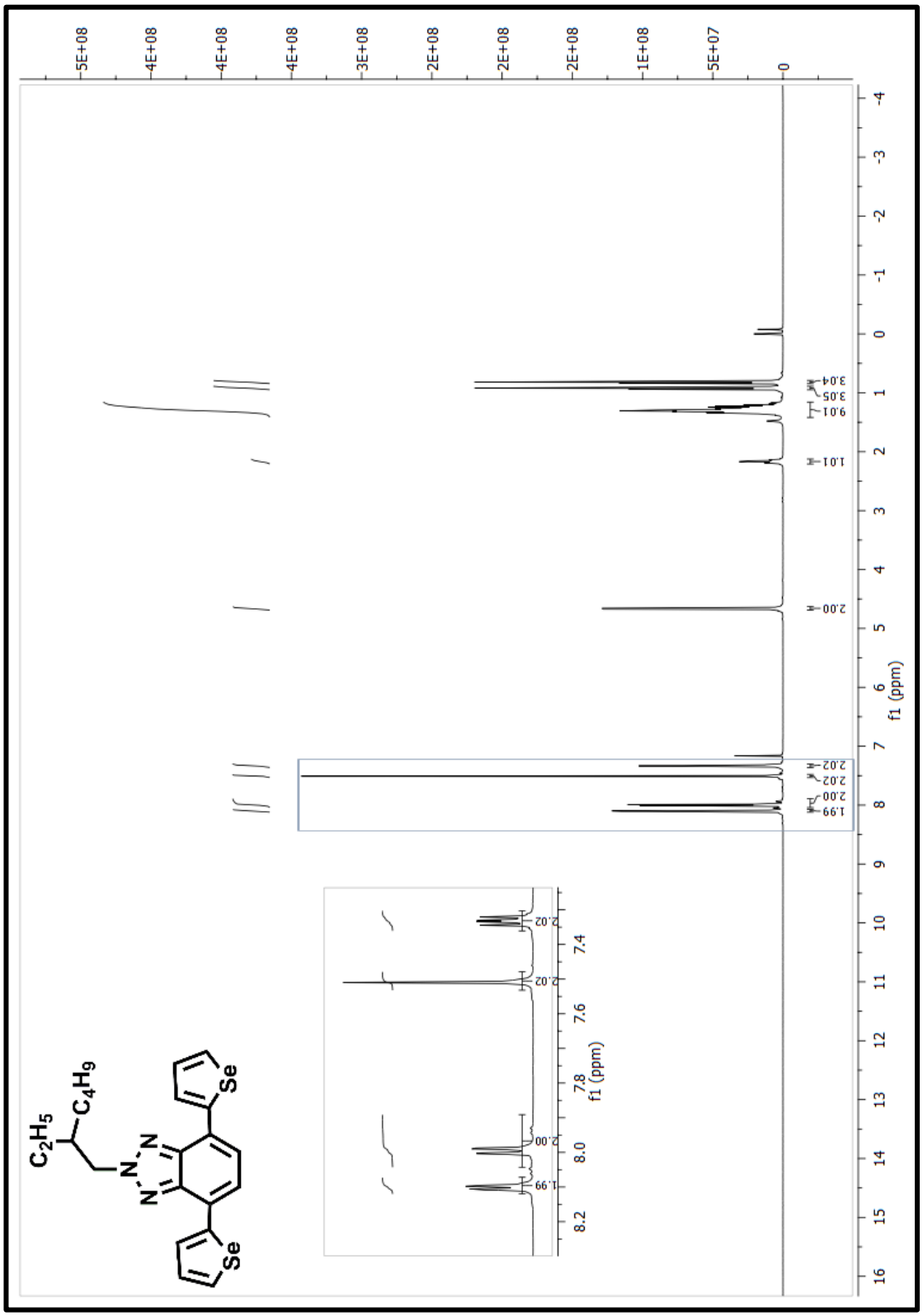

Figure A. 13. [1]H NMR of 2-(2-ethylhexyl)-4,7-di(selenophen-2-yl)-2H-benzo[d][1,2,3] triazole

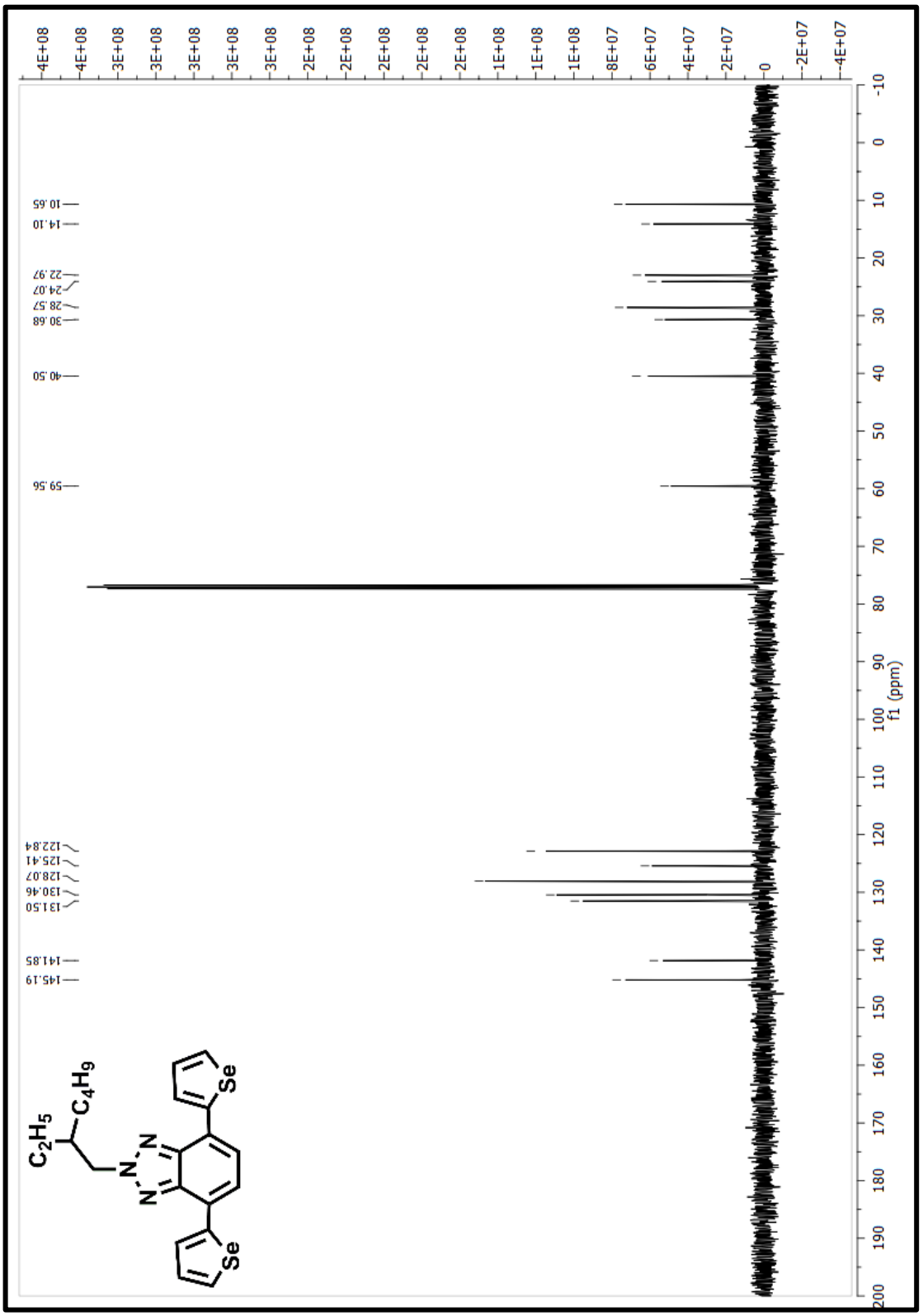

Figure A. 14. ^{13}C NMR of 2-(2-ethylhexyl)-4,7-di(selenophen-2-yl)-2H-benzo[d][1,2,3] triazole

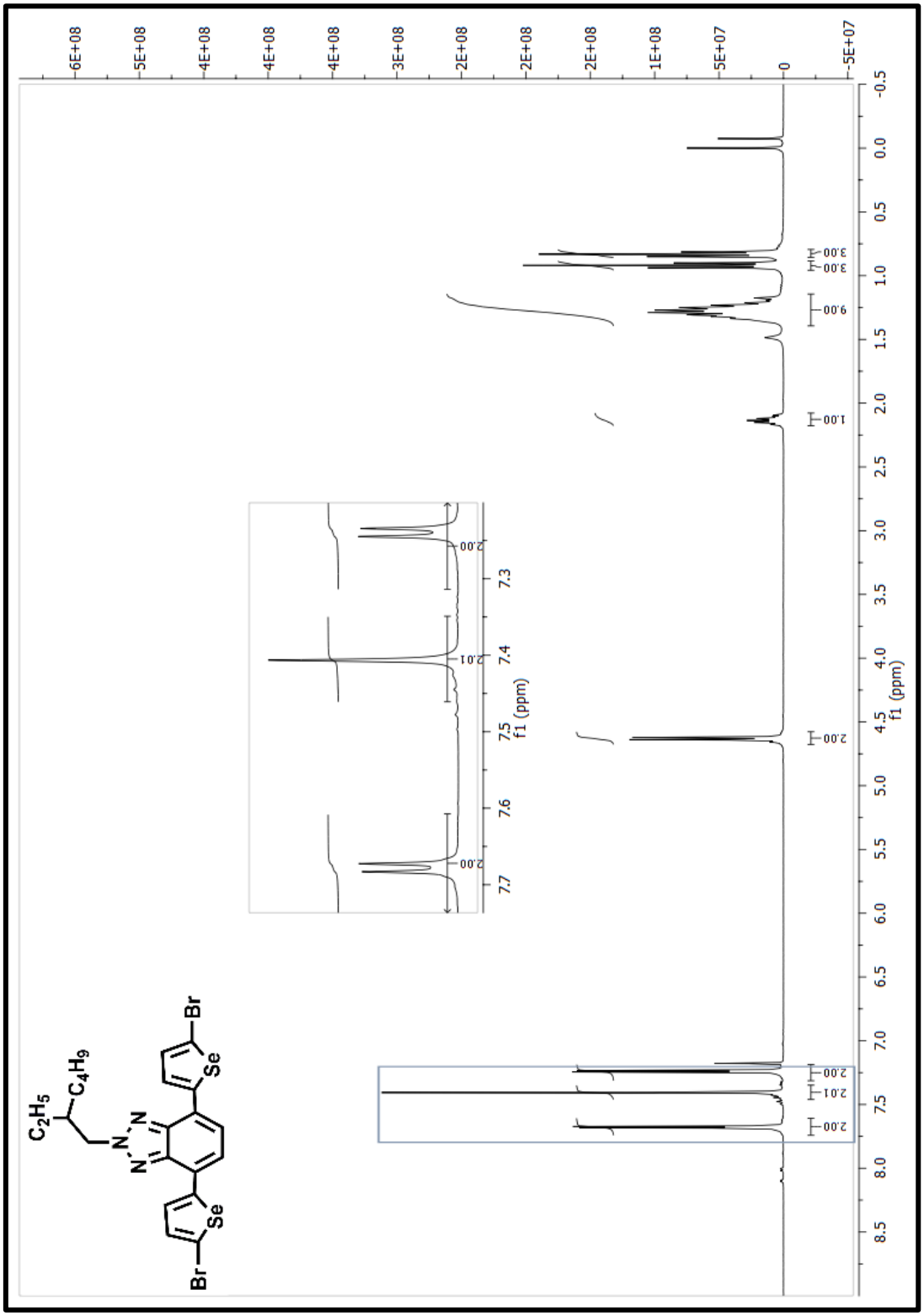

Figure A. 15. ^{1}H NMR of 4,7-bis(5-bromoselenophen-2-yl)-2-(2-ethylhexyl)-2H-benzo[d][1,2,3]triazole

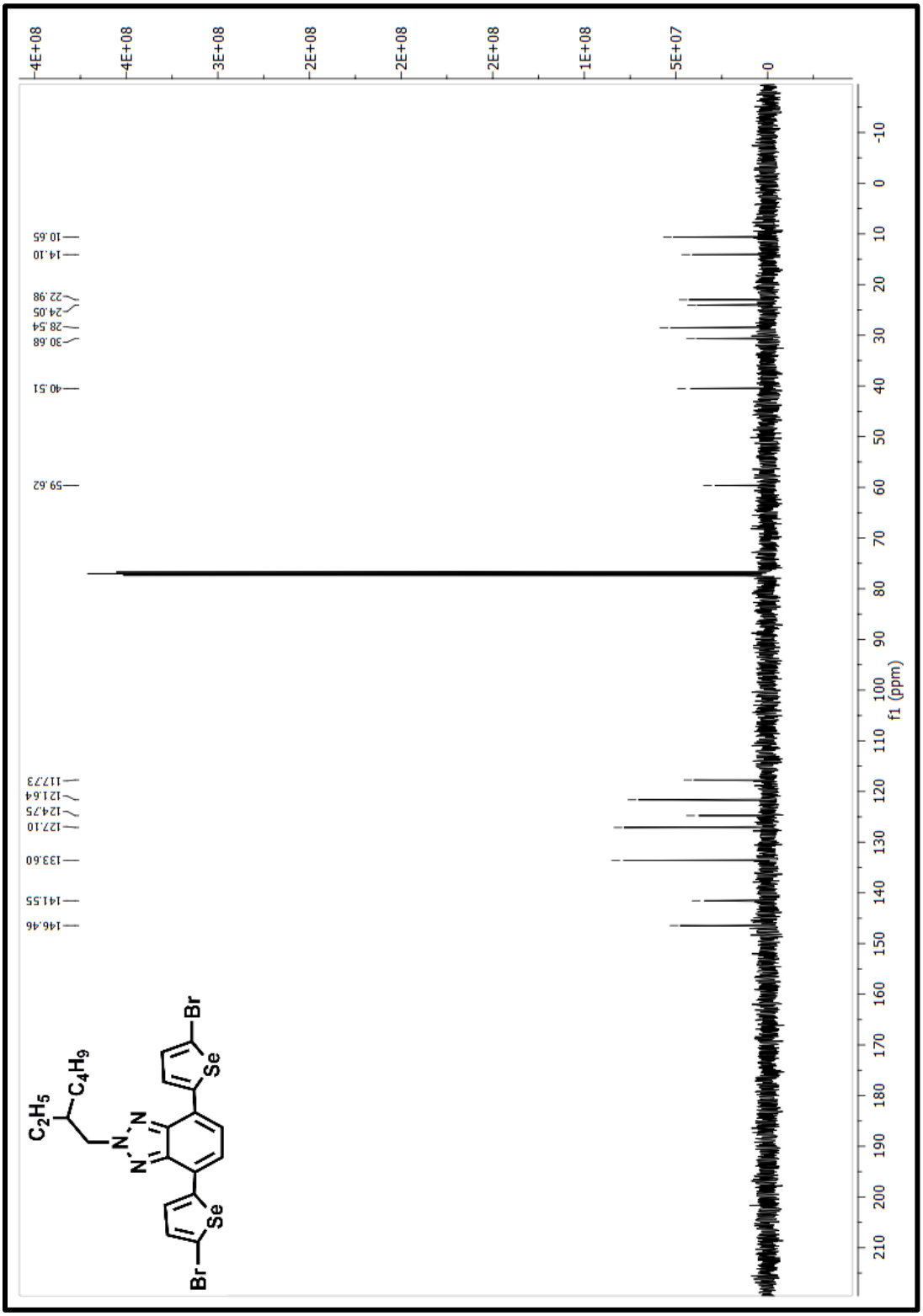

Figure A. 16. ^{13}C NMR of 4,7-bis(5-bromoselenophen-2-yl)-2-(2-ethylhexyl)-2H-benzo[d][1,2,3]triazole

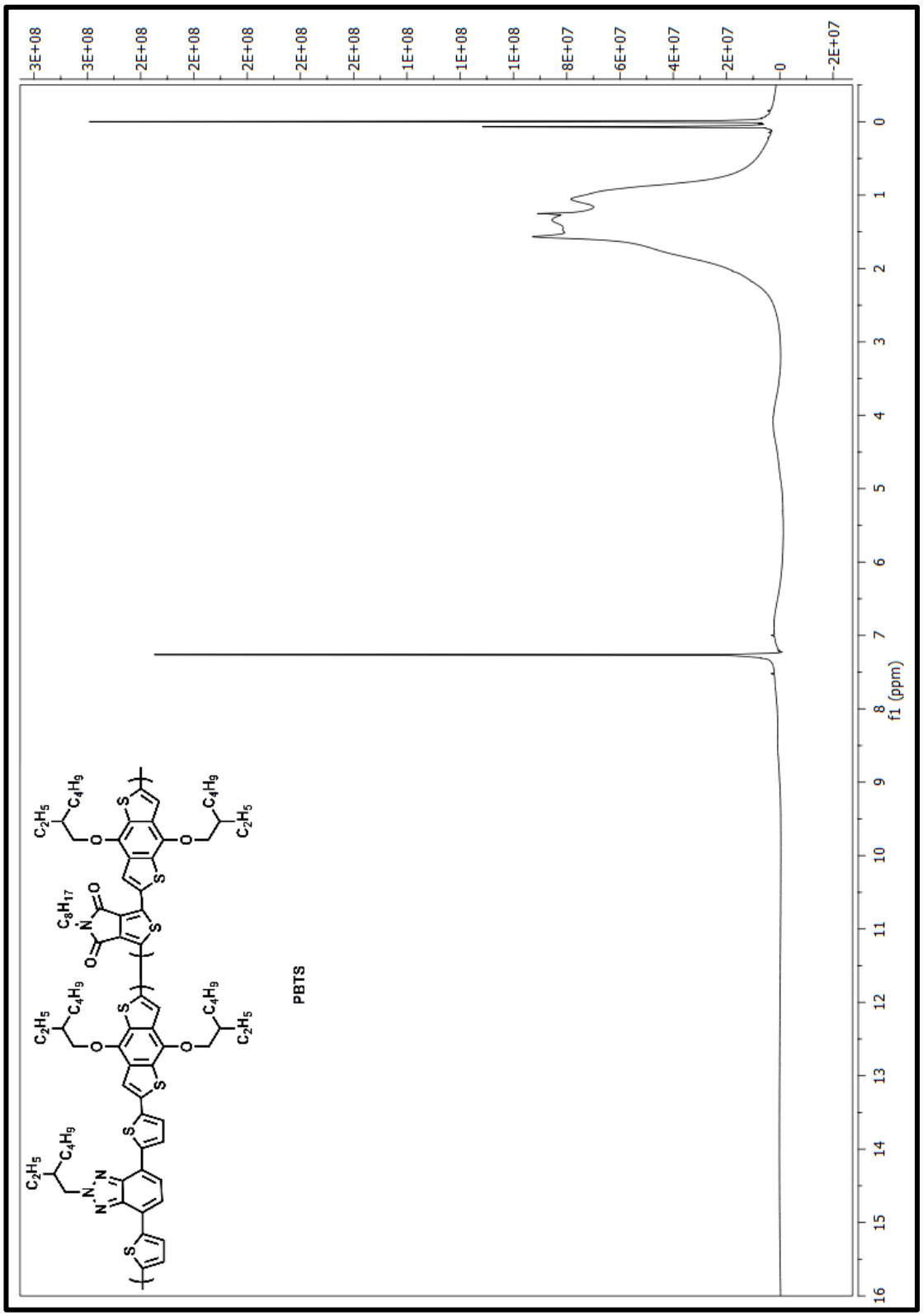

Figure A. 17. [1]H NMR of PBTS

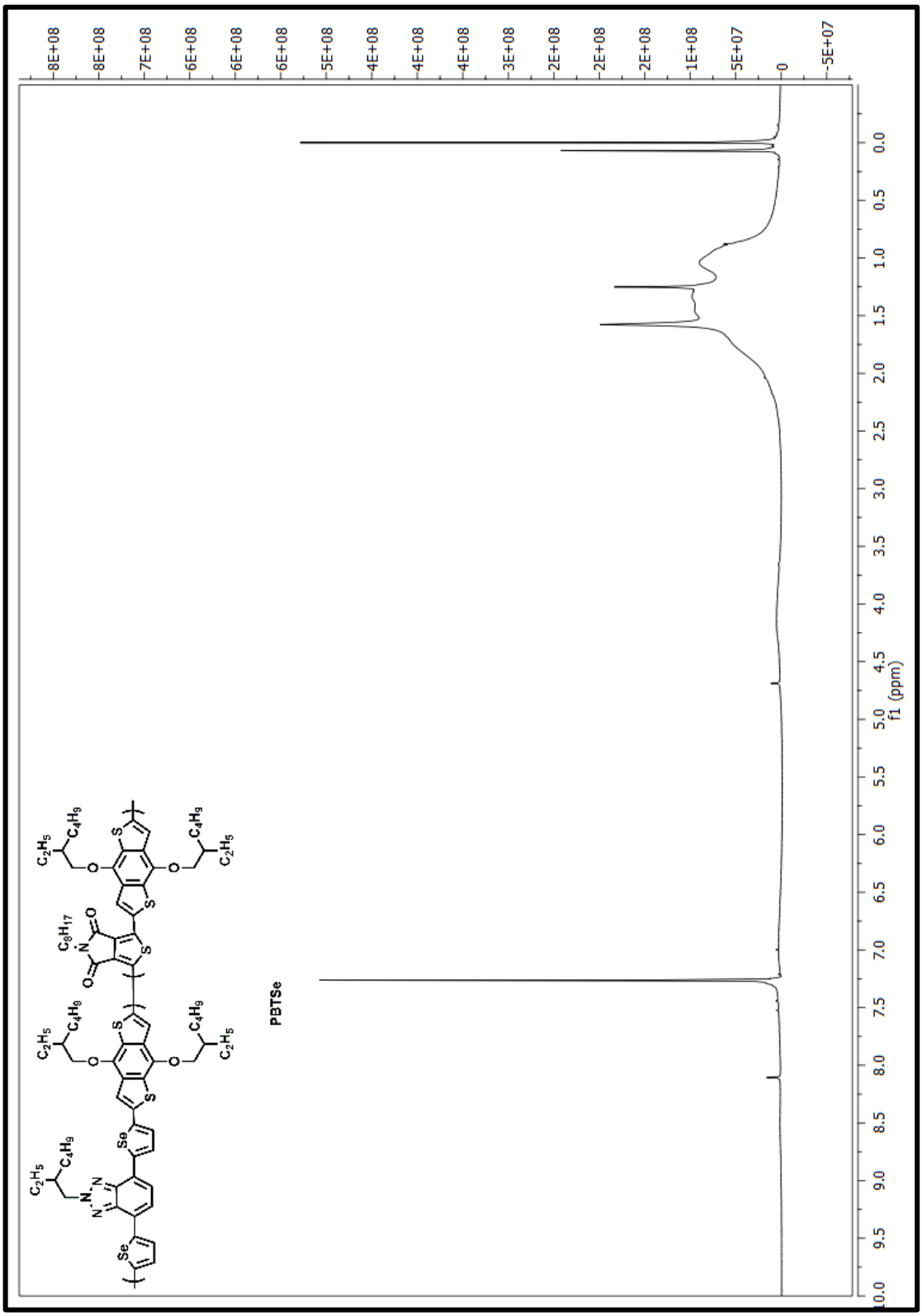

Figure A. 18. ^{1}H NMR of PBTSe

B. THERMAL ANALYSIS DATA

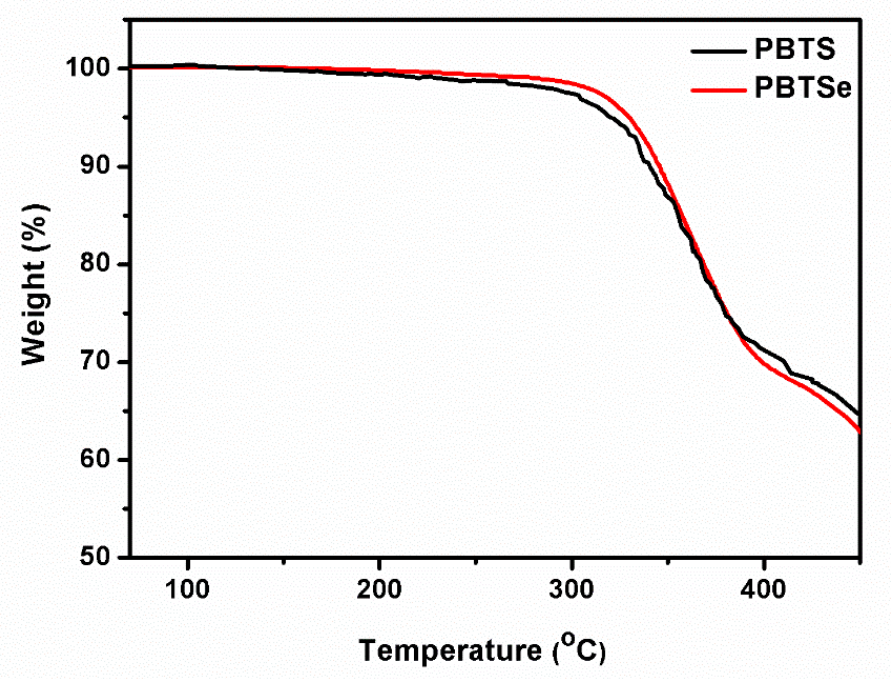

Figure B. 1. TGA Curves of PBTS and PBTSe

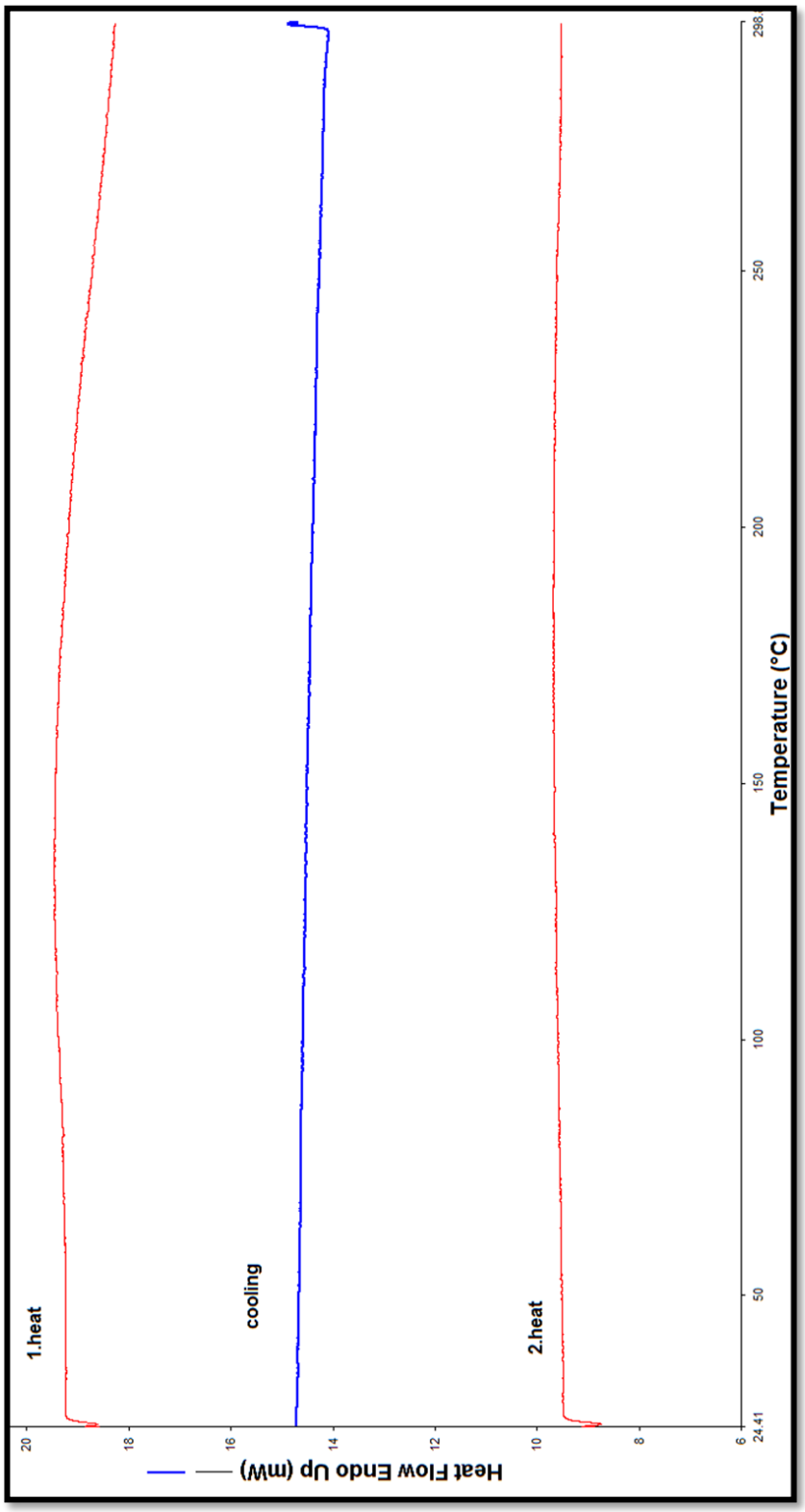

Figure B. 2. DSC curve of PBTS

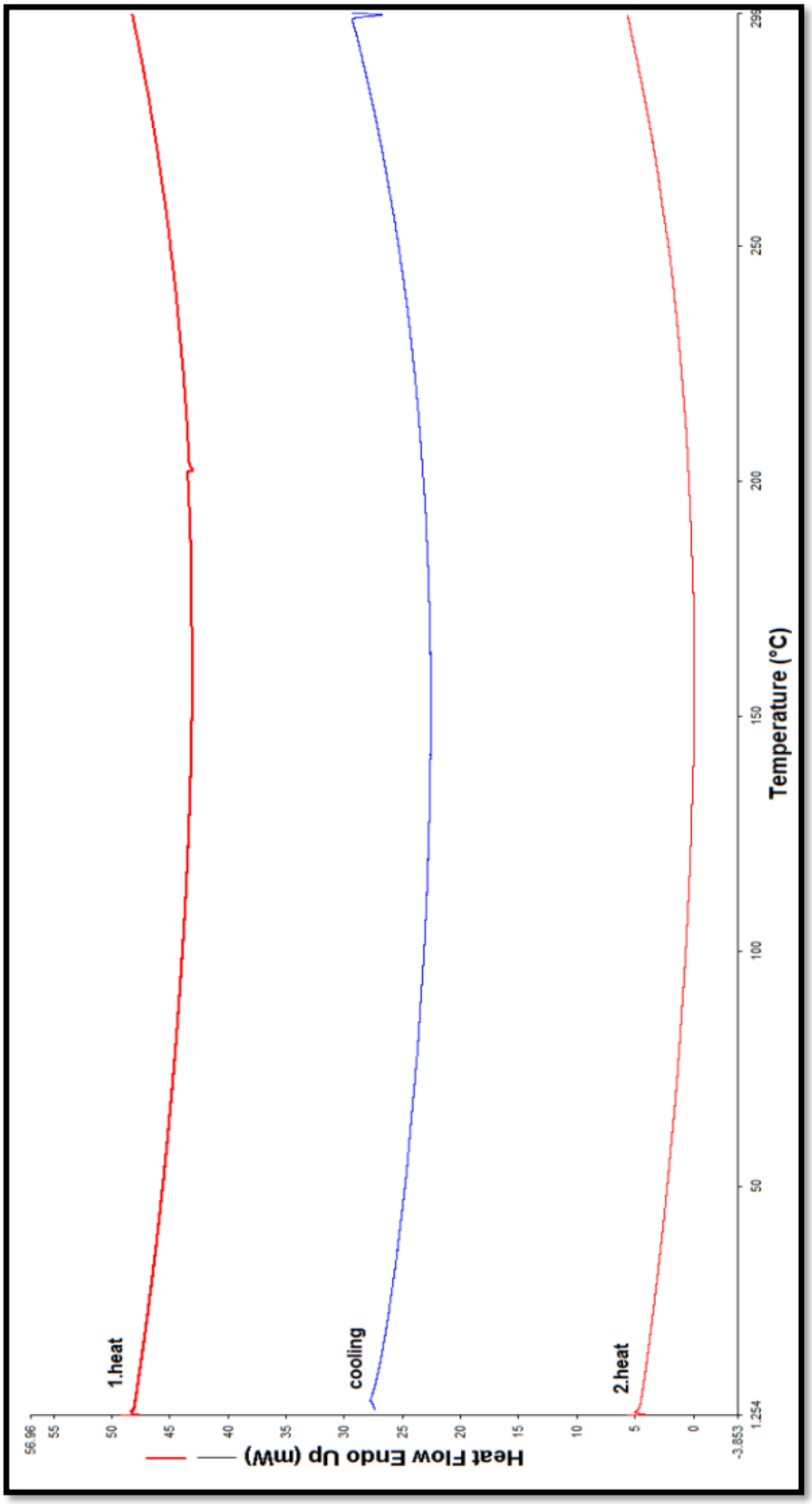

Figure B. 3. DSC Curve of PBTS*e*